UNIVERSITÀ DI PARMA

Università degli studi di Parma

DOTTORATO DI RICERCA IN MEDICINA MOLECOLARE

CICLO XXXIV

Characterization of repetitive ventricular responses and tachyarrhythmias induced by single ventricular premature stimulation during sinus rhythm.
An epicardial mapping study in normal adult rats.

Coordinatore:

Chiar.mo Prof. Prisco Mirandola

Tutore:

Chiar.mo Prof. Emilio Macchi

Dottorando: Luca Magnani

Anni Accademici 2018/2019 – 2020/2021

Index

List of abbreviations.

AP	action potential
APD	action potential duration
AT	activation time
AT1	earliest activation time of the premature beat
AT2	earliest activation time of the reentrant beat
BBR	bundle branch reentry
BCL	basic cycle length
BTP	breakthrough point
CI	coupling interval
DAD	delayed after depolarization
EAD	early after depolarization
ECG	electrocardiogram
EG	electrogram
ERP	effective refractory period
IVR	intraventricular reentry
IVR-P	non-sustained IVR through terminal Purkinje system
IVR-M	non-sustained figure 8 reentry
IVF	idiopathic ventricular fibrillation
IVS	interventricular septum
LBB	left bundle branch
LBBB	left bundle branch block
LV	left ventricle
PMJ	Purkinje muscle junction
PVC	premature ventricular complex
RBB	right bundle branch
RBBB	right bundle branch block
R-on-T	short coupled R-on-T arrhythmia
RT	recovery time
RV	right ventricle
RVOT	right ventricular outflow tract
RVR	repetitive ventricular responses
RW-S	premature stimulation applied during sinus rhythm
S_1-S_2	programmed stimulation
S_1	basic drive beat
S_2	premature beat
SCD	sudden cardiac death
SE	standard error
S-I	strength-interval
UCB	unidirectional conduction block
VF	ventricular fibrillation
VT	ventricular tachycardia

Abstract.

Introduction. The mode of onset of life-threatening ventricular tachycardia and fibrillation (VF) has been well described in patients with organic heart disease and long QT syndromes. However, less is known about the mode of onset of VF initiated by premature ventricular complexes (PVCs) with very short coupling intervals in rare patients who have no evidence of organic heart disease or identifiable etiology. Hence, the aim of this work was to identify the reentry circuits induced by critical PVCs that initiate VF in normal ventricular myocardium.

Methods. Unipolar potentials were measured by means of a high resolution epicardial electrode array in seventeen normal rats. Single premature stimulation was performed during normal sinus rhythm at test sites of the epicardial array or single endocardial electrodes. Strength was gradually increased from near diastolic threshold (100 μA) to 10 mA. For each strength, coupling interval was gradually decreased until absence of ventricular response. All premature stimulations and induced arrhythmias through a test site were summarily represented in a characteristic strength-interval plane. Electrical data were processed off line as electrogram, isopotential and isochrone maps.

Results. Critical premature stimuli triggered repetitive ventricular responses (RVRs) and tachyarrhythmias. RVRs are defined as one or more (but less than five) non-stimulated ventricular beats after a paced ventricular premature beat. RVRs include two types of reentry: bundle branch reentries (BBRs), characterized by reentry circuit through the conducting system and the myocardium of both ventricles, and intraventricular reentries (IVRs) characterized by reentry circuits within the same stimulated ventricle either through terminal Purkinje fibers and myocardium (IVR-P) or through myocardium alone (IVR-M, figure 8 reentry). Tachyarrhythmias occurred when very short coupled IVRs induced VF.

Discussion. Our findings show that VF induced by low strength premature stimuli (less than 1 mA) was characterized by the initial occurrence of very short coupled IVR-Ps with focal pattern followed by sustained arrhythmia. Moreover, focal IVR-Ps could be followed by multiple IVR-Ms with figure 8 reentry pattern before degenerating into sustained arrhythmia. Hence, our findings suggest that, in some instances, the initial reentry beats act like "premature stimulus equivalents" (i.e. S2, S3, S4) aiding the emergence of sustained ventricular tachyarrhythmias.

Alternatively, VF induced by high strength premature stimuli (more than 5 mA) was often characterized by the initial occurrence of IVR-Ms with figure 8 reentry pattern that eventually became sustained.

Preface.

Idiopathic ventricular fibrillation (IVF) is defined as ventricular fibrillation (VF) which occurs in patients with no apparent structural or electrical heart disease after extensive investigations and it is reported in 6,8% of all patients who survive to sudden cardiac death (SCD), but it is much more frequent in young adults where it becomes the most frequent cause of unexplained SCD; indeed, in the population under the age of 35 years, 35% of SCD cases remain unexplained. It is known from the literature that IVF is triggered by extremely short-coupled spontaneous extrasystoles; however, it is not fully understood how such premature spontaneous extrasystoles are able to trigger IVF. The aim of the present work is to characterize the circuit of the first reentrant beat of VF and ventricular tachyarrhythmias triggered by short coupled spontaneous extrasystoles in the normal heart. For this purpose, experiments were performed on normal rat hearts in vivo using a high-resolution grid positioned on the epicardium which allowed to simulate the spontaneous premature extrasystole using the single premature stimulation technique applied during sinus rhythm and to map the reentry triggered by the stimulated extrasystole. The single premature stimulation technique applied during sinus rhythm is the most realistic technique to simulate spontaneous extrasystoles and the recording of the epicardial unipolar potential allows to obtain high resolution maps for the identification of the reentry circuit. In chapter 2 of this work, basic concepts of cardiac arrhythmias, the main mechanisms and the electrophysiological basis of arrhythmias will be illustrated, with particular emphasis on arrhythmias due to abnormal impulse conduction, unidirectional conduction block (UCB) and reentry circuit. In the third chapter the methods used in the present experimental work will be illustrated in detail. In the fourth chapter, examples of arrhythmias induced through the methods described in the previous chapter will be presented; particular emphasis will be placed on non-sustained arrhythmias (repetitive ventricular responses, RVR, which include bundle branch reentries, BBRs, and intraventricular reentries, IVRs) and on VFs (sustained arrhythmia). In the fifth chapter, the aforementioned arrhythmias will be discussed with emphasis on their vulnerability, on the methods used for their identification and on the events at the base of their induction.

1. Introduction.

1.1. Cardiac anatomy.

The heart is a hollow organ located in the thoracic cavity in the middle mediastinum. In the adult it has an average weight of 250-300 g, a length of 13-15 cm, a width of 9-10 cm and a thickness of 6 cm.

It is located between the third and sixth ribs, between the fifth and eighth vertebrae and its anatomical relationships are shown in figure 1.

Anatomically it is in contact with:

- Inferiorly it rests on the diaphragm.
- Anteriorly it is in relationship with the costal cartilages, thoracic muscles, sternum, pulmonary propagation and pleura and with the internal mammary vessels.
- Laterally it is related to the pulmonary hila.
- Superiorly with the great vessels, bronchi and thymus.
- Posteriorly with descending aorta, esophagus, vagus nerves, azygos and hemiazygos veins and the lower tracheo-bronchial lymph nodes.

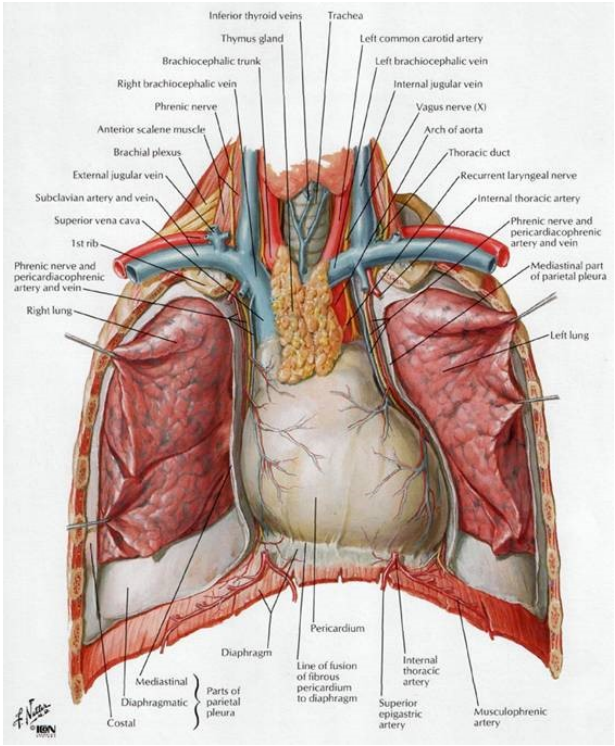

Figure 1: heart anatomical relationships. Reported from Atlas of Human Anatomy, F. H. Netter

The heart has four chambers, two atria (located superiorly) and two ventricles (located inferiorly).

The right side of the heart, consisting of the right atrium and right ventricle, receives deoxygenated blood and sends it into the pulmonary circuit. The left side, consisting of the left atrium and left ventricle, receives oxygenated blood and sends it into the systemic circuit. In physiological conditions, there is no blood exchange between right and left sides of heart.

A wall called the interatrial septum divides the atria, and they are separated from the ventricles by the atrioventricular valves**.** The tricuspid valve separates the right atrium from the right ventricle, and the mitral valve separates the left atrium and the left ventricle. Two other heart valves separate the ventricles and the large blood vessels that carry blood leaving the heart. These valves are called the pulmonic valve**,** which separates the right ventricle from the pulmonary artery leading to the lungs, and the aortic valve, which separates the left ventricle from the aorta.

Heart anatomical elements are shown in figures 2 and 3, from different views.

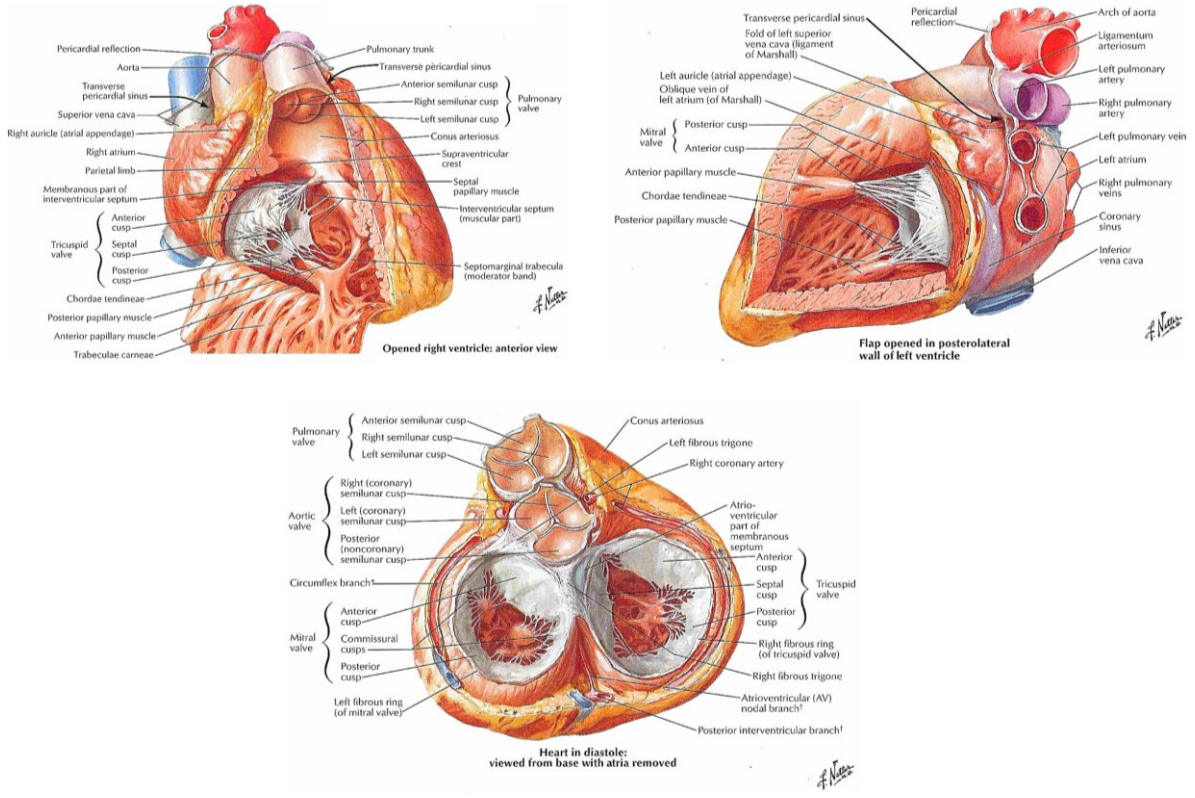

Figure 2: heart anatomical views.
Upper left panel: opened RV, anterior view.
Upper right panel: flap opened in posterolateral wall of LV.
Lower panel: heart viewed from base.
Adapted from Atlas of Human Anatomy, F. H. Netter

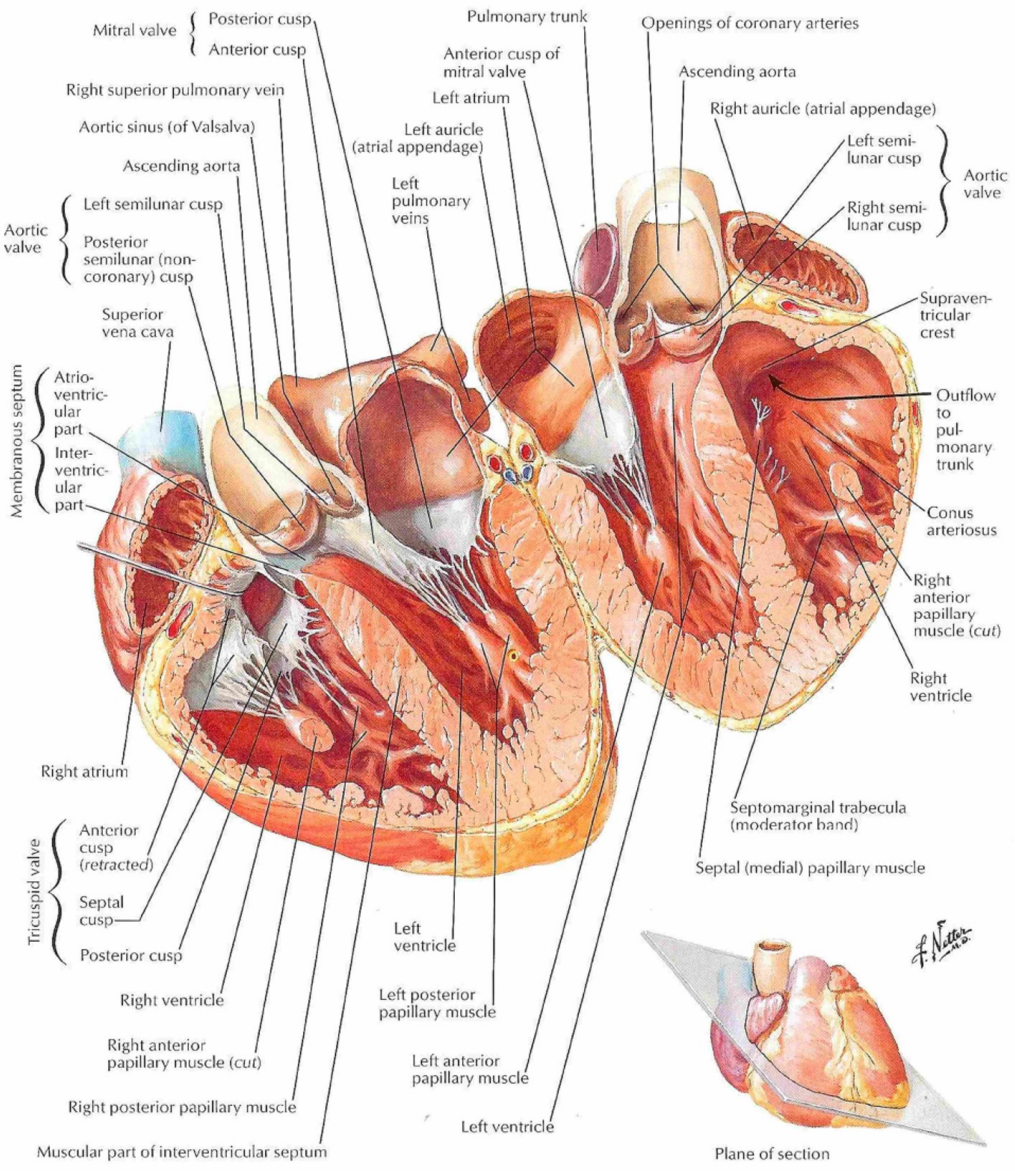

Figure 3: main heart anatomical elements. Reported from Atlas of Human Anatomy, F. H. Netter

Blood vessels carrying blood away from the heart are called arteries. Two coronary arteries branch off at the beginning of the aorta and divide into a network of smaller arteries that provide oxygen and nourishment to the muscles of the heart. Blood vessels that carry blood back to the heart are called veins. They contain valves that prevent blood from flowing backward.

The heart wall is made up of three layers:

- Endocardium. Ventricular endocardium is composed of five distinct layers: the endothelial layer, the inner connective tissue layer, the elastic tissue layer, the smooth muscle cell layer, and the outer connective tissue layer or subendocardial layer.
- Myocardium. It is composed by striated muscle tissue and connective tissue: it is the portion that acts as a pump.
- Pericardium.

The pericardium is a large serous sack, which isolates the heart from the nearby organs and is composed of two parts:

1) External, of a connective nature, called fibrous pericardium, which is linked to the surrounding formations by means of small fibrous cords: the ligaments of the pericardium, which help to maintain its outer expanse surface.
2) Internal, serous, called serous pericardium. This, like all the serous membranes, is formed by a parietal leaflet which adheres to the inner surface of the fibrous pericardium and a visceral leaflet which is applied to the myocardium and forms with the epicardium the most outer tunica of the walls of the heart.

The three layers of heart wall are shown in figure 4.

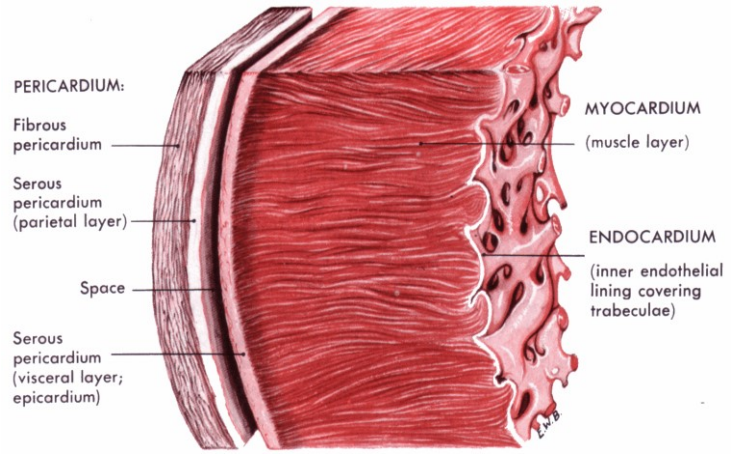

Figure 4: schematization of the heart wall. Source: https://slidesharetips.blogspot.com/2020/06/three-layers-of-heart-wall-identify_24.html

The cardiac wall has different thicknesses in different regions. In particular, the thickness of the myocardium is different in relation to the contractile force that each cavity has to exert to thrust the blood. It follows that the wall of the atria is thin, while that of the ventricles is

thicker. In particular, the left ventricular wall is three times thicker than that of the right ventricle, because it has to thrust the blood in the aorta and therefore in the large circulation.

The myocardium, that determines the major part of cardiac wall, can be divided into cardiomyocytes, with contractile function, and specific cells that forms the conducting system, with pacemaker function.

The conducting system is characterized by special cells characterized by automaticity. From the conducting system the impulse propagates to the various parts of the heart according to a well-defined sequence. In detail, the heart conducting system (shown in figure 5) consists of:

1) Sinoatrial node (SA node) or Sinus node, located in the rear wall of the right atrium at the "terminal sulcus" that separates the outlet of superior vena cava from the right atrium. The SA node is the structure where the automaticity has the highest frequency and, for this reason, it determines the heart rate.
2) Atrioventricular node (AV node). It is located in the right rear part of the interatrial septum near the tricuspid valve. It is characterized by automaticity but with a shorter rate compared to SA node. Physiologically, it is the only structure that allows the propagation of the impulse from the right atrium to the ventricles
3) His bundle, which starts from the AV node, descends into the interventricular septum and splits into two majors, right and left, bundle branches. The two branches divide then into further ramifications.
4) Left bundle branch splits into three main fascicles from which Purkinje fibers have origin.

   Right bundle branch splits directly into Purkinje fibers without originating separated fascicles.

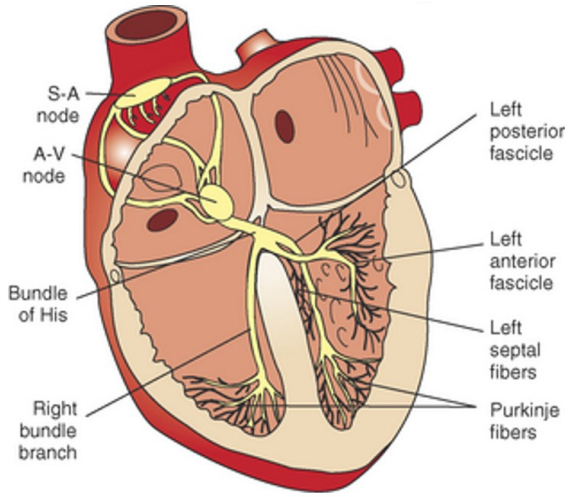

Figure 5: Schematic representation of the heart conducting system. Source: https://veteriankey.com/electrocardiography-2/

Physiologically, the impulse has origin in the SA node and reaches the AV node through right atrial muscle: the fastest preferred bundle is the crista terminalis. The impulse passes from the right atrium to the left atrium via the bundle of Bachmann.

The impulse cannot pass freely from the atrium to the ventricle because the fibrous ring which acts as an insulator and the AV node represents the only way of passage for the impulse. The AV node slows the conduction (to about 0.05 m/sec) allowing complete atrial activation and contraction before initiation of ventricular activation.

In pathological conditions there may be accessory bundles that can favor macro reentry tachycardias, such as the bundle of Kent.

From the AV node the impulse propagates in the His bundle, in the bundle branches and in the Purkinje fibers.

Purkinje fibers are electrically connected to the ventricular muscle and are histologically localized between the endocardium and the myocardium, as shown in figure 6.

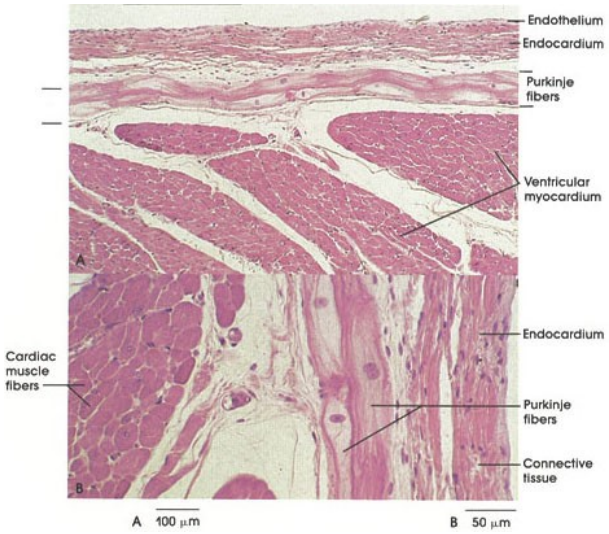

Figure 6. Histological localization of Purkinje fibers in the ventricular wall. Source: https://www.anatomyatlases.org/MicroscopicAnatomy/Section08/Plate08151.shtml

The role of the conducting system is to synchronize and speed up ventricular muscle contraction in order to make its pump function efficient.

For this reason, Purkinje fibers are characterized by the maximum conduction velocity (about 2-4 m/sec).

At ventricular level, the impulse propagates from the portion of myocardium closer to the endocardium to the portion of myocardium closer to epicardium and from the apex to the base. Consequently, blood is pushed toward the base of the heart allowing an efficient pump function.

1.2. Cardiac electrophysiology

The myocardium is able to respond to supraliminal stimuli through an active electrical process called action potential (AP). An action potential is a rapid sequence of changes in the voltage across a membrane which follows the "all or none" law. The "all or none" law indicates the fact that the amplitude of an action potential is independent of the amount of current that triggers it. Hence, action potentials are said to occur fully or not to occur at all in response to a stimulus. The "all or none" characteristic of AP is due to the active role of the cellular membrane in the genesis of an AP. Particularly, the excitability of the membrane depends on the presence of voltage-gated channels and the AP is the result of the activation and inactivation of the correspondent different ionic currents.

The AP in cardiac cells can be schematically divided into two groups (shown in figure 7):

1) Action potentials of fast response cells, which concerns working muscle cells of atria and ventricles, and cells of His bundle and of Purkinje fibers.
2) Action potentials of slow response cells, which concerns cells of SA node and AV node.

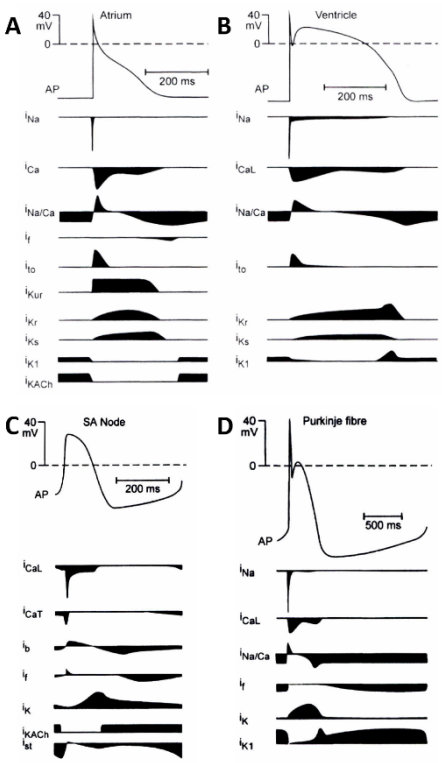

Figure 7.
Cardiac action potentials and correspondent ionic currents of atrial cell (A), ventricular cell (B), sinoatrial node (C), Purkinje fibre (D).
Inward currents (depolarizing): Na^+ and L-type Ca^{2+}currents (i_{Na} and i_{CaL}).
Outward (repolarizing) K^+currents: i_{to} transient outward, i_{Kur} ultra-rapid delayed rectifier, i_{Kr} rapid delayed rectifier, i_{Ks} slow delayed rectifier, i_{K1} inwardly rectifying, i_{KACh} acetylcholine activated.
Adapted from Cardiac Cellular Electrophysiology, E. Carmeliet and J. Vereecke

The terms “fast and slow” indicate the rate of depolarization during the phase 0 of the AP, which can be fast (when mediated by i_{Na}) or slow (when mediated by i_{CaL}).

The action potential in typical cardiomyocytes (fast cells) is composed of 5 phases (0-4), beginning and ending with phase 4:

- Phase 4 (or resting diastolic phase)
- Phase 0 (or depolarization)
- Phase 1 (or early repolarization)
- Phase 2 (or plateau)
- Phase 3 (or late repolarization)

Phase 4: The resting diastolic phase.

The resting potential in a cardiomyocyte is −90 mV due to a constant outward leak of K^+ through inward rectifier channels (current i_{K1}). Na^+ and Ca^{2+} channels are closed at resting transmembrane potential.

Phase 0: Depolarization.

An action potential triggered in a neighboring cardiomyocyte or pacemaker cell causes the transmembrane to reach the activation threshold. When the stimulus is above the activation threshold it leads to the opening of the channels to Na^+ generating an inward current higher than the outward current of K^+, which causes depolarization and fast opening of other Na^+ channels, through a self-regenerating mechanism. The speed of the upstroke (which is proportional to the net ionic current) is almost exclusively determined by the current of Na^+ (i_{Na}). After reaching the peak, the Na^+ current undergoes a rapid decline, caused by a decrease in driving force (the membrane potential is close to that of E_{Na}) and the inactivation of the channel. The large Na^+ current rapidly depolarizes the transmembrane potential to and slightly above 0 mV (~ + 40mV) for a transient period of time called the overshoot.

Phase 1: Early repolarization.

It is mainly determined by the rapid inactivation of the Na+ channels by the inner gate (inactivation gate) and by the transient outward potassium current i_{to} which leads the transmembrane potential to a value equal to 0 mV. In phase 1 of AP, a gradual increase of Ca^{2+} occurs by slow opening of L-type Ca^{2+} channels. This early repolarization results in the notch between the end of the upstroke and the beginning of the plateau. The size of the notch varies among cardiac cells and depends on i_{to} channels density in their membrane.

Phase 2: The plateau phase.

The plateau phase is generated by an ionic equilibrium due to outward (i_{kr} and i_{ks}) and inward (i_{CaL}) currents, with a slightly dominance of outward currents that allows a very slow repolarization and a maintenance of the membrane potential to positive values close to 0 mV. Voltage-regulated L-type Ca^{2+} channels are activated by depolarization of membrane potential to about -40 mV and inactivate slowly.

i_{Ks} and i_{Kr} are activated very slowly in phase 1 and K^+ efflux augments in phase 2 and more significantly in phase 3 of the AP.

Phase 3: Late repolarization.

It is determined by the closure of the L-type Ca^{2+} channels while slow delayed rectifier (i_{Ks}) K^+ channels remain open. The final repolarization is also mediated by the inwardly rectifying K^+ current, i_{K1}. The delayed rectifier K^+ channels close when the membrane potential is restored to about -85 to -90 mV, while I_{K1} remains conducting throughout phase 4, which helps to set the resting membrane potential.

Slow response cells action potentials are divided into three phases:

- Phase 4 is the spontaneous depolarization that triggers the action potential once the membrane potential reaches the threshold (between -40 and -30 mV). It is mainly mediated by the funny current i_f which allows the depolarization from -60 mV to -40 mV. When it is reached a value of membrane potential equal to -50 mV, the current i_{CaT} contributes to reach the threshold.
- Phase 0 is the depolarization phase of the action potential and it is mediated by i_{CaL} current.
- Phase 3 is the repolarization and it is mediated by inactivation of i_{CaL} current and by the repolarizing current i_K. Phase 3 is then followed immediately by a new Phase 4 mediated by i_f.

Cardiac muscle presents different properties, including automaticity, excitability, conduction, contractility and refractoriness.

1) Automaticity is the ability of cardiac pacemaker cells to generate their own electrical impulses spontaneously without external stimulation. This characteristic is specific to the pacemaker cells localized in the conducting system (i.e., SA node, AV node, His bundle and Purkinje fibers).
2) Excitability is the ability of cardiac muscle to respond to adequate stimuli by generating a propagated action potential. This characteristic is shared by all cardiac cells.
3) Conduction is the ability of cardiac cells to propagate action potentials. The propagation of action potentials is guaranteed by electrotonic currents.

Considering two contiguous regions, when an AP develops in one of the two regions while the other is at rest, a difference in membrane potential is established between the two regions. This difference involves the development of an intracellular current, which flows through the gap junctions, from the activated region to the resting region. The variation in the space of this intracellular current is the depolarizing electrotonic current, which allows the threshold to be reached in the resting region. Consequently, an AP will develop in the region which was at rest (propagation of the AP from the activated region to the one initially at rest).

Conduction of AP occurs with anisotropy; this means that conduction velocity is not uniform in the myocardium.

Particularly, conduction velocity is higher along fiber direction and lower across fiber direction. This difference is due to the fact that intracellular resistance is not uniform in cardiomyocytes. The non-uniform intracellular resistance in cardiomyocytes is due to their morphology (roughly rectangular, measuring 100–150 μm by 30–40 μm) and because of distribution of the gap junctions in their membrane (mainly located at the intercalated disk, along cardiomyocytes direction). Consequently, the transverse resistance is higher than the longitudinal one and the conduction is faster in longitudinal (0,6 m/s) than in transverse direction (0,3 m/s).

4) Contractility is the ability of cardiac cells to shorten and cause cardiac muscle contraction in response to an electrical stimulus. The contraction of cardiomyocytes is determined by the increase in intracellular calcium. Since the increase in intracellular calcium is determined by the action potential (i_{CaL} current which determines further release of calcium from the sarcoplasmic reticulum), this event is indicated as excitation-contraction process. The term excitation-contraction, therefore, indicates the fact that the contraction

of cardiomyocytes is always determined and occurs after their excitation (development of the action potential).

5) Refractoriness is the inability for a period of time to respond to a supraliminal stimulus with a propagated response (action potential). It is due to the presence of voltage-dependent ion channels that are also characterized by inactivation.

   There are different states of refractoriness throughout the action potential (as shown in figure 8):

   a. Absolute refractory period (ARP): period in which the myocardium is unable to respond to any stimulus (corresponds to that phase in which the sodium channels are inactivated).
   b. Effective refractory period (ERP): period of absolute refractoriness with a stimulus given at a specific strength. As the strength increases, the ERP decreases. At maximum strength, the ERP coincides with the ARP.
   c. Relative refractory period (RRP): period in which the myocardium is able to respond to intense stimuli, above the diastolic threshold (corresponds to that phase in which some sodium channels are still inactive, while others are closed and openable).
   d. Supernormal period (SNP): period in which the myocardium responds to stimuli weaker than diastolic threshold. It is a very short period that corresponds to that phase in which all the sodium channels are closed and the membrane potential is higher than the resting membrane potential.

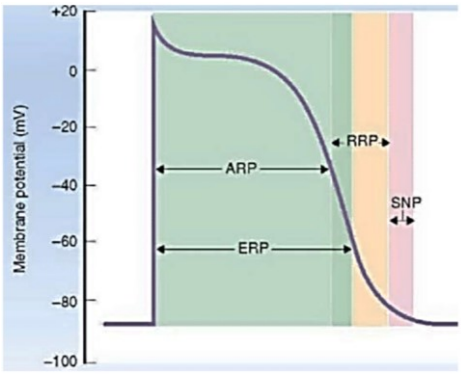

Figure 8. Schematization of cardiac refractoriness. Source: https://www.researchgate.net/figure/Refractory-periods-of-the-ventricular-action-potential-The-effective-refractory-period_fig7_330411041

1.3. Purkinje fibers.

Purkinje fibers are made of Purkinje cells assembled longitudinally and are insulated from working cardiomyocytes by connective tissue[1-2-3]. The cells of Purkinje fibers are larger (50 µA of diameter) compared to cardiomyocytes, and therefore have a larger capacitance.

Purkinje cells are differentiated from cardiomyocytes, from a cellular point of view, by the absence of T-tubules, distinctive mitochondria, and large glycogen density[3-4].

Membrane electrical properties remain the most remarkable distinctions between these two cell types.

Electrophysiological and morphological properties of Purkinje system cells are different from those of other cardiomyocytes.

The Purkinje action potential, compared to ventricular cardiomyocytes, is characterized by:

- faster upstroke velocity (dV/dt_{max}). Particularly, in the Purkinje system, upstroke velocity is the fastest recorded in the heart (500-1000 V/s), as the result of high density of Na^+ channels[5].
- larger amplitude.
- more pronounced early repolarization (phase 1) and more negative plateau potential due to larger i_{to} density[6].
- much longer action potential duration and refractoriness.

Another difference between Purkinje cells and ventricular cardiomyocytes is provided by ion-channel expression, most notably those associated with Ca^{2+} handling[7]. Particularly, compared to ventricular cardiomyocytes, in which RyR2 is the only Ca^{2+}-release channel expressed, intracellular Ca^{2+} mobilization in canine Purkinje cells is governed by three different channels in the membrane of the endoplasmic reticulum, which are IP3R, RyR2, and RyR3. Therefore, distinct proarrhythmic Ca^{2+}-mediated mechanisms can lead to the development of triggered activity in the Purkinje cells.

Early afterdepolarizations (EADs) and delayed afterdepolarizations (DADs) occur in Purkinje fibers[8-9-10].

EADs occur during phase 2 and phase 3 of the action potential and are caused by the reactivation of inward currents (I_{CaL} and/or late Na^+)[11].

DADs occur Purkinje cells during phase 3 and phase 4 of the action potential and are due to intracellular Ca^{2+} load[11].

Purkinje–muscle junctions have the function to activate the myocardium and at the same time to protect from retrograde excitation.

Abnormal excitation patterns can however lead to unidirectional block that predisposes to arrhythmias[12]. Because myocardium is a large volume and Purkinje system can be considered as a cable, Purkinje network must overcome the large electrical source–load mismatch where it couples to the myocardium. For this reason, Purkinje cells are characterized by a high density of membrane Na^+ channels and have a large size in order to improve source strength.

In Purkinje-muscle junctions, transitional cells are localized between Purkinje cells and cardiomyocytes. These transitional cells have the function to amplify impulses and shield the Purkinje system from electrotonic loading.

Because junctional transmission is delayed in the anterograde direction by 3–12 ms[13], it is suggested a low safety factor[14] of propagation in this direction. On the contrary, in retrograde direction, the conduction delay is much shorter (about 1 ms). This situation can lead in some conditions to determine anterograde block and retrograde conduction[15].

Purkinje fibers have longer action potential duration (and refractoriness) compared to ventricular cardiomyocytes. Action potential duration (and refractoriness) is not uniform in the Purkinje system. Maximal action potential and refractoriness occur at 2–3 mm from the Purkinje-muscle junctions and then they shorten proceeding towards the junctions. Electronic interactions at the junctions can account for this distal shortening of action potential duration, as suggested by modelling studies[12]. The same electrotonic interactions can lead to local myocardial action potential prolongation, which amplifies repolarization heterogeneity and can be proarrhythmic in pathological conditions.

Many junctions might normally be quiescent and become active with myocardial uncoupling[16]. This theory is supported by studies demonstrating that a critical level of coupling is needed for propagation across an abrupt tissue expansion[17].

Purkinje system can be related to ventricular arrhythmias such as isolated ectopies, monomorphic VT, polymorphic VT and VF, in patients with or without structural heart disease.

Regarding to VF, Purkinje system can be involved in its initiation (trigger) and in its maintenance (substrate)[18].

1.4. Ventricular fibrillation and sudden cardiac death.

Ventricular fibrillation (VF) is a ventricular arrhythmia characterized by ventricular chaotic electrical activity which leads desynchronized ventricular contractions until the stop blood flow into the body causing sudden cardiac death (SCD), which is defined as an unexpected death caused by the loss of mechanical pump function of the heart.

Every year, SCD causes 350,000 deaths in the USA, 700,000 deaths in Europe, more than 1 million deaths in Asia[19] and in the young it causes 7% of deaths[20]. Sudden cardiac death occurs in more than 50% of cases in presence of pathological conditions (the main component is represented by coronary problems), in the other cases, occurs in victims which are apparently healthy[21]. Furthermore, SCD can be caused by VF, which is the most frequent cause[22], pulseless electrical activity (PEA) and asystole.

Idiopathic VF (IVF) is defined as VF which occurs in patients with no apparent structural or electrical heart disease after extensive investigations[23]. Ventricular fibrillation is initiated by premature ventricular complexes (PVCs) or by a transition from ventricular tachycardia (VT).

Sudden cardiac death is most commonly caused by congenital alterations and structural heart diseases which lead to the development of VF, albeit a significant number remain unexplained after comprehensive autopsy. In these unresolved cases, channelopathies are considered the first potential cause of death.

Channelopathies are a group of cardiac diseases, of genetic origin, characterized by a structurally normal heart leading to VF and SCD.

Some of these channelopathies do not determine changes in the electrocardiogram (ECG), making them more difficult to diagnose[24].

The common mechanism by which some channelopathies (Brugada syndrome, early repolarization syndrome, long QT syndrome and short QT syndrome) lead to VF is the amplification of transmural dispersion of repolarization (TDR) which promotes the development of very closely coupled extrasystole via phase 2 reentry resulting in an R-on-T phenomenon that can initiate polymorphic VT or VF.

In patients with IVF, PVCs that trigger VF originate from Purkinje fibers in up to 93% of cases and more rarely from the right ventricular outflow tract (RVOT) or papillary muscles[25]. These premature extrasystoles are mostly caused by abnormal automaticity or triggered activities and more rarely by reentries[26] and are characterized by short coupling R-on-T intervals[27-28]. Ventricular fibrillation is then sustained by reentrant activities and multiple wavelets[29] and lately by Purkinje system that maintains long-duration VF[30]. Idiopathic VF is

a rare cause of SCD and it is reported in 6,8% of all patients who survive to SCD but it is much more frequent in young adults and it becomes the most frequent cause of unexplained SCD in young patients under the age of 35[25].

1.5. Cardiac arrhythmias.

Cardiac arrhythmias can be classified as:

- Cardiac Arrhythmias:
  - Impulse initiation;
    - Abnormal automaticity
      - Reduced automaticity (bradycardia)
      - Enhanced automaticity (tachycardia)
    - Triggered activity
      - Early after depolarization (EAD)
      - Delayed after depolarization (DAD)
  - Impulse conduction;
    - Conduction block
    - Reentry
      - spiral wave re-entries
      - figure 8 reentries
      - reflection re-entries
      - phase 2 reentries
      - repetitive ventricular responses
  - Combination between impulse initiation and conduction

In detail, enhanced automaticity can occur when atrial or ventricular myocardial cells develop automaticity resulting in the development of repetitive impulse initiation, a phenomenon defined depolarization-induced automaticity. The rate of abnormal automaticity is substantially higher than that of normal automaticity of sinoatrial (SA) node causing tachycardia. Abnormal automaticity in the Purkinje fibers likely results from a deficient calcium regulation by the sarcoplasmic reticulum[18], or can be caused by hypokalemia.

Early after depolarizations are depolarizations that occur during phase 2 or phase 3 of the action potential, and can be caused by pathological conditions such as injury, hypoxia and acidosis, by pharmacologic agents, or by more physiological situations such as transient electrolyte disturbances and increased exposure to catecholamines. Early after depolarizations develop when the balance of current active during phase 2 and or 3 of the action potential shifts in the inward direction, thus causing depolarization. More frequently, EADs are caused by a reduction of potassium currents active during phase 2 and 3 (I_{Kr} and I_{Ks}) of an action

potential. I_{Kr} and I_{Ks} reductions can be caused by hypokalemia, drugs (class IA and III antiarrhythmic agents), and catecholamines. Early after depolarizations can also be caused by an increase in the sodium-calcium exchange current (I_{NCX}) (due to an increase of Cai activity or upregulation of the I_{NCX}) and an increase in late sodium current (late I_{Na}).

Delayed after depolarizations are depolarizations that occur during phase 4 of the action potential and are caused by conditions that augment intracellular calcium, such as hypercalcemia, enhanced exposure to catecholamines, increased heart rate, and heart failure.

Early after depolarizations and DADs are commonly recorded in the Purkinje cells and can result from Ca^{2+} overload[31].

Reentry can occur when an activation wavefront meets an anatomic or functional unidirectional conduction block (proximal side), propagates around the unidirectional conduction block (UCB), and from the distal side of UCB it can re-excite the proximal side. Successful reentry can occur only when the impulse conduction is sufficiently delayed during the circumvention of the UCB to allow the expiration of the refractory period in the tissue at the proximal side of UCB. The general rule is that the length of the circuit (path length) must exceed or be equal to that of the wavelength which is defined as the product of the conduction velocity by refractory period of the proximal side of UCB. Hence, reduction of conduction velocity or refractory period can both significantly reduce the path length required for the development or maintenance of reentry.

1.5.1. Spiral wave reentries

Spiral wave reentries (or rotors) are characterized by a central region (core) of UCB. The central refractory region prevents the centripetal waves from short circuiting the circus movement and maintains the reentry. This central refractory region can be structural (due to pathologies) or functional (due to dispersion of refractoriness). When the core is functional, it is maintained by centripetal wavelets that collide with each other and recordings near the center of the circus movement show only subthreshold responses. Functional spiral wave reentries were obtained and described for the first time by Allessie et al. [32] in 1973.

1.5.2 Figure 8 reentries

Figure 8 reentries are characterized by an arch of UCB that can be structural or functional. During figure 8 reentries, the wavefront circulates from the proximal side of UCB in both directions around the lines of conduction block and once reached the distal side of the block it re-excites the proximal region breaking through the arch of block. The reentrant activation continues as two circulating wavefronts that travel in clockwise and counterclockwise directions around the two arcs in a pretzellike (figure 8) configuration. Figure 8 reentry due to structural UCB (infarction) has been described by El-Sherif et al.[33] in 1981. Figure 8 reentry due to functional UCB (dispersion of repolarization) has been described by Gotoh[34] et al. in 1997. In his work "Cellular Graded Responses and Ventricular Vulnerability to Reentry by a Premature Stimulus in Isolated Canine Ventricle" Gotoh was able to induce VF by means of S1-S2 programmed stimulation applied on epicardial slices (30×38×2 mm) of canine ventricle. Baseline S1 stimuli were applied at the edge and the S2 at the center of the tissue. The line connecting the S1-S2 sites was parallel to the long axis of the fiber orientation. Isochrone activation maps were obtained through 56 (in 16 experiments) and 480 (in 14 experiments) bipolar electrodes. In addition to bipolar extracellular potential, two transmembrane action potentials were recorded simultaneously from the most superficial (first three) epicardial cell layers through machine-pulled glass-capillary electrodes with two differential amplifiers; one recording was from the area of S2-induced conduction block and the second from the region of the earliest activation after the S2. In this work, Gotoh utilized the "propagated graded response hypothesis", proposed for the first time by Chen[35] et al. in 1988, to explain the mechanism underlying the development of VF following programmed stimulation. The same hypothesis was also used and inserted into a broader mechanism,

denoted by the term “critical point”, in a subsequent work by Frazier[36] et al. (in which linear stimulation was utilized during programmed stimulation instead of point-like stimulation) in 1989. The same graded response hypothesis was then used again in a later work of Chen[37] et al. in 1993. According to this hypothesis, the first reentry of VF induced by means of S1-S2 premature stimulation, is caused by the ability of S2-induced graded responses to prolong refractoriness near the S2 site and second to propagate away from the S2 site. The propagated graded responses encounter recovered cells and initiate activation at a site distant from the S2 site. The distally originated wave front propagates in all directions but blocks near the S2 site, where graded response occurred, as a result of the prolongation of the refractoriness by the same S2-induced graded response. The wave front propagates around both sides of the functional conduction block, reaches the distal side of UCB and re-enters through the proximal side of UCB when it is no longer refractory, initiating in this way the first reentry of VF. Furthermore, in the same work, Gotoh has characterized the properties of the graded responses.

In Fig.9A, it is shown the activation pattern following S1 stimulation during regular pacing (600-ms pacing cycle length). Pacing site (*) was at the lower edge of the figure, and S1 was applied at twice the diastolic threshold with a duration of 2 ms. As it is visible from the map, the source resulted localized around the stimulation site and propagation occurred anisotropically without UCB (higher conduction velocity along than across fiber direction, 70 versus 52 cm/s).

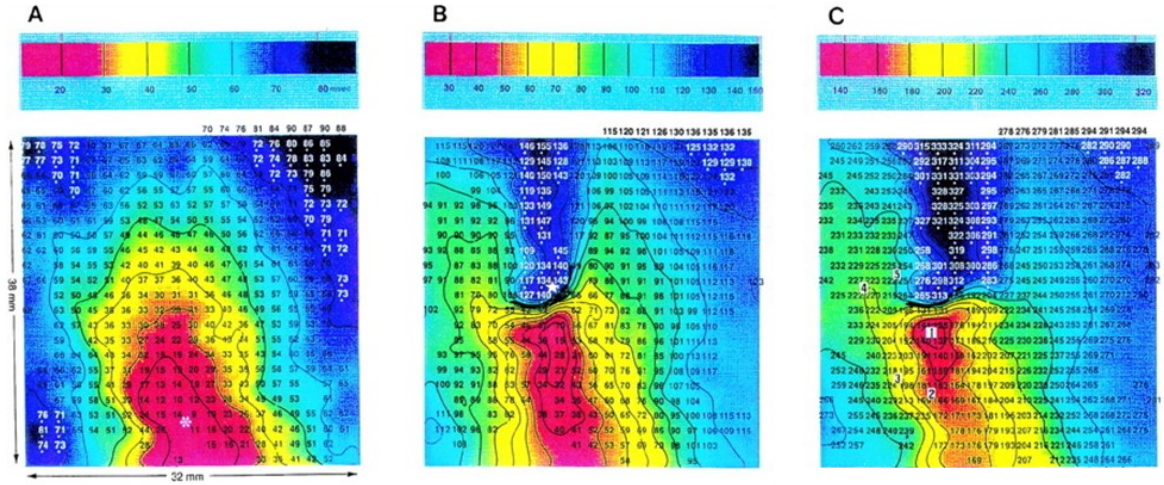

Figure 9. A: S1 activation pattern; B: S2 activation pattern; C: first figure 8 reentry, of VF, activation pattern. Fiber orientation was north-south. Adapted from Gotoh et al., 1997.

In Fig.9B, it is shown the activation pattern following S2 premature stimulation with a stimulation strength of 10 mA and a coupling interval of 130 ms. S2 was applied from the center of the tissue (☆). Because premature stimulation was applied at a critical coupling interval, tissue around the stimulation site could not respond immediately with a full action potential and graded response occurred in the south direction. For this reason, the source did not result localized around the S2 stimulation site but resulted in localized 3.2 mm away from S2 in south direction (isochrone 10 ms in red color); functional UCB (due to graded response which prolongs refractory periods) was present as indicated by thick black lines in the center of the map. Wavefront originating from the source turned around the UCB and reached the distal side of the UCB after 140 ms.

In Fig.9C, wavefront, which reached the distal side of UCB at 140 ms in Fig.9B, re-excites the proximal side of UCB at 141 ms, initiating in this way the first figure 8 reentry.

Graded responses are particular responses that characterize the tissue when a critical premature stimulation is applied; both passive and active ionic mechanisms are implied in graded responses.

Following the data reported by Gotoh, the graded response:

- tends to increase in amplitude and duration, increasing the stimulation strength at a fixed coupling interval (Fig.10A).
- tends to increase in amplitude and duration, increasing the coupling interval of the S2 at a fixed current strength (Fig.10B).
- tends to increase in amplitude as the takeoff potential becomes more negative at a fixed current strength and to increase in amplitude, increasing stimulation strength, at a fixed takeoff potential (Fig.10C).
- tends to propagate in a decremental and anisotropic fashion (Fig.10D).
- is characterized by a slower conduction velocity compared to regenerative responses.

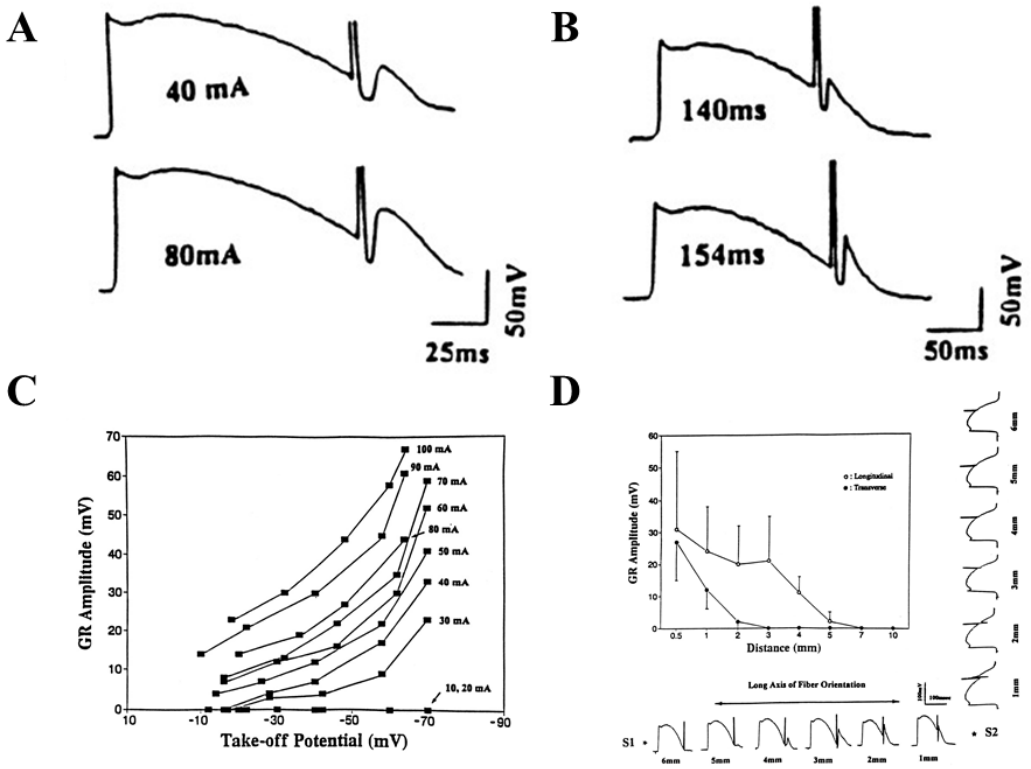

Figure 10. A: effects of increasing S2 current strength from 40 mA to 80 mA at a given coupling interval on graded response amplitude and duration. B: effects of increasing S2 coupling interval from 140 ms to 154 ms at a given stimulation strength on graded response amplitude and duration. C: effects of take-off potential at a given stimulation strength on graded response amplitude and effects of stimulation strength at a given take-off potential on graded response amplitude. D: anisotropic propagation of graded responses. S2 was applied with a current strength of 50 mA and a coupling interval 140 ms. The graded response has a higher amplitude and propagates further along fibers direction. Adapted from Gotoh et al., 1997.

1.5.3 Reflection reentry

Reflection reentries can occur in presence of a large dispersion of refractoriness. The site with delayed recovery serves as a virtual electrode that excites its already recovered neighbor, resulting in a reentrant re-excitation. Reflection reentry has been described by Antzelevitch et al.[38] in 1980. In this work, an ion-free isotonic sucrose solution was used to create a narrow (1.5 mm to 2 mm) central unexcitable zone (gap) in unbranched Purkinje fibers mounted in a 3-chamber tissue bath. Stimulation of the proximal (P) segment elicits an action potential that propagates to the proximal border of the sucrose gap (Fig.11). Active propagation across the sucrose gap is not possible because of the ion-depleted extracellular medium, but local circuit current continues to flow through intercellular low-resistance pathways provided. This electrotonic current gradually gives rise to a depolarization that manifests as a either a subthreshold response (last distal response) or as a threshold response in the distal (D) segment (Fig.11). In the second case, active impulse propagation stops and then resumes after a delay that can be as long as several hundred milliseconds. When anterograde (P to D) transmission time is sufficiently delayed to permit recovery of refractoriness at the proximal end, electrotonic transmission of the impulse (D to P) in the retrograde direction is able to re-excite the proximal tissue, thus generating a closely coupled reflected reentry. Reflected reentries have also been described in isolated ventricular tissues[39] (Fig.11).

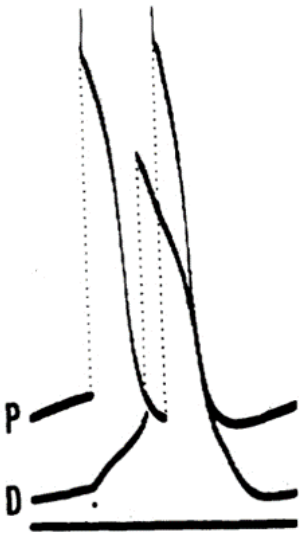

Figure 11. Example of reflection re-entry. P = recordings from segments proximal to the sucrose gap, D = recording from segments distal to the sucrose gap. Conduction time to D from the driven response in P was 290 ms, and the corresponding interval in the reverse direction was 100 ms; the resulting coupling interval in P was 390 ms. Adapted from Antzelevitch et al., 1980.

1.5.4. Phase 2 reentry.

Phase 2 reentries can occur in presence of a large dispersion of refractoriness. Phase 2 reentry occurs thanks to depolarizing electrotonic currents which flow from the action potential dome of one site to a close site which has already returned at rest causing in this way its re-excitation and thus the generation of a closely coupled extra-systole. Severe spatial dispersion of repolarization is needed for phase 2 reentry to occur. Because the epicardial action potential is characterized by a pronounced dome, phase 2 reentry tends to occur more frequently in this region. Phase 2 reentry has been theorized, demonstrated and described by Antzelevitch et al.[40] in 1993. In this work, the authors utilized Flecainide (a sodium channel drug) in order to create dispersion of refractoriness in slices of right ventricular epicardial strips (2x1.5x0.2 cm) of dog hearts; epicardial preparations were obtained by razor blade shavings made parallel to the fiber orientation in the right ventricular free wall. Transmembrane potentials were recorded from one or more sites with the use of glass microelectrodes connected to a high-input impedance amplification system. The maximal rate of rise of the action potential upstroke (dV/dt_m, or V_{max}) was measured with a differentiator adjusted for linearity within the range of 50-500V/sec. The duration of the action potential (APD) was measured as the interval between the upstroke and 50% (APD_{50}) or 90% (APD_{90}) repolarization of the action potential. Programmed stimulation was used, with basic cycle lengths (BCL) ranging from 200 ms to 2,000 ms using rectangular stimuli (1-3 ms-duration, 2.5 times diastolic threshold intensity) delivered through silver bipolar electrodes. Premature stimulation (S2) was delivered after every 15^{th} basic beat (S1). The S1-S2 coupling interval was increased progressively from the end of the refractory period. The effective refractory period was defined as the longest S1-S2 interval at which S2 failed to elicit a propagated response. At the epicardial level, after 40 minutes of exposure to flecainide, action potential results characterized by an all-or-none repolarization, loss of the action potential plateau or dome and a marked abbreviation of APD. Loss of the dome in epicardium was usually heterogeneous; while after S1 stimuli all the sites were characterized by loss of dome, after premature stimulation a marked dispersion of repolarization was observed with some sites showing loss of dome and others still showing it. Phase 2 reentries were induced through programmed stimulation in six of nine experiments on epicardial ventricular preparations treated with Flecainide. Electrical heterogeneity in response to flecainide after premature stimulation induced reentrant re-excitation of the tissue. The large voltage gradient that developed between the short and long APD sites could indeed generate significant local

circuit currents that could act to electrotonically depolarize sites exhibiting brief refractory periods, thus effecting reentrant re-excitation of the tissue. Figure 12 shows an example of an induced reentry with the protocol aforementioned; both P and D sites are characterized by the absence of the dome during S1 (due to Flecainide activity). After S2, P site is still characterized by absence of dome, while D site shows a partial dome in trace 1 and a complete dome in trace 2. Reentry occurs in P site when D site shows the complete dome. The lack of a reentrant response after the shorter distal S2 responses (trace 1) may be due to a weaker and briefer electrotonic influence expected under these conditions.

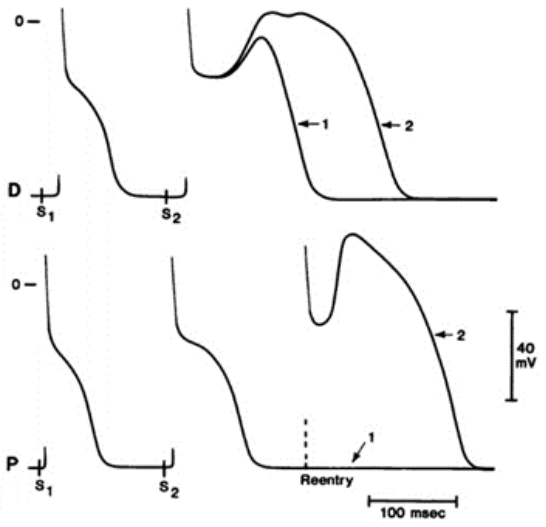

Figure 12. Example of Phase 2 reentry. Transmembrane recordings obtained from proximal (P) and distal (D) sites to thestimulating electrodes in an epicardial preparation exposed to flecainide. Adaptedfrom Antzelevitch et al., 1993.

1.5.5. Repetitive ventricular responses.

Repetitive ventricular responses (RVR) are non-sustained reentrant arrhythmias which can require the participation of both myocardium and conducting system or of the myocardium only. When the circuit includes the conducting system, the UCB tends to be functional and to occur at conducting system level because of its longer refractoriness compared to myocardium. When a premature extrasystole occurs, its wavefront can meet refractory Purkinje fibers close to the origin site of the PVC, then it propagates through myocardium to the opposite ventricle and run across in retrograde direction its conducting system, reaching His bundle. Then, it descends in anterograde direction the Purkinje system of the ventricle, where the PVC originated, completing in this way the reentry. Repetitive ventricular responses have been described for the first time by Akthar et al.[41] in 1974 and have been defined by Akthar[42] in 1981 as "the occurrence of one or more (but less than five) nonstimulated ventricular beats after a paced ventricular premature beat (V2) either during basic atrial (sinus or atrial paced) or ventricular rhythms".

Repetitive ventricular responses have been subdivided in four main categories by Akthar:

1) RVR within the His-Purkinje system also referred to as bundle branch reentry (BBR), where the reentrant circuit incorporates the bundle of His and both the right and left bundle branches. 2) RVR localized to more peripheral areas in the Purkinje-muscle system, also referred to as intraventricular reentry (IVR), local reentry or non-BBR.

3) Atrioventricular nodal reentry.

4) Reentry using retrograde conduction via the accessory and subsequent antegrade conduction over the normal pathway with aberrant intraventricular conduction.

Bundle branch reentry is considered a physiologic phenomenon that occurs in approximately 50% of subjects with normal intraventricular conduction, while IVR is considered an abnormal response.

In his first work on RVR "Demonstration of Re-entry within the His-Purkinje System in Man" Akhtar was able to induce BBR in 15 of 24 patients by means of ventricular programmed stimulation applied at right ventricular apex or outflow tract. During this procedure, the author could register His bundle activity (HBE) through a tripolar electrode catheter positioned in the region of the tricuspid valve while a high right atrial electrogram (HRA) was obtained by means of a quadripolar electrode catheter percutaneously introduced into an antecubital vein and fluoroscopically positioned against the lateral wall of the right

atrium near its junction with the superior vena cava. In addition to intracardiac electrograms, standard ECG leads 1, 2, 3 and V1, were used in this study (Fig.13).

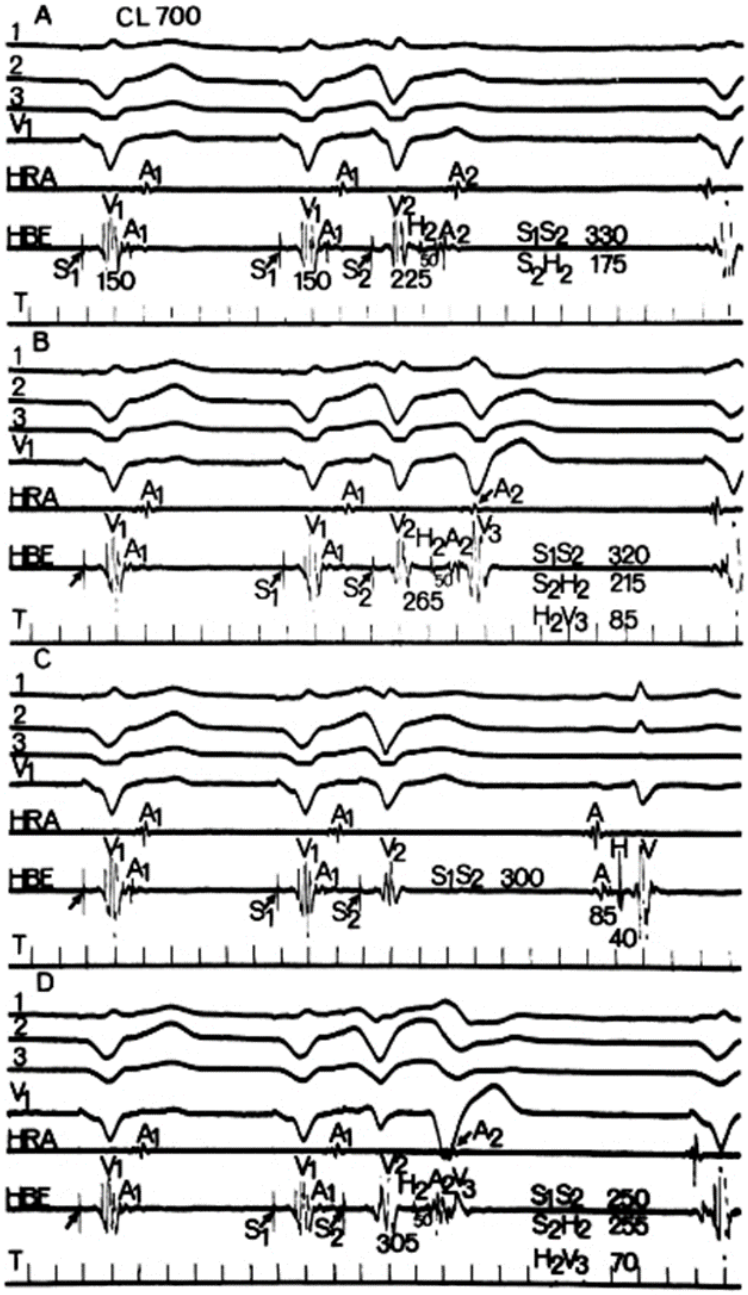

Figure 13. A: example of premature stimulation applied at long S_1-S_2 coupling intervals (330 ms); RVR is not induced. B: example of premature stimulation (S_1-S_2 coupling interval = 320 ms) followed by RVR. C: example of gap phenomenon $_{during}$ premature stimulation (S_1-S_2 coupling interval = 300 ms). D: example of RVR induced at shorter coupling interval (S1-S2 = 250 ms) after gap phenomenon. S1, V1, and A1, represent stimulus artifact, ventricular, His bundle and atrial electrograms, respectively, of the basic ventricular drive beats. S2, V2, H2, and A2 represent stimulus artifact, ventricular, His bundle and atrial electrograms, respectively, of the premature ventricular beats. When BBR occurred, as in panel B and panel D, it was indicated as V3. Reported from Akhtar et al., 1974.

In Fig.13A, the basic ventricular drive (S_1-S_1) is constant at 700 ms, retrograde conduction time to atrium (S_1-A_1) measures 150 ms, S_2 is applied with a coupling interval of 330 ms (S_1-S_2 = 330 ms), S_2 is associated with a retrograde conduction time to atrium of 225 ms (S_2-A_2 = 225 ms), retrograde conduction time to His bundle measures 175 ms (S_2-H_2 = 175 ms), retrograde conduction time from His bundle to atrium measures 50 ms (H_2-A_2 = 50 ms). V_3 was not obtained with this S_1-S_2 coupling interval. The mechanism at the base of the absence of V_3 in panel C and its re-obtaining at even lower S_1-S_2 coupling in panel D is explained by the retrograde gap phenomenon described by Akthar et al.[43]; with the coupling interval S_1-S_2 of 250 ms (panel D), a further delay in the His-Purkinje system, compared to the one of the coupling interval S_1-S_2 of 300 ms (panel C), occurs so that His bundle can recover its excitability and V_3 can occur. V_3 beats obtained in this study resulted characterized by QRS morphology and axis orientation similar to the preceding V_2 but with a QRS duration generally greater than V_2.

Figure 14 of the same work represents the possible events which follow right ventricular stimulation at different coupling intervals.

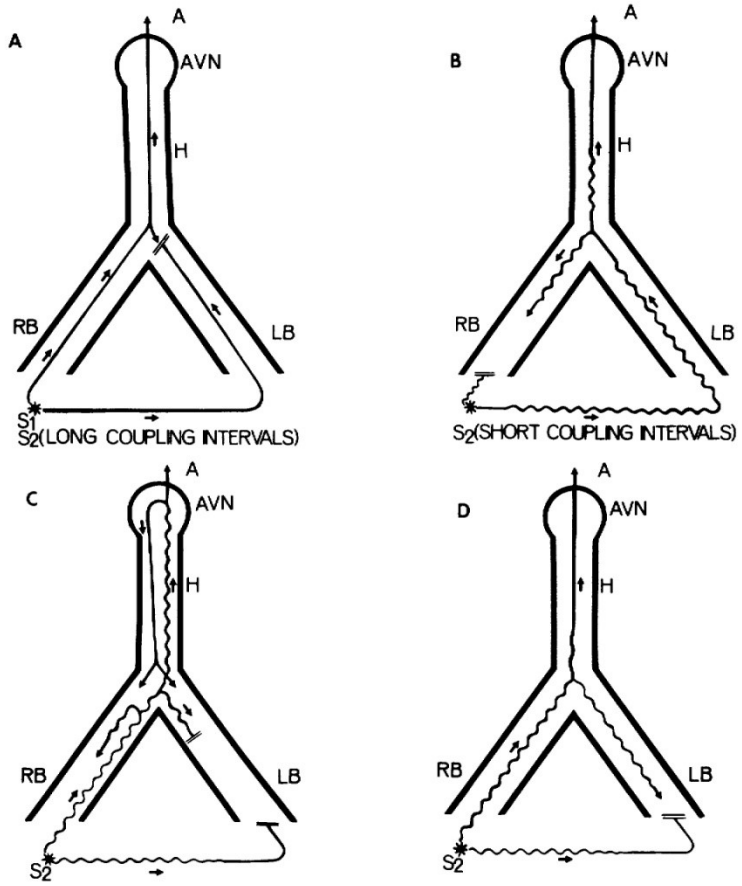

Figure 14. A: Schema of events occurring after right ventricular premature stimulation applied at long coupling intervals. B: Schema of events occurring after right ventricular premature stimulation applied at shorter coupling intervals. C: Schema of RVR occurring due to longitudinal dissociation within the RB or due to reentry at AVN level. D: Schema of BBR occurring when LB presents longer refractoriness compared to RB. A = atrium; AVN = A-V node; H = bundle of His; RB = right bundle branch system; LB = left bundle branch system; S_1 = basic ventricular drive stimulus; S_2 = premature ventricular stimulus. Reported from Akhtar et al., 1974.

In Fig.14A it is shown what happens during S_1 and during S_2 at long S_1-S_2 coupling intervals. Due to the lack of any significant retrograde delay within the His-Purkinje system (HPS) as well as the proximity of the stimulating site to the RB, both of these impulses preferentially depolarize the His bundle via the RB. The same impulse traversing the LB finds the bundle of His refractory. Hence, V_3 cannot occur. In Fig.14B, S_2 is applied at closer coupling intervals and may retrogradely block within the RB or within ventricular muscle-Purkinje fiber junctions because they are still refractory from the preceding basic drive beat (S_1). Depolarization of the ventricular muscle proceeds and the arrival of the S_2 impulse at the LB permits retrograde conduction to the His bundle, after which the impulse is antegradely conducted within the RB. If sufficient time has elapsed to permit recovery of both the RB and ventricular muscle, V_3 can be obtained and will be characterized by a QRS morphology of similar to that of V_1 and V_2. Fig.6C represents V_3 obtained by means of longitudinal dissociation within the RB or due to reentry at AVN level. The latter mechanism of re-excitation of the ventricles can be added to the previous figures (Fig.14A and B) and to the following figure (Fig.14D). The events shown in figure 14 are theoretically possible if the refractoriness of the LB markedly exceeds that of the RB. The premature ventricular impulse (S_2) may therefore block in the left bundle, propagate along the RB and re-excite the LB. In this case V_3 would be characterized by a right bundle branch block (RBBB) QRS pattern. This kind of V_3 was obtained by Akthar in this study only in one patient who had a complete RBBB pattern during sinus rhythm.

Another important work on RVR has been made by Mehdirad et al.[44] in 1994. The purpose of this study was to delineate retrograde His-Purkinje system conduction and reentry during left ventricular extra-stimulation and compare them with right ventricular extra-stimulation. Retrograde and anterograde routes of impulse propagation were determined on the basis of the sequence of His (H) and right bundle (RB) potentials, H-RB intervals, as well as the QRS configuration and axis of V_3 beats. Programmed ventricular stimulation S_1-S_2 was performed at right and left ventricular apexes in all patients and in six patients ventricular extra-stimulation was also applied the left ventricular free wall. During right ventricular extra-stimulation retrograde conduction of V_2 occurred through the LB and the V_3, when induced, resulted characterized by a LBBB QRS pattern. V_3 was induced in 8 of 13 patients; in 7 of them V_3 had a LBBB QRS pattern and therefore retrograde conduction of V_2 must have been through LB. In the last patient, V_3 was induced only at one S_1-S_2 coupling interval and it

showed a RBBB QRS pattern; the route of retrograde conduction could not be determined in this case.

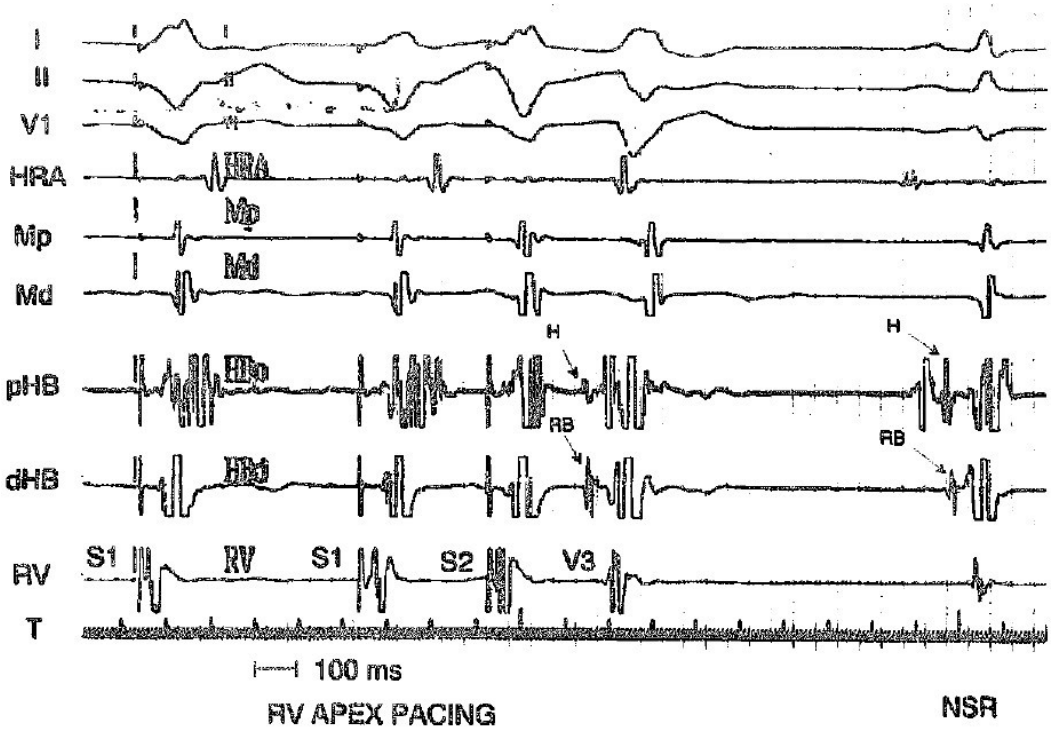

Figure 15. Example of BBR induced during right ventricular premature stimulation showing LBBB QRS pattern. HRA = high right atrium, Mp = recording from proximal electrode pairs in the left ventricular apex of the mapping catheter, Md = recording from distal electrode pairs in the left ventricular apex of the mapping catheter, pHB = proximal His, dHB = distal His, HBp = Right bundle, HBd = Right bundle, RV = right ventricle, T = time, NSR = normal sinus rhythm. Reported from Mehdirad et al., 1994.

Figure 1 of this work, here reported in Fig.15, shows a typical example of V_3 obtained through right ventricular extra-stimulation with LBBB QRS pattern. V_3 induced during right ventricular premature stimulation resulted characterized by LBBB QRS pattern. His bundle results to be activated before than RB and the H-RB interval preceding V_3 is only of 5 ms compared to the H-RB interval preceding normal sinus rhythm. During left ventricular extra-stimulation retrograde conduction of V_2 occurred only through LB. Only one exception occurred during a premature stimulation applied with a coupling interval of 320 ms in one patient; in this case, retrograde His-Purkinje system propagation improved suddenly, and impulse conduction was through RB, as indicated by the RB-H interval which resulted equal but of opposite sequence to the one of sinus rhythm.

Left ventricular extra-stimulation was able to induce V_3 in 5 of 13 patients; in four of them the induced V_3 beats resulted characterized by RBBB QRS morphology (fascicular reentry),

while in the last V_3 resulted characterized by LBBB QRS morphology. In four of five patients in whom V_3 was induced, retrograde conduction of V_2 occurred in LB.

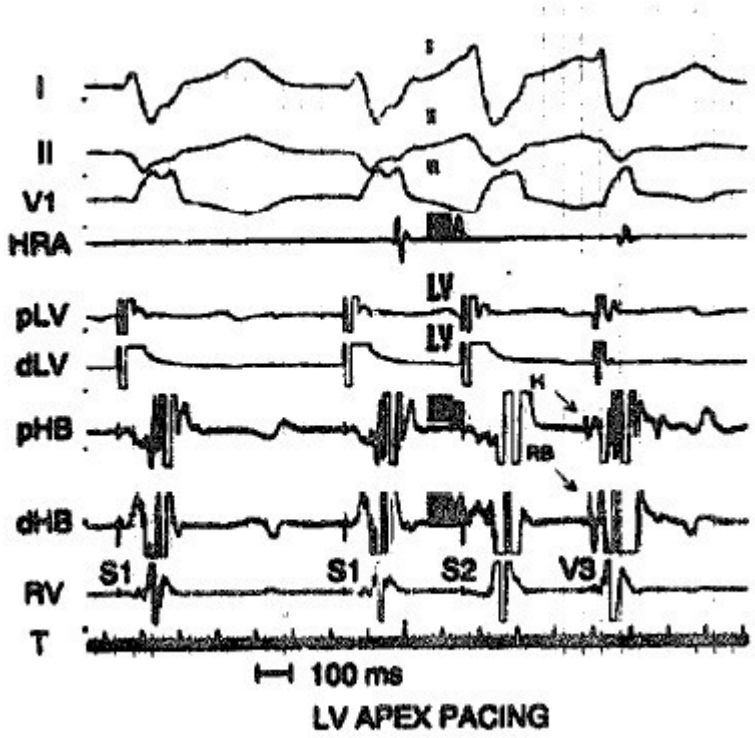

Figure 16. Example of fascicular reentry induced during left ventricular premature stimulation showing RBBB QRS pattern. Reported from Mehdirad et al., 1994.

Figure 2 of the original work, here reported in Fig.16, shows an example of V_3 induced by means of left ventricular extra-stimulation and characterized by RBBB QRS configuration (thus indicating that the anterograde route occurs in the LB) with retrograde conduction of V_2 occurring in the LB (fascicular reentry), as indicated by H-RB activation sequence after the left sided V_2. The results obtained by Mehdirad indicate that LB is the preferred retrograde conduction pathway regardless the site of stimulation; the authors suggest that this preference is due to the shorter retrograde refractory period of the LB compared to RB[45].

In the same work, Mehdirad indicates the existence of three main typologies of RVR described by the following Fig.17.

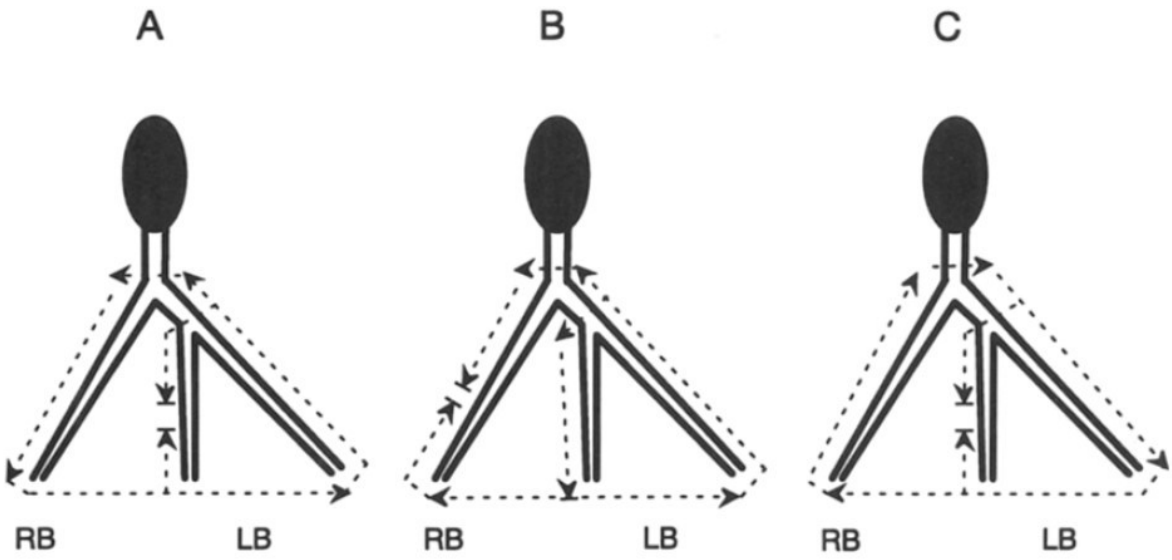

Figure 17. A: Schema of BBR with retrograde conduction through LB and anterograde conduction through RB. B: Schema of fascicular reentry. C: Schema of BBR with retrograde conduction through RB and anterograde conduction through LB. Reported from Mehdirad et al., 1994.

In Fig.17A, retrograde conduction occurs by means of LB and the anterograde conduction through the RB. In this case V_3 would be characterized by a LBBB QRS pattern. This is the most common form of BBR. In Fig.17B, retrograde conduction occurs by means of one of the left-sided fascicles and the anterograde conduction through the other left-sided fascicle (fascicular reentry). In this case, V_3 would be characterized by a RBBB QRS pattern. In Fig.17C, retrograde conduction occurs by means of the right-sided His-Purkinje system and the anterograde conduction through one of the left-sided fascicles. In this case, V_3 would be characterized by a RBBB QRS pattern. Fascicular reentry can be distinguished from BBR with RBBB QRS pattern using the H-RB activation sequence; during fascicular reentry the H-RB interval is shortened or simultaneous, while during BBR with RBBB QRS pattern, RB potential should precede the one of His by an interval similar to the H-RB interval of sinus rhythm.

RVR has been described more recently by Mark Josephson[46] in his book "Clinical cardiac electrophysiology: techniques and interpretations". In this book, the author subdivides RVR in three main categories: BBR, reentry within the A-V node and IVR.

BBR is reported to be the most common form of RVR, occurring in approximately 50% of normal individuals and it is a form of reentry using the His–Purkinje system and ventricular muscle. The mechanism at the base of their induction, explained in this book, is the same pointed out by Akhtar and Mehdirad; during right ventricular stimulation at close coupling

intervals, progressive retrograde conduction block occurs in the RBB such that the retrograde His-bundle activation occurs via the LBB. When a critical degree of retrograde His–Purkinje delay (S_2-H_2) is attained, the impulse can return down the initially blocked RBB to excite the ventricles producing a V_3 characterized by LBBB QRS pattern (Fig.18). In patients with normal hearts, BBR is rarely sustained and usually it is self-terminating in one or two complexes.

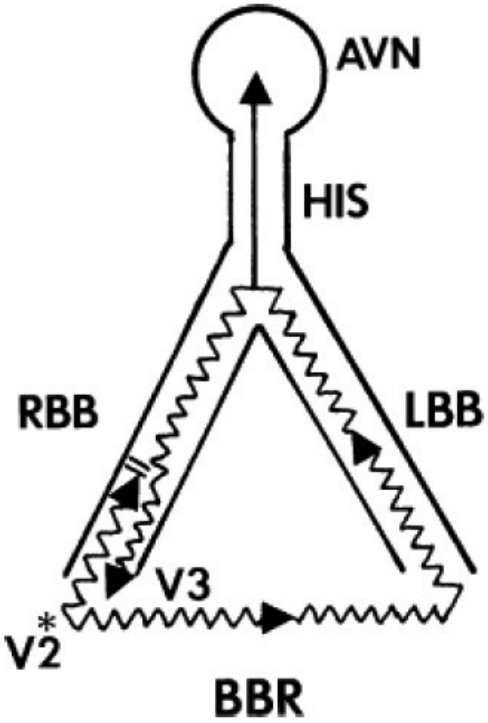

Figure 18. Schema of BBR.
V2 = stimulation site in right ventricle; RBB = right bundle branch; LBB = left bundle branch. Reported from M. Josephson.

The most common reason for failure to sustain BBR is a retrograde block in the LBB system. As shown in Fig.19, BBR is induced only at the S_1-S_2 coupling interval of 230 ms, at which, the retrograde His-Purkinje delay (VH) reaches 165 ms. QRS of the BBR has a LBBB left-axis deviation. At longer S_1-S_2 coupling intervals (250 ms and 240 ms), retrograde His-Purkinje delays are shorter (140 ms and 150 ms) and BBR is not induced. A variant of bundle branch reentry is intra-fascicular reentry which occurs more often in patients with pre-existent complete RBBB and either left anterior or posterior fascicular “block” on the ECG. The fascicular “block” is usually due to very slow conduction. Ventricular extra-stimuli can conduct retrogradely through the slowly conducting fascicle and anterogradely through the “good” fascicle, giving rise to an extra beat that looks almost identical to the (altered) sinus complex.

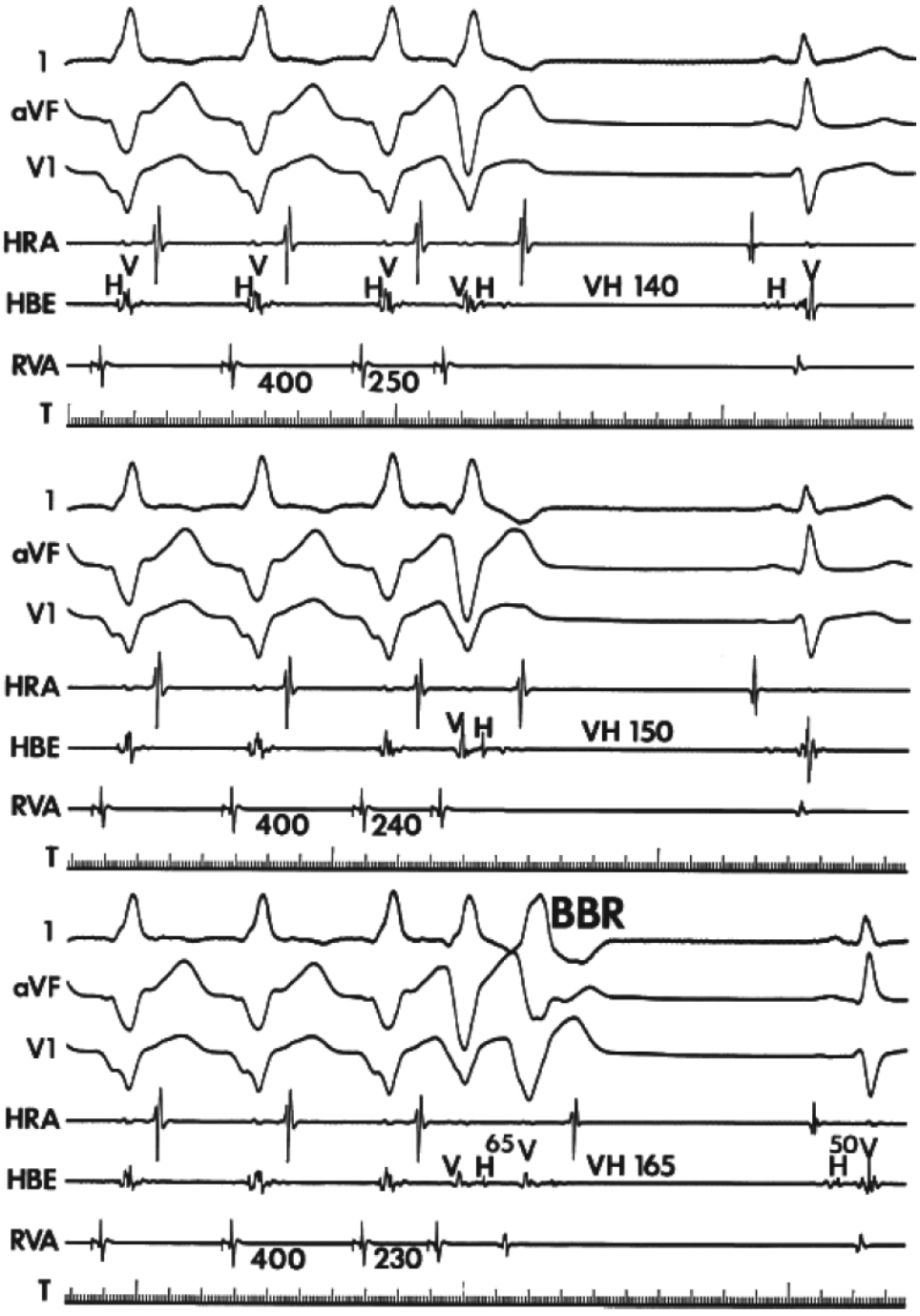

Figure 19. A: example of BBR induction at short S1-S2 coupling intervals. HRA = electrogram from high right atrium; HBE = electrogram from His bundle; RVA = electrogram from right ventricular apex. Reported from M. Josephson.

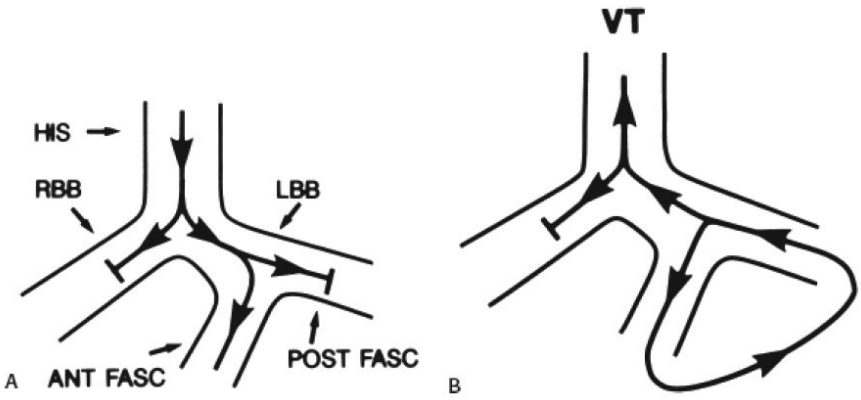

Figure 20. Schema of intra-fascicular re-entry. A: sinus activation in presence of RBBB and fascicular block. B: circuit at the base of ventricular responses in presence of RBBB and fascicular block. RBB = right bundle branch; LBB = left bundle branch. Reported from M. Josephson.

In Fig.20 it is represented, in panel A, sinus activation in presence of RBBB and fascicular block; in panel B it is represented the circuit at the base of ventricular responses in presence of RBBB and fascicular block. In this case the reentrant beat would be characterized by a QRS almost identical to the one of sinus rhythm.

Reentries within the A-V node are reported to be the second most common RVR occurring in normal patients; echo due to reentry within the A-V node occurs in approximately 15% of patients and it appears when a critical degree of retrograde A-V nodal delay is achieved. This kind of ventricular echo is produced by retrograde conduction through the slow pathway and antegrade conduction through the fast pathway of A-V node (Fig.21).

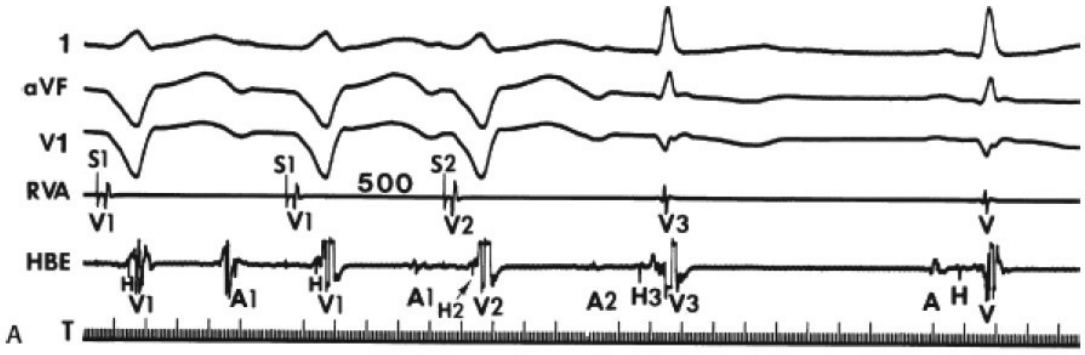

Figure 21. Example of echo due to reentry within A-V node induced by ventricular programmed stimulation. HBE = electrogram from His bundle; RVA = electrogram from right ventricular apex. Reported from M. Josephson.

With critical H2-A2 or V2-A2 (if H2 cannot be seen), an extra beat with a normal antegrade QRS morphology (V3) may be obtained. Atrial activity also precedes the His deflection before the extra QRS complex. This phenomenon may occur at long or short coupling intervals and depends only on the degree of retrograde A-V nodal delay. In the example reported in Fig.21, the basic drive cycle length (S1-S1) is 600 ms. Each S1 is followed by a retrograde His deflection on the basic drive complexes. An S2 is delivered at a coupling interval of 500 ms (S1-S2 = 500 ms) and a retrograde H-A delay occurs (H2-A2 interval is longer than H1-A1 interval). V3 is obtained and it is characterized by a normal QRS (similar to sinus rhythm).

The third type of RVR, reported by M. Josephson, is the IVR; it is reported to occur most often in presence of a cardiac pathologic condition, particularly coronary artery disease with prior infarction. IVRs usually occur at short coupling intervals and are more often characterized by RBBB QRS pattern than LBBB in patients with prior myocardial infarction. In normal patients using single ventricular extra-stimuli at twice threshold, intraventricular reentries occur less than 15% of the time and up to 24% with double extra-stimuli. In patients with prior VT, VF and cardiac disease, IVR occurs in 70% to 75% of instances in response to single or double extra-stimuli.

IVRs are usually non-sustained (1 to 30 complexes), typically polymorphic and in occasional instances they may even degenerate into VF. In patients without prior clinical arrhythmias, such responses have not been found to have clinical significance. IVRs should be considered “normal” responses and should not be treated in patients with normal hearts and no clinical ventricular arrhythmias.

Contrary to what happens for BBRs, IVRs do not require V-H prolongation for their occurrence; IVR can occur in absence of retrograde His potentials, or with His potentials with an H-V interval less than that observed during sinus rhythm. In contradistinction to BBRs, IVRs, frequently have a QRS configuration distinctly different from that of the S_2. IVRs have been described in detail in a clinical study of A. Farshidi et al.[47] in 1980. In Fig.22 it is reported an example of IVR (V_4) obtained through double premature stimulation in the right ventricle; basic cycle length was of 600 ms (S_1-S_1 = 600 ms); S_2 was delivered with a coupling interval of 250 ms (S_1-S_2 = 250 ms), while S_3 was delivered with a coupling interval of 180 ms (S_2-S_3 = 180 ms). Stimuli were applied at twice diastolic threshold and were of 1 ms in duration. IVR is characterized by a different QRS pattern compared to paced complexes.

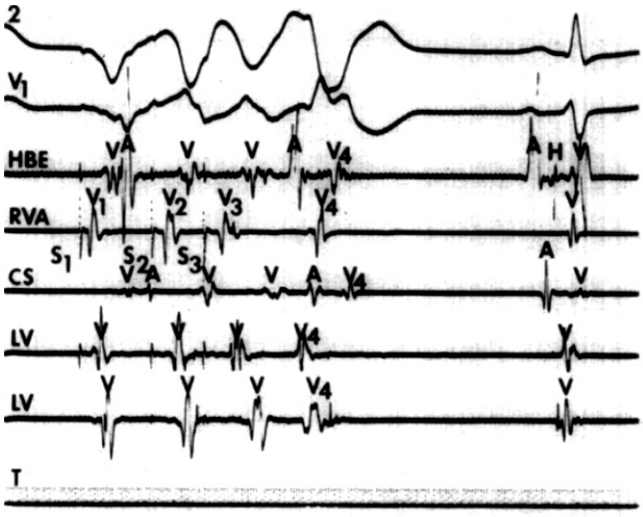

Figure 22. Example of IVR (V_4) following double extra-stimulation (S_1-S_2-S_3) applied in the right ventricle. 2 = surface electrogram; V1 = surface electrogram; HBE = intracardiac electrogram from His bundle; RVA = intracardiac electrogram from right ventricular apex; CS = intracardiac electrogram from coronary sinus, LV = electrogram from left ventricle (LV); T = timeline. Reported from A. Farshidi et al., 1980.

In Fig.23 it is reported an example of VT induced by double premature stimulation in the right ventricle; double premature stimulation was applied, in the same patient, with the same characteristics described previously in relation to Fig.22. In this case IVR is followed by a short run of VT. IVR (V_4) of Fig.23 is identical to the IVR of Fig.22 and very similar to the other VT complexes.

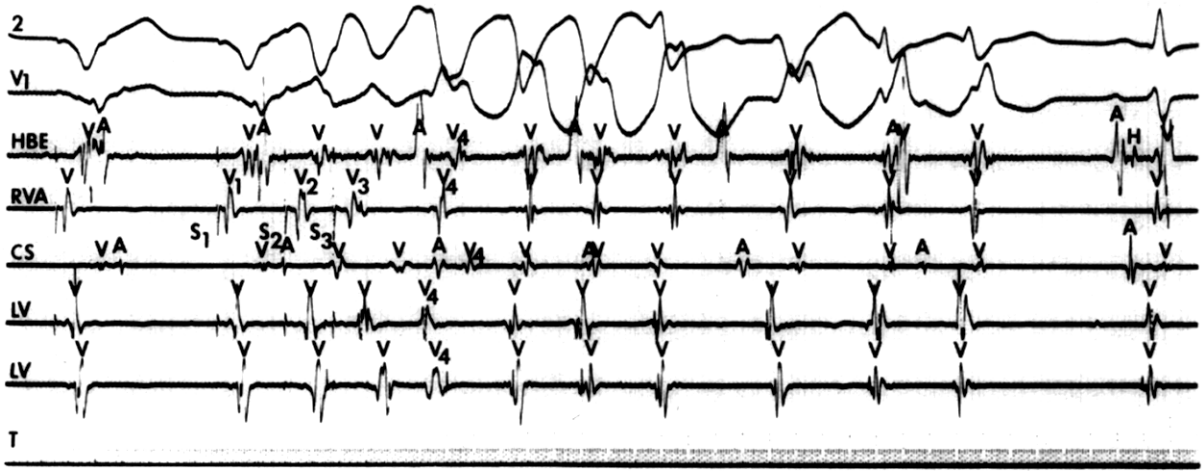

Figure 23. Example of VT induced by means of double extra-stimulation (S_1-S_2-S_3) applied in the right ventricle. 2 = surface electrogram; V_1 = surface electrogram; HBE = intracardiac electrogram from His bundle; RVA = intracardiac electrogram from right ventricular apex; CS = intracardiac electrogram from coronary sinus, LV = electrogram from left ventricle (LV); T = timeline. Reported from A. Farshidi et al., 1980.

1.6. Conducting system properties

The conducting system is a specialized system which allows impulse propagation from the atrioventricular (A-V) node to ventricular muscle. It is composed by the bundle of His, right and left bundle branches, peripheral ramifications of the branches, and subendocardial Purkinje network. Recordings of transmembrane action potentials from single cells with intracellular microelectrodes have shown that action potential durations in the conducting system increase from the bundle branches distally up to an area of maximum action potential duration, localized about 2 mm proximal to the termination of Purkinje cells in muscle, and then the durations progressively decrease through a sequence of Purkinje cells, transitional cells, and muscle cells. Because of recording of transmembrane action potentials from single cells with intracellular microelectrodes has shown that the refractory period of individual cells after a depolarization is primarily related to the duration of the action potential so that the refractory period is prolonged as the duration of the action potential increases, the refractory period at different levels of the conducting system follows the action potential duration trend showed in Fig.24.

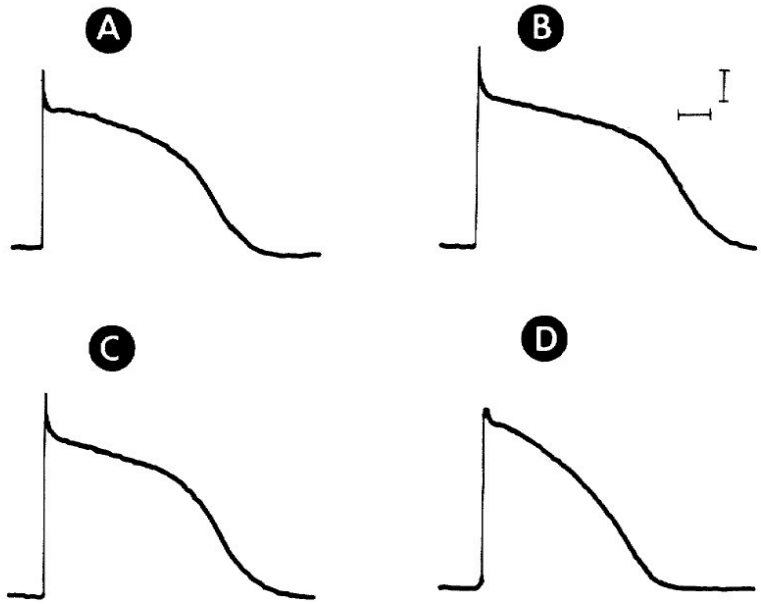

Figure 24. Action potential durations at the following levels: bundle branch (A), the area of maximum action potential duration (B), conducting tissue in the subendocardium distal to the area of maximum action potential duration (C), muscle cell in the free wall of the ventricle (D). Reported from J. Myerburg, 1971.

Thus, the area of maximum action potential duration is also the area having the longest local refractory period. Because of these functional properties, the area of maximum action

potential duration can act as a gate, determining the minimum possible coupling interval between a driven impulse and a premature impulse that allows conduction from bundle branches to terminal Purkinje fibers and muscle cells and vice versa. All this has been experimentally demonstrated in the dog heart by Myerburg[48].

Fig.25 shows at the top a scheme of the preparation used by Myerburg, which consists of a single free-running false tendon from RBB to the FWRV; in the middle section, the graph demonstrates that the changes in APD along the length of the preparation are paralleled by changes in RP. From RBB there is a progressive increase in APD and RP to a maximum of 290 ms, followed by a sharp fall up to the FW.

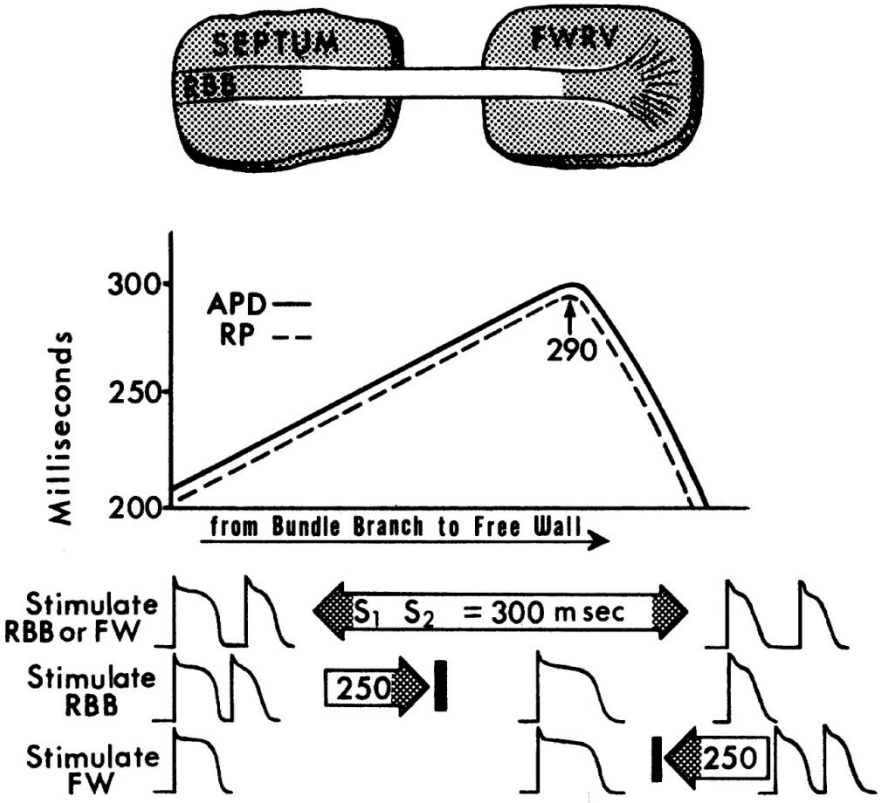

Figure 25. Demonstration of the gating mechanism. APD = action potential duration; RP = refractory period; RBB = right bundle branch; FW = ventricular free wall; FWRV = free wall of the right ventricle. Reported from J. Myerburg, 1971.

As it is shown in the lower section of the figure, because the RP in the maximum APD area (gate area) measured 290 ms, when a premature stimulation with a coupling interval of 300 ms was applied at RBB level or at FW level, conduction could occur through the gate area.

At the opposite, when the premature stimulation was applied with a coupling interval of 250 ms, the impulse could not be conducted through the gate area and remained confined in the side of stimulation.

In accordance with Fig.26, following the gate system principle, the conducting tissue from the HB through the distal gates has progressively lengthening refractory periods and then, after the distal gates, it has progressively shortening refractory periods.

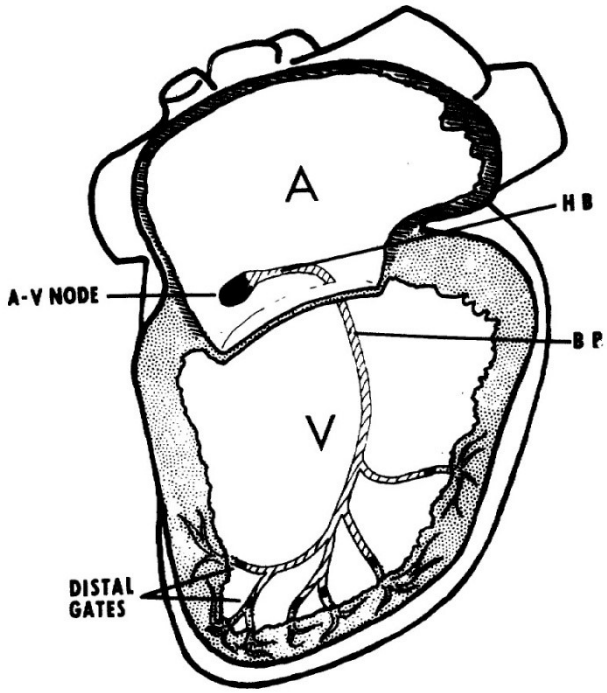

Figure 26. Scheme of the gating system of the conducting system. A = atrium; V = ventricle; HB = His bundle; BB = bundle branch. Distal gates are shown in black. Reported from J. Myerburg, 1971.

1.7. Electrotonic current.

The electrotonic current is essential for the propagation of the action potential in the myocardium. Considering two contiguous regions, when an action potential develops in one of the two regions while the other remains at rest, a spatial transmembrane potential gradient ΔVm is established. Such potential gradient involves the development of an intracellular current Ii from the activated region to the region at rest (according to Ohm's law, $\Delta V = IiRi$, where ΔV is the potential, Ii is the intracellular current and Ri is the intracellular resistance). The variation in the space of this intracellular current is the outgoing electrotonic transmembrane current $i_m = \Delta Ii$, which determines a depolarization in the region at rest, favoring the reaching of the threshold and therefore the propagation of the action potential. It also plays an important role in the modulation of the repolarization process, resulting in a slowing down of the aforementioned process in physiological conditions. In this case, considering two contiguous regions, one in repolarization and the other in depolarization, a potential difference arises between the two regions. Such potential difference involves the development of an intracellular current from the depolarized region to the repolarizing region. The spatial variation of this intracellular current is the outgoing electrotonic current in the region under repolarization. In a repolarizing region, an outgoing (and therefore depolarizing) electrotonic current slows down the repolarization process.

Electrotonic current has been described in depth[49-50-51-52-53-54]. From a biophysical point of view, the electrotonic current (i_m) is a transmembrane current equal to the sum of the capacitive current (i_c) and the resistive current (i_{ion}). The i_c is a displacement of ionic charges on either side of cell membrane without movement across the membrane. For an ion deposition on one side of the membrane, an ion withdrawal of the same sign occurs on the opposite side. Consequently, it is a current that does not require channels.
From a physical point of view, $i_c = c_m \times \partial V_m / \partial t$. In the reported equation, c_m is the membrane capacitance per unit length of the cell, V_m is the membrane potential; V_m is the difference between the intracellular potential (V_i) and the extracellular potential (V_e). Hence, $V_m = V_i - V_e$. The i_{ion} consists of ions that physically cross membrane ion channels; it is resistive, through passive ion channels, and active through voltage-gated, ligand-gated or mechanosensitive ion channels. The i_{ion} is physically defined by the following equation: $i_{ion} = g (V_m - E)$. In the reported equation, g is the conductance of the ionic species taken into consideration ($g = 1/r$), E is the equilibrium potential of the same ionic species taken into consideration.

E is defined by Nernst equation, and it is the membrane potential at which an ionic species would reach its thermodynamic equilibrium and would stop moving across the membrane.

$$E = \frac{RT}{zF} ln \frac{[ion\ outside\ cell]}{[ion\ inside\ cell]}$$

In Nernst equation, R is the ideal gas constant, T is the temperature in kelvins, z is the charge of the ion taken into consideration, F is Faraday's constant.

In accordance with Ohm's law, changes in V_i per unit length equal the axial intracellular current (I_i) times resistance/unit length.

For the same law, changes in V_e per unit length equal the axial extracellular current (I_e) times resistance/unit length.

Consequently, $I_i = -1/r_i \times (\partial V_i/\partial x)$ and $I_e = -1/r_e \times (\partial V_e/\partial x)$.

In the reported equations, r_i is the intracellular axial resistance per unit length, r_e is the extracellular axial resistance per unit length, and ∂x is the axial variable.

Current flows following the potential gradient, from higher to lower potential values.

When part of I_i crosses the membrane, then the axial decrease is initially transformed into I_m and then I_e increases.

Because of charge conservation physical principle, the changes in axial current per unit length must precisely equal the transmembrane current per unit length.

Consequently, $I_m = -\partial I_i/\partial x = \partial I_e/\partial x$.

Deriving twice both members of $V_m = V_i - V_e$, it is possible to obtain the following equation defining I_m: $I_m = 1/(r_i+r_e) \times (\partial^2 V_m/\partial x^2)$.

To summarize, the electrotonic current is a transmembrane current with depolarizing action when outgoing.

Physiologically it has two fundamental roles:

1) it allows the propagation of the action potential, determining the achievement of the threshold in the region at rest, ahead of the wave front.

2) it slows down the repolarization process, behind the wave front.

In less physiological conditions such as in the presence of a reversible functional UCB it is able to speed up the repolarization process at the proximal side of UCB, such as at a ventricular Purkinje-muscle junction (PMJ). This effect could promote arrhythmias in critical

conditions. This was experimentally proved by Mendez[50]. The lower panel, of the Fig.27, shows schematically the preparation used by Mendez in his experiment; the experimental preparation involved the use of the anterior papillary muscle (which provides muscle fibers) of a dog's right ventricle and a connected false tendon (which provides Purkinje fibers).

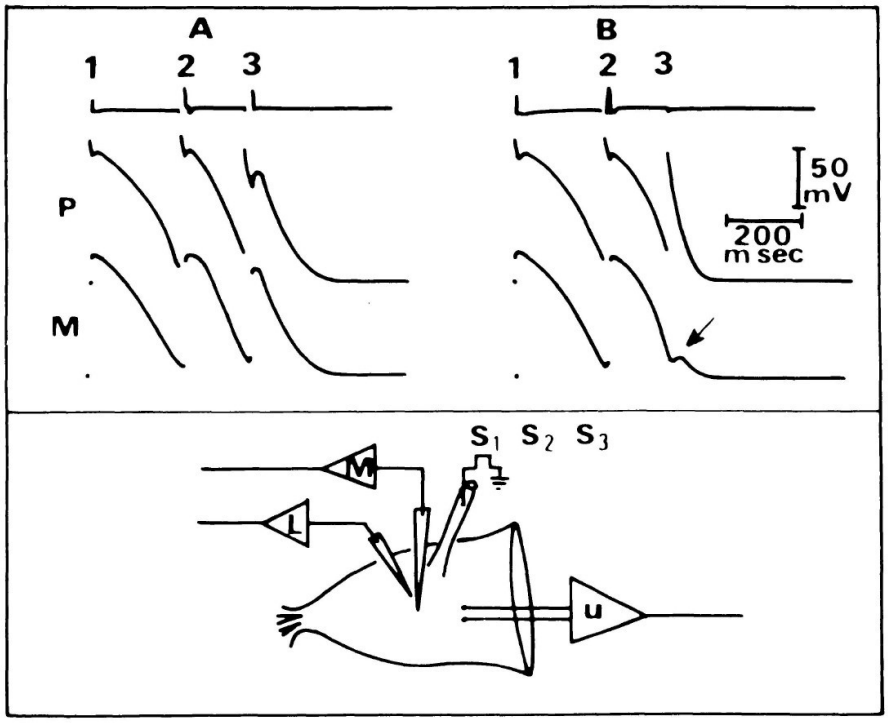

Figure 27. Experimental demonstration of repolarization shortening effect of electrotonic current. In the superior figure: P = Purkinje fiber, M = muscle fiber. In the inferior figure: L = transmembrane potential of a muscle fiber, M = transmembrane action potential of a terminal Purkinje fiber, U = bipolar electrogram. Reported from C. Mendez, 1983.

In such experimental preparation, extracellular electrodes were used to obtain bipolar electrograms of papillary muscle activity (upper trace in superior figure), intracellular microelectrodes were used to obtain transmembrane action potentials of a terminal Purkinje fiber (middle trace in superior figure) and of a neighboring muscle fiber (lower trace in superior figure). Double premature stimulation (S_1-S_2-S_3) was applied at false tendon level.
In panel A, the shortest S_2-S_3 coupling interval capable of evoking a response at muscle level was used; hence, both Purkinje and muscle fibers were able to respond actively to S_3.
In panel B, a shorter S_2-S_3 coupling interval was used and S_3 failed to evoke a response in the muscle fiber. Correspondingly, Purkinje fiber resulted to be characterized by an extremely brief action potential. Mendez explained these results in this way: when UCB takes place in cardiac tissues, a marked potential difference is established between the proximal active

segment and the inactive distal inactive region. Consequently, local circuits are generated that supply insufficient electrotonic currents to depolarize the distal region (outward electrotonic current) whose membrane remains polarized at resting potential (source-sink mistmatch). Hence, the same current returns at the extracellular level to the active region. At this level it acts as an external anode causing an acceleration of the repolarization process (inward electrotonic current). The drastic shortening of the action potential in Purkinje fibers can promote the development of reentries. This was experimentally demonstrated by Mendez in an experiment conducted on a preparation very similar to the one just described (Fig.28).

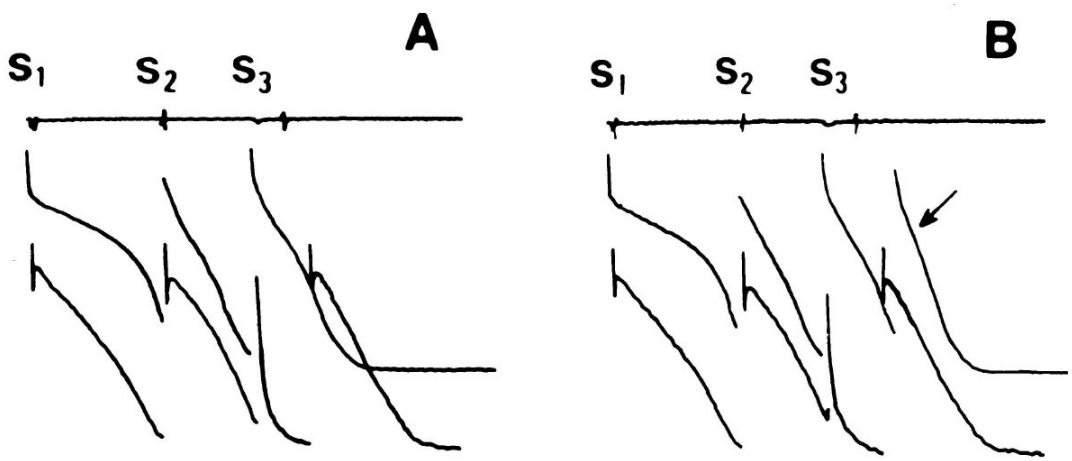

Figure 28. Examples of abortive reentry (A) and of complete reentry (B) in a canine right anterior papillary muscle preparation. Upper trace = bipolar electrogram (indicating global activity of papillary muscle); middle trace = transmembrane action potential of a Purkinje fiber in the false tendon; lower trace = transmembrane action potential of a terminal Purkinje fiber. S_1, S_2 and S_3 were applied at false tendon level. Reported from C. Mendez, 1983.

In panel A it is reported an example of partial reentry induced by S_3 premature stimulation; as it is visible, from the figure here reported, S_3 was able to activate the Purkinje fiber in the false tendon and the terminal Purkinje fiber but it was not able to activate the corresponding muscle junction (as indicated by the extremely brief action potential of the terminal Purkinje fiber). However, at other junctions propagation to the muscle occurred (as indicated by bipolar electrogram). The muscular activity reached the terminal Purkinje fiber which was able to respond again with an action potential (because its previous action potential had been extremely brief). The returning impulse was anyway unable to activate anew the Purkinje in the false tendon. In panel B, however, complete reentry took place as indicated by the arrow.

2. Materials and Methods.

2.1. Ethical Statement, Animal Preparation, and Outline of the Experimental Protocol.

The study was conducted in conformity with the American Physiological Society guiding principles in the care and use of vertebrate animals in research and training. The protocol was submitted to and approved by the Veterinary Animal Care and Use Committee of the University of Parma and adheres to the National Ethical Guidelines of the Italian Ministry of Health. All surgery was performed under anesthesia. Rats used in this study (Rattus norvegicus, wild-type Groningen) were obtained from the University of Groningen (Groningen, The Netherlands) and bred in our animal care center under conventional conditions. Studies were performed on the in-situ heart of 17 healthy rats, which were anesthetized with ketamine chloride (Imalgene; Merial, Milan, Italy; 50 mg/kg ip) plus medetomidine hydrochloride (Domitor; Pfizer Italia, Latina, Italy; 0.4 mg/kg ip). Under artificial respiration, the heart was exposed through a longitudinal sternotomy and suspended in a pericardial cradle. Body temperature was maintained constant at 37°C with infrared lamp radiation.

2.2. Epicardial Mapping

In order to investigate ventricular vulnerability to arrhythmia, unipolar epicardial potentials were measured in 17 normal rats by means of a 64-electrode array with electrodes placed at a distance of 1 mm from each other. In the 17 experiments the total points of stimulation were 57. In the present study, 8 x 8 row and column electrode arrays, with 1-mm-resolution square mesh covering an area of 49 mm^2, were fabricated on surgical cotton gauze and used. In addition to the 64 electrodes, used to record the extracellular unipolar potential, 4 outermost electrodes were used at the end of each experiment to apply burns on the epicardial surface. The four burns were applied to allow the identification of the epicardial grid position for histological investigation of the underlying ventricular wall (Fig.29).

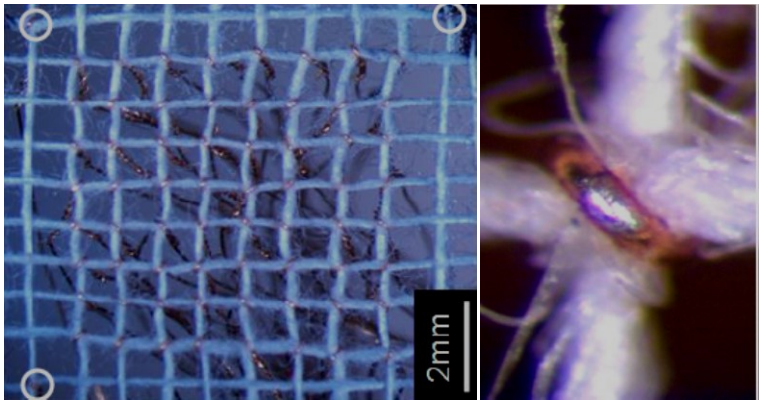

Figure 29. Left Panel: Photography of an electrode array. The three white circles identify three of the four electrodes used to apply the burns at the end of the experiment. Right panel: Photography of one of the 64 silver electrodes of the array. Note that only the portion that comes into contact with the epicardial surface is deprived of the insulating coating.

The gauze moistened by the thin liquid layer adhered firmly to the epicardium, and all electrodes made a stable contact (Fig.30).

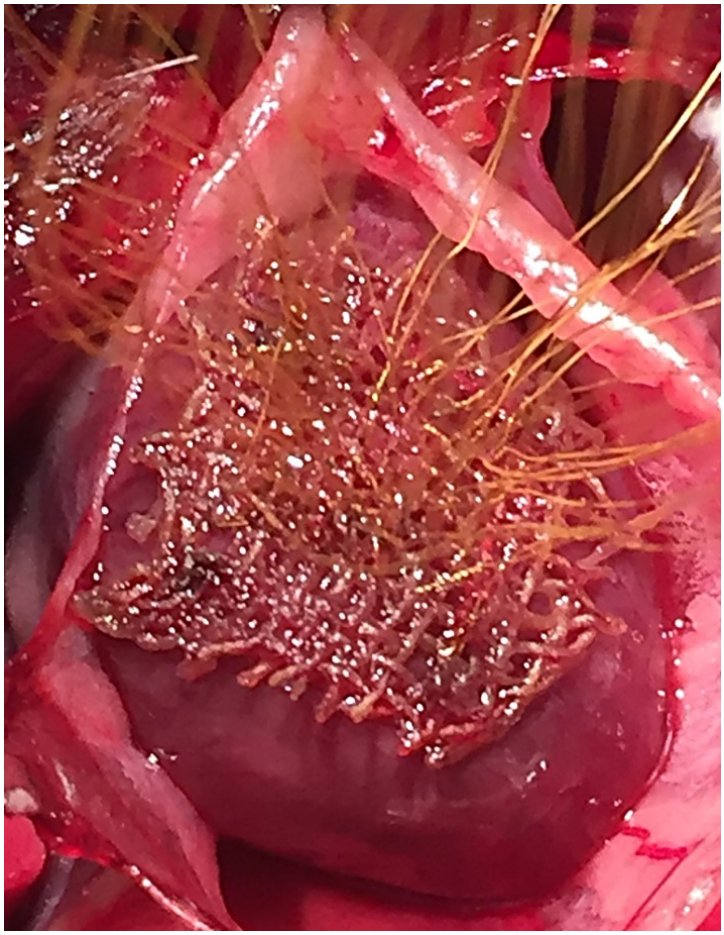

Figure 30. Photography of an array positioned on the epicardium of rat heart. Note that in this case (experiment of 04 August 2017) the grid covered a large portion of the anterior surface of the right ventricle, the epicardial projection of the septum and a smaller part of the left ventricle.

At the end of cardiac mapping, animals were euthanized and the epicardial position of the electrode array was identified by fiducial marks (Fig.31).

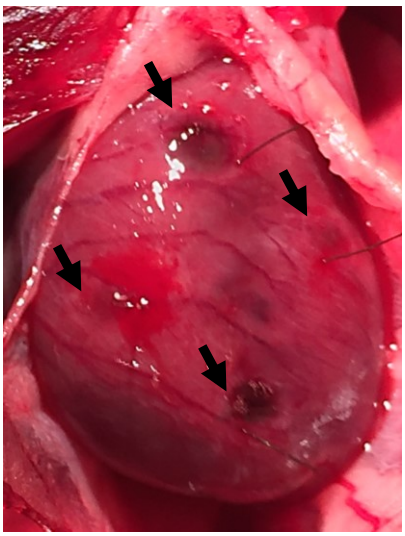

Figure 31. Photography of the four burns (indicated by the black arrows) applied at the end of the experiment (of 04 August 2017).

The high-resolution epicardial electrode array was used to stimulate through one of the electrodes (test site) and for unipolar potential recording from all other electrodes around the test site. In 14 of 17 experiments one or two endocardial electrodes were used to stimulate the endocardium and in this case all the electrodes of the grid were used to record unipolar epicardial potentials. Subendocardial pacing was performed via a 50 μm diameter silver wire that was insulated except at the tip. The wire was threaded through a 25-gauge needle (0.51-0.26 mm) with the tip of the wire bent to form a 1-2 mm barb and inserted through the ventricular wall with the needle (Fig.32). The needle was then removed and the wire pulled back to anchor on the endocardium (Fig.32). Electrical stimuli were given through the wire from a constant current source, controlled by a stimulator.

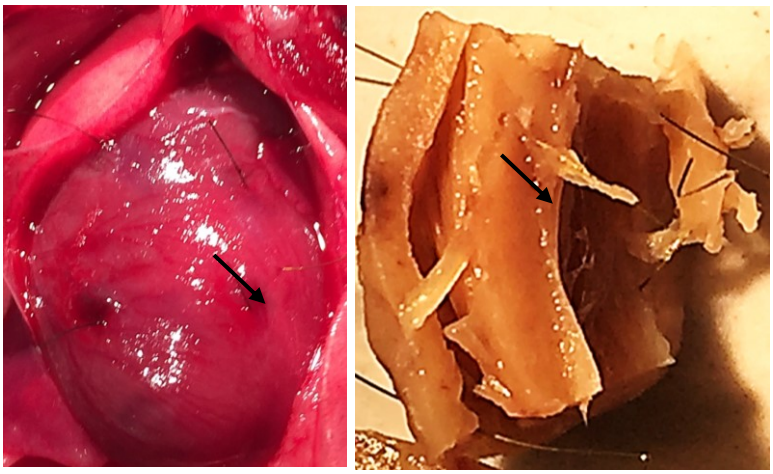

Figure 32. Left Panel: Photography of the insertion point of the endocardial pacing electrode (indicated by the black arrow) inserted into the left ventricle. Right Panel: Photography of the attachment point at the endocardial surface of the intracavitary electrode (indicated by the black arrow) inserted into the left ventricle (experiment of 26 July 2017).

In each experiment, unipolar epicardial electrograms (EGs) were simultaneously recorded differences between each electrode of the array, and a common reference electrode placed on the left hind leg, during SR and ventricular stimulation. The ground electrode was inserted subcutaneously into the right hind leg. Electrodes were connected to alternating current (AC)-coupled, variable-gain differential amplifiers of a 256-channel mapping system. The entire set of unipolar EGs was continuously monitored on an analog oscilloscope screen during recording sessions for quality control. Data were recorded at a bandwidth of 0.03–500 Hz, input impedance of 10^{12} Ω, and sampling rate of 1 kHz/channel. No additional filtering was used to avoid EG waveform distortion. During stimulation protocol, from a few seconds to a few minutes recordings of digitized EG waveforms with 12-bit resolution were sequentially stored on hard disk at the overall rate of 256 kHz. However, continuous data recording, up to several minutes, was occasionally performed during prolonged ventricular stimulation to capture repetitive and sustained arrhythmic events. Spatial distributions of EGs, instantaneous unipolar potentials (isopotential maps), and activation times (isochrone maps) were displayed off-line for data quality control and analysis by means of custom-written software. EG waveforms were interpreted in terms of biophysical principles underlying the interaction between the geometry and direction of propagation of the wave front and the architecture of the fibers through which electrical excitation was spreading.

2.3. Ventricular Stimulation

Unipolar stimulation at ventricular epicardial or endocardial test sites was performed from one of the array electrodes with a battery-powered constant current (CC) stimulator (biphasic stimulator, model 301; Crescent Electronics, Sandy, UT), which provided square wave current pulses of variable duration (from 10 μs to 10 ms) and strength (from 1 μA to 10 mA), or from an electrode external to the grid and placed in ventricular cavity. The CC stimulator was triggered at a cycle length (CL) set by a programmable four-channel biomedical stimulator (model 425; Crescent Electronics). The negative pole (cathode) of the CC stimulator was connected to test site electrode while the positive pole (anode) was set to an indifferent electrode placed subcutaneously in the chest wall, close to the heart. In the present study, pulse strength was varied within the intensity range of the CC stimulator, while pulse duration was always kept constant at 1 ms.

2.4. Diastolic Stimulation Threshold

Diastolic stimulation threshold at each test site was determined by applying cathodal current pulses at a CL slightly shorter than SR for ventricular capture according to the following protocol. Current strength was initially set to a value above diastolic threshold. Next, current strength was decreased by 10- μA steps until capture was lost and successively increased by 2- μA steps until capture was resumed. Diastolic stimulation threshold was defined as the minimum current strength required to induce at least one propagated response during a 6-s drive interval.

2.5. Stimulation protocols

Two premature stimulation protocols were used, RW-S and S1-S2.

RW-S protocol consists of a sequence of 8 sinus beats followed by a premature stimulation (S) applied at a variable coupling interval after the R wave (RW) of the QRS of the last sinus beat.

Figure 33. Example of premature stimulation applied during sinus rhythm. The coupling interval between the R wave of the sinus complex and the premature stimulation was of 75 ms. RW = R wave of sinus QRS complex; PS = premature stimulation.

S1-S2 protocol consists of a train of 8 induced beats at constant time distance (S1) followed by a premature stimulation (S2) applied at variable coupling interval after the last S1 stimulus (Fig.34).

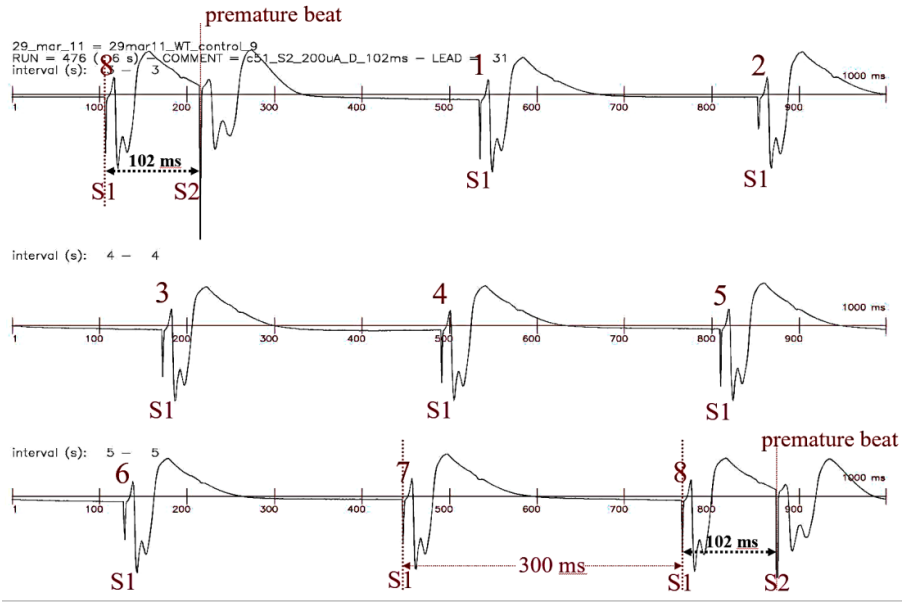

Figure 34. Example of premature stimulation (S2) applied during paced rhythm (S1). S1-S1 coupling interval was of 300 ms, S1-S2 coupling interval was of 102 ms. Note that premature beat is characterized by a larger QRS (compared to S1), indicating a slower conduction due to relative refractoriness.

During RW-S protocol, stimulation strength was gradually increased from 100 µA to 1 mA with steps of 100 µA and from 1 mA to 10 mA with steps of 1 mA; for each stimulation strength, RW-S coupling interval was gradually decreased with steps of 10 msec from 150 ms until the myocardium was not enabled to respond. Subsequently RW-S coupling interval was gradually increased with steps of 2 ms to reach ERP.

In S1-S2 protocol, S1 stimuli were applied with a strength twice the diastolic stimulation threshold, S2 stimulus was applied with a strength four times S1, i.e. 8 times diastolic stimulation threshold. S1-S2 coupling interval was gradually decreased from 150 ms, with steps of 10 ms, until capture was lost, and then gradually increased with steps of 2 ms until capture was resumed. To characterize myocardial activation above ERP, the RW-S coupling interval and the S1-S2 coupling interval were increased by 2 ms steps from ERP to ERP + 6 ms. In both protocols, in case of arrhythmia or fibrillation at any given strength and interval, further stimulations at higher or lower coupling intervals of 2, 3 or 5 ms were repeated, in order to define with precision the arrhythmia vulnerability time window.

2.6. Effective Refractory Period.

To To obtain a measure of the tissue refractoriness within the mapped area, ERPs were determined through S1-S2 and RW-S protocols; with S1-S2 protocol ERPs were measured only once at 8 times diastolic stimulation threshold intensity at each electrode site of stimulation (Fig.35).

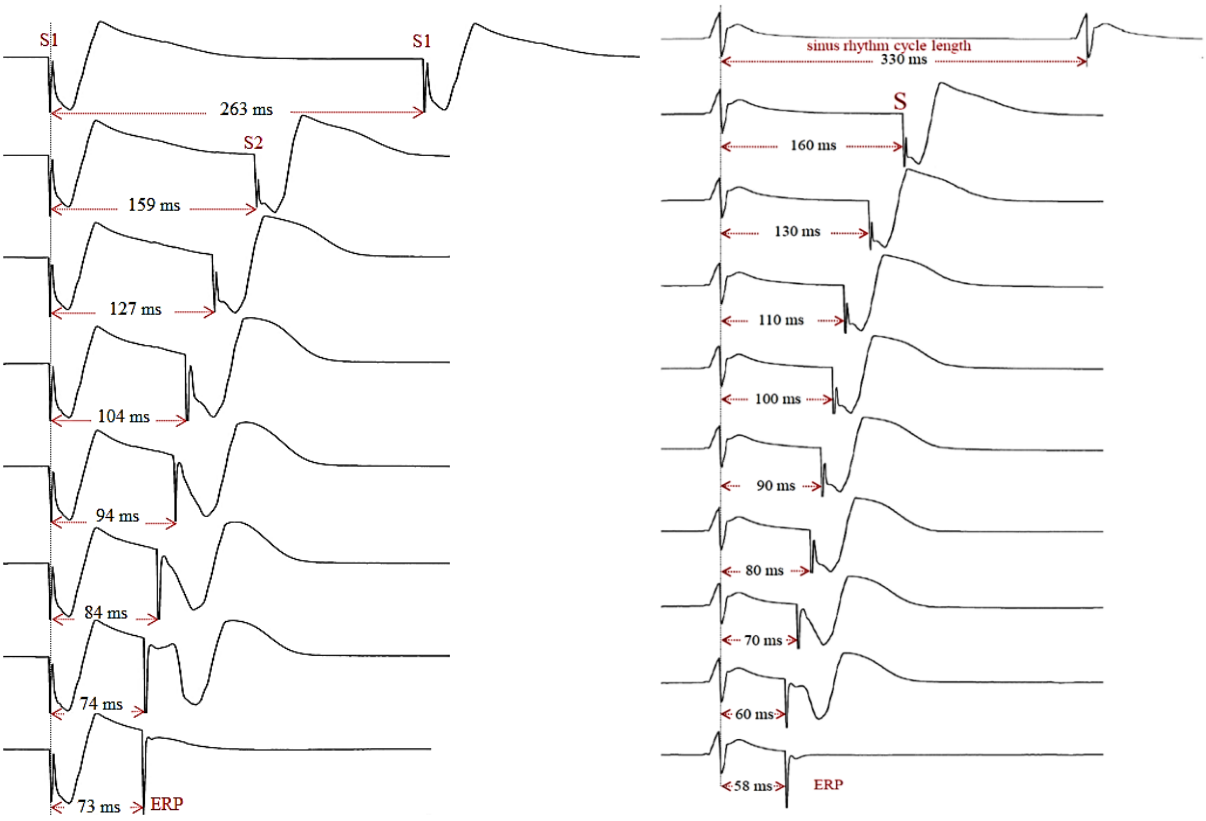

Figure 35. Left Panel. Example of ERP measurement using S1-S2 premature stimulation protocol. Note that from 159 ms to 104 ms of coupling interval, tissue responds without response latency to the premature stimulation. At the coupling intervals of 94 ms and 84 ms, premature beats begin to show response latency and a weaker intrinsic deflection; at the coupling interval of 74 ms, response latency increases further. At 73 ms of coupling interval, premature stimulation is not followed by a propagated muscular response, indicating ERP was reached. Right Panel. example of ERP measurement using RW-S protocol. Note that from 160 ms to 80 ms of coupling interval, tissue responds without response latency to the premature stimulation. At the coupling interval of 70 ms, premature beat begins to show latency and a slower intrinsic deflection; at the coupling interval of 60 ms, latency increases further. At 58 ms of coupling interval, premature stimulation is not followed by a propagated muscular response, indicating ERP was reached.

With RW-S protocol, ERPs were measured at each intensity of stimulation at each test site. The coupling interval between sinus beat and premature stimulation was obtained as follows. The programmable stimulator operated in external trigger mode with its master clock set to sinus rhythm by a reference EG signal R wave (RW) fed to its internal Schmitt trigger

comparator circuit. In turn, the programmable stimulator was set to sense eight successive R waves and to trigger the CC stimulator after a selectable delay interval from the eighth R wave. Right after, the programmable stimulator was inhibited for a sufficiently long time interval to avoid being re-triggered by the T wave of the premature response. The procedure allowed for a reliable R wave-premature stimulation coupling interval to be set for premature stimulation during sinus rhythm. ERP was defined as the longest R wave-premature stimulation coupling interval failing to generate a propagated response during a 6-s time interval. Since ERP durations were measured at each test site by using the R wave amplitude threshold of the same reference EG, true local ERP duration was computed off-line as the interval between sinus beat activation time at that test site and successive premature stimulation onset.

2.7. Strength Interval Plane.

S-I planes were obtained for a total of 57 ventricular test sites in 17 rats. For each test site, S-I planes reported graphically ERPs and all stimulation responses obtained through RW-S and S1-S2 protocols. In the S-I plane, the abscissa represents RW-S or S1-S2 coupling intervals and the ordinate the corresponding stimulation strength. Consequently, each S-I point is therefore univocally identified by its strength and coupling interval. In each S-I plane multiple parameters and events were displayed. Specifically, parameters and events shown in each S-I plane are ERP, response latency and UCB, bundle branch reentries (BBRs), non-sustained intraventricular reentries through the terminal Purkinje system (IVR-P), non-sustained intraventricular figure 8 reentries (IVR-M), ventricular tachycardias (VTs), ventricular fibrillations (VFs). For each type of arrhythmia, in the S-I plane, the interval between activation during the paced beat and activation during the first of the first repetitive response was reported.

In Figure 36 below reported, black points indicate, for each stimulation strength, the measured ERP.

White points indicate all the premature (stimulated) beats which were not followed by arrhythmias.

Red points indicate all the premature beats which induced BBRs with longer AT1-AT2 intervals.

Dark red points indicate all the premature beats which induced BBRs with shorter AT1-AT2 intervals.

Yellow points indicate all the premature beats which induced IVR-M.

Purple points indicate all the premature beats which induced IVR-P.

Green points indicate all the premature beats which induced non sustained VTs.

Cyan points indicate all the premature beats which induced VFs.

Horizontal cyan lines indicate, in each stimulation strength, premature beats which were characterized by response latency.

Horizontal orange lines indicate, in each stimulation strength, premature beats which were characterized by a visible UCB at the epicardial level in the activation maps.

Numbers above the S-I points of the plane indicate the interval in ms (AT1-AT2) between activation time at test site during the paced beat (AT1) and earliest activation time during the first arrhythmia reentry (AT2).

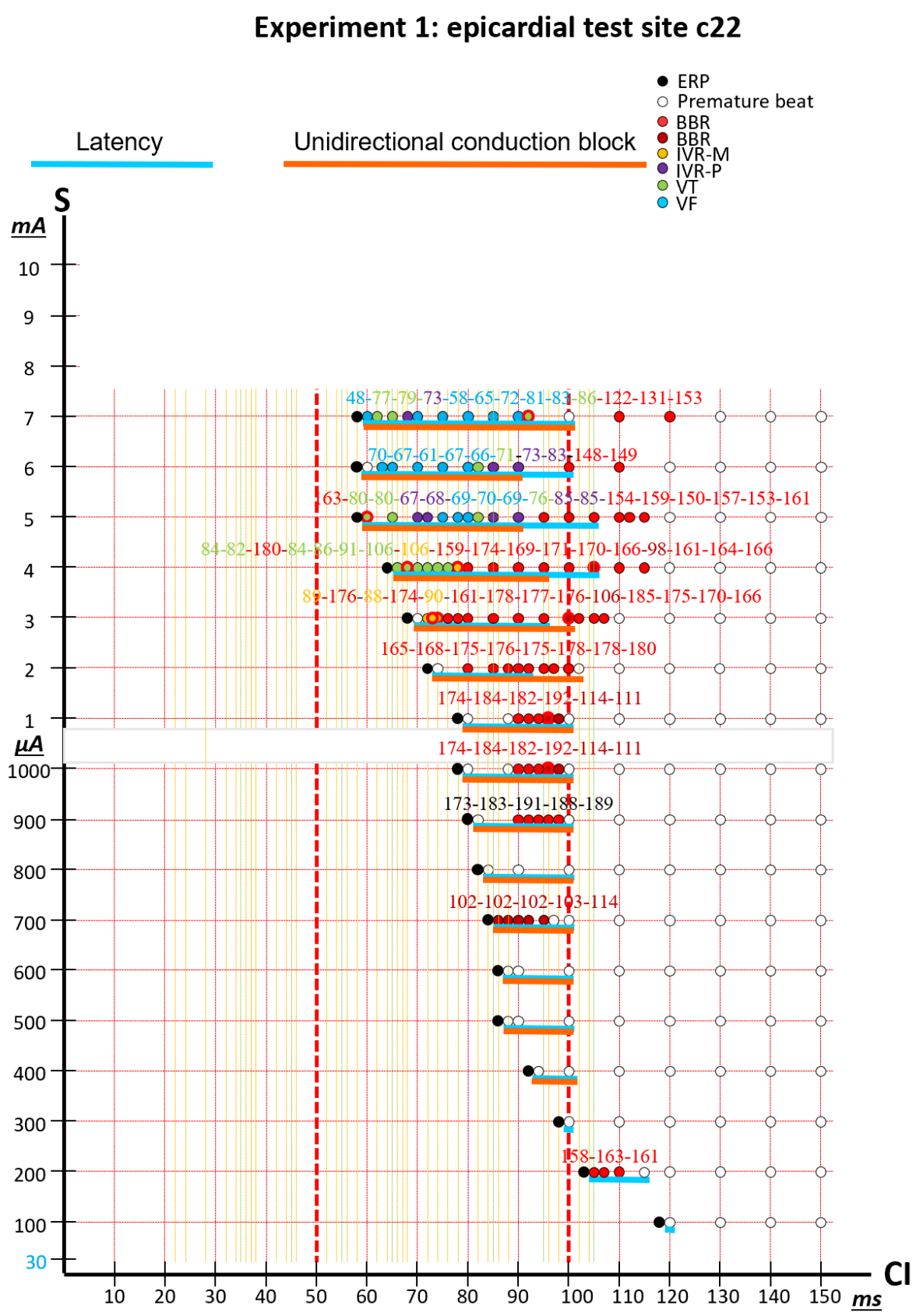

Figure 36: example of S-I plane (relative to the experiment 1, epicardial stimulation point through lead 22 of the grid).

2.8. Premature response activation latency graphs.

For each stimulation strength of a test site a response latency graph of the premature beat was built reporting on the abscissa the coupling interval of the premature stimulation and on the ordinate the response activation latency (Fig.37). In the present study response activation latency is defined as the time interval in ms between the instant of premature stimulation (S) and the earliest activation time of the premature beat (AT1).

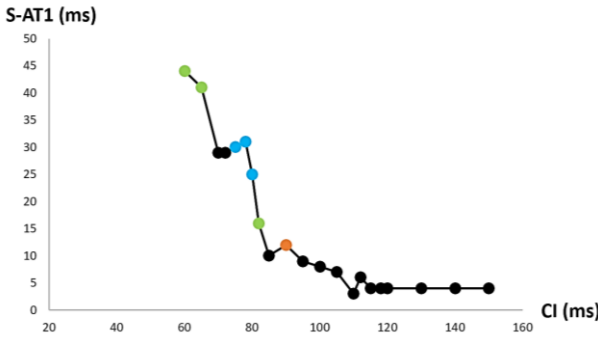

Figure 37. Example of response latency graph (relative to the experiment of 12 May 2017, epicardial test site, electrode 22 of the grid) for the stimulation strength of 5 mA. Premature stimulation was applied during sinus rhythm. Response latency had an initial value of 4 ms from 150 ms to 115 ms of coupling interval and reached its maximum value (44 ms) with the shortest coupling interval (60 ms). Black points indicate premature stimulations that did not induce reentries. Orange point indicates the RW-S coupling interval from which unidirectional conduction block occurred at the epicardial level in the premature beat. Green points indicate premature stimulations which induced VTs. Cyan points indicate premature stimulations which induced VFs.

2.9. Stimulation-reentry interval graphs.

For each stimulation strength, for each test site, a stimulation-reentry activation time graph (S-AT2) was built (Fig.38) reporting on the abscissa the coupling interval of the premature stimulation (S) and on the ordinate the earliest activation time of the reentrant beat (AT2). Activation isochrone map of the reentrant beat was built using the instant of premature stimulation as reference time.

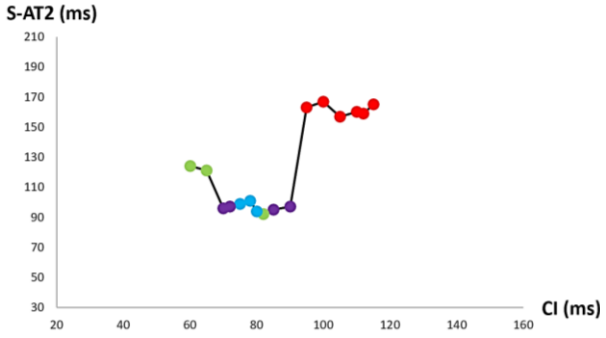

Figure 38. Example of stimulation-reentry (S-AT2) graph (relative to the experiment 1, epicardial test site, electrode 22 of the grid) for the stimulation strength of 5 mA. Premature stimulation was applied during sinus rhythm. Red points indicate premature stimulations which induced BBRs. Purple points indicate premature stimulations which induced IVR-Ps. Green points indicate premature stimulations which induced VTs. Cyan points indicate premature stimulations which induced VFs.

2.10. Premature beat-reentry interval graphs.

For For each stimulation strength, of a test site, a premature beat-reentry graph (AT1-AT2 interval) was built (Fig.39) reporting on the abscissa the coupling interval of the premature stimulation (S) and on the ordinate the difference between the earliest activation time of the reentrant beat (AT2) and the earliest activation time of the premature beat (AT1).
Isochrone maps of premature and reentrant beats were built using the instant of premature stimulation as reference time. Hence, the premature beat-reentry interval represents the stimulation reentry-interval not taking into account the premature beat activation latency.

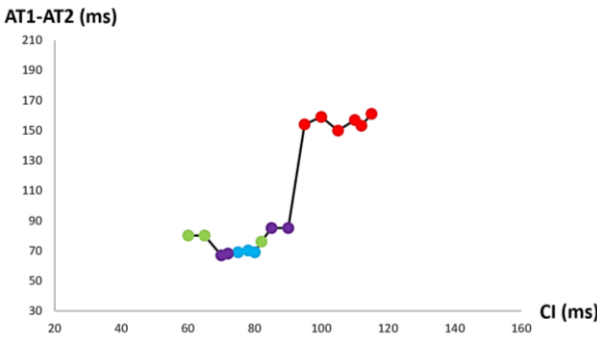

Figure 39. Example of premature beat-reentry (AT1-AT2) graph (relative to the experiment of 1, epicardial test site, electrode 22 of the grid) for the stimulation strength of 5 mA. Premature stimulation was applied during sinus rhythm. Red points indicate premature stimulations which induced BBRs. Purple points indicate premature stimulations which induced IVR-Ps. Green points indicate premature stimulations which induced VTs. Cyan points indicate premature stimulations which induced VFs.

2.11. Activation Isochrone maps.

Activation isochrone maps during RW-S protocol were built using the following reference times:

- Sinus beat reference time was set at the beginning of the QRS complex. Accurate detection of low-voltage QRS onset during SR was obtained by taking the logarithm of the root-mean-square (RMS) signal calculated from the 8x8 EGs.
- Premature beat reference time was set at the instant of stimulation.
- Reentry beat reference time was set at the instant of stimulation.

Activation isochrone maps during S1-S2 protocol were built using the following reference times:

- For S1 beat, reference time was set at the instant of stimulation of S1 beat.
- For S2 beat, reference time was set at the instant of stimulation of the S2 beat.

- For reentry beat, reference time was set at the instant of stimulation of the S2 beat.

Ventricular activation times were defined as the minimum time derivative of QRS intrinsic deflection (dV/dtmin). From the spatial distribution of activation times of a specific beat, the corresponding activation isochrone map was obtained.

In the activation isochrone maps, red circle indicates the position of the electrode 1 of the grid, while blue circle indicates the position of the electrode 8 of the grid.

2.12. Recovery isochrone maps.

Recovery times were computed as the times of the minimum of the time derivative (dV/dtmin) during the downslope of the T wave. From the spatial distribution of recovery times of a specific beat, the corresponding recovery isochrone map was obtained. Recovery isochrone maps were used to determine the dispersion of repolarization of the beat under consideration.

Recovery isochrone maps were built using the same reference times used to obtain the corresponding activation isochrone maps.

In the recovery isochrone maps, red circle indicates the position of the electrode 1 of the grid, while blue circle indicates the position of the electrode 8 of the grid.

2.13. Isopotential maps.

For each beat, different maps are built and printed at time intervals of 1 ms from each other, starting from the stimulus artifact or from the beginning of QRS during sinus rhythm; each map represents the explored area. Each of them reports the instantaneous potential values and by joining the points that are at the same potential, instantaneous maps of the equipotential lines are obtained. The equipotential lines define the configuration of the potential field of the explored region, and its evolution over time. Blue lines highlighted negative potentials while red lines highlighted positive potentials.

Isopotential maps were mainly used to localize the position of endocardial test sites which corresponds to the position of minimum value of extracellular potential at the instant of stimulation. In the isopotential maps, red circle indicates the position of the electrode 1 of the grid, while blue circle indicates the position of the electrode 8 of the grid.

2.14. Statistical analysis

Data were expressed as mean ± SEM. The normal distribution was checked by the Kolmogorov-Smirnov test. Statistics of variables included unpaired Student's t-test, Kruskal-Wallis (post hoc analyses: Dunn's multiple comparisons), and one-way ANOVA (post hoc analyses: Bonferroni test or Games-Howell test, when appropriate). GraphPad 6.0 software (Prism) was used to assess the normality of the data and for the statistical calculation. P values of <0.05 were considered to be significantly different.

2.15. Animals and stimulation points.

To investigate ventricular vulnerability to arrhythmia and fibrillation, 17 normal rats were used in 17 experiments.

1) In the experiment 1, one epicardial test site (c22) in the RV was studied.
2) In the experiment 2, two epicardial test sites were studied. The first electrode of stimulation, c43, resulted located in the interventricular septum (IVS). The second electrode of stimulation, c22, was located in the RV at the sinus BTP level.
3) In the experiment 3, three test sites were studied, two epicardial and one endocardial in the LV. The first electrode of stimulation, c43, was epicardial and located on LV. The second electrode of stimulation was endocardial and located into the LV. The last electrode of stimulation, c46, was epicardial and located at the IVS.
4) In the experiment 4, two epicardial test sites were used. The first electrode of stimulation was c42, localized in RV close to the IVS. The second electrode of stimulation was c14 whose location coincided with the sinus beat BTP in the RV.
5) In the experiment 5, three test sites were studied, two epicardial in the RV and one endocardial in LV. The first electrode was c46 (located at the sinus BTP level), the second was c19 and the third was the endocardial in the LV.
6) In the experiment 6, three electrodes test sites were studied, two epicardial and one endocardial in the RV. The first electrode of stimulation was c19 and it applied stimulations in correspondence of the sinus BTP. The second electrode of stimulation was c22. The third electrode of stimulation was the endocardial electrode in the RV.
7) In the experiment 7, four test sites were studied, two epicardial and two endocardial. The first and the second electrode of stimulation, c43 and c22 respectively, stimulated

the RV. The third electrode of stimulation was the endocardial electrode located in the LV, while the fourth was the endocardial located in the RV.

8) In the experiment 8, one endocardial test site in the RV was studied.
9) In the experiment 9, two test sites were studied, c34 and the endocardial electrode in the RV. C34 resulted located in the RV between the two BTPs of the sinus beat.
10) In the experiment 10, two test sites were studied, the epicardial test site c13 in the RV and the endocardial electrode in the RV.
11) In the experiment 11, three test sites were studied, two epicardial in the RV and one endocardial in the RV. The two epicardial test sites were c27, localized between the two BTPs of sinus beat, and c37, localized at the level of a BTP of sinus beat.
12) In the experiment 12, four test sites were studied, three epicardial in the RV (c49, c29 and c34) and one endocardial in the RV. C49 resulted located at BTP level of sinus beat.
13) In the experiment 13, five test sites were studied, two epicardial in the RV (c28 and c31), one epicardial in the LV (c50), one endocardial in the RV and one endocardial in the LV.
14) In the experiment 14, five test sites were studied, two epicardial in the RV (c22 and c46), one epicardial in the IVS (c26), one endocardial in the RV and one endocardial in the LV.
15) In the experiment 15, three test sites were studied, one epicardial in the RV (c53) at the BTP level, one endocardial in the RV and one endocardial in the LV.
16) In the experiment 16, three test sites were studied, one epicardial in the RV (c14) at the BTP level, one endocardial in the RV and one endocardial in the LV.
17) In the experiment 17, five test sites were studied, two epicardial in the RV (c22 and c05), one epicardial in the LV (c34), one endocardial in the RV and one endocardial in the LV. C22 resulted localized at sinus BTP level.

2.16. Definitions.

Latency. In the present study response activation latency is defined as the time interval in ms between the instant of premature stimulation (S) and the earliest activation time of the premature beat (AT1).

Breakthrough point. In the present study breakthrough point (BTP) is defined as an outcrop at the epicardium of a wavefront coming from the endocardium and which is visible in activation maps as a circular or elliptical region of activation characterized by shorter activation times. BTPs are usually visible in activation maps of sinus beats and of arrhythmias due to reentry through Purkinje system (BBRs and IVRs).

Collision. In the present study the term "collision" is used to indicate the clash between two distinct wavefronts which end to merge in a single wavefront. Collisions are often visible in activation maps of sinus beats (collision between wavefronts deriving from different BTPs) and of premature beats characterized by an arch of UCB (collision between wavefronts turning around the UCB at the distal site of the latter).

Graded response. In the present study “graded response” is used to indicate a particular response (sustained by active and passive elements) of myocardium which occurs when the stimulus is applied prematurely during the phase of relative refractoriness. Graded response is indirectly visible in activation maps of premature beats when the source (region of earliest activation) of the premature beat is localized at a distance (of one or more millimetres) from the test site. In these circumstances, graded response allows the onset of an action potential in the source localized away from the test site. Consequently, the region in which graded responses take place is the region between the test site and the source of the stimulated beat.

Experimental ERP. In the present study the term “experimental ERP” is utilized to indicate the ERP measured experimentally, which corresponds to the longest coupling interval which is not followed by a propagated response.

Real ERP. In the present study “real ERP” is utilized to indicate the longest coupling interval which lead to a stimulated beat whose activation map shows a source which is not localized anymore around the test site but it is localized away from the test site.

2.17. Tissue morphometry.

At the end of each experiment, the epicardial position of the electrode array was identified by fiducial marks burned onto the tissue by constant current flow through four electrodes external to the electrode array. Hence, under a stereo microscope, epicardial fibre direction was visually inspected in the area covered by the electrode array. In a few experiments, fiber direction, myocardial fibrosis, and myocyte transverse diameter were assessed across the wall of ventricular myocardium underlying the measurement area.

Briefly, small-diameter tungsten wires were inserted perpendicularly to the epicardial surface across the fiducial marks to deepen the epicardial marks into myocardial tissue. Thereafter, the heart was rapidly removed from the chest, weighed, and fixed in 10% buffered formalin solution for 24–48 h. The ventricular wall comprising the fiducial marks was excised from the heart and embedded into a paraffin block with the epicardial surface facing upward.

25-gauge steel needles were inserted into a perpendicularly predrilled, Plexiglas frame that was placed in contact with the paraffin block. Perpendicular insertion of the needles into the block allowed for later alignment of sections via the needle track reference holes. Subsequently, the block was fully sectioned parallel to its epicardial surface, and 500 consecutive 4-µm-thick histological sections were usually obtained. Sections were stained with hematoxylin and eosin (H & E) for fiber direction and myocyte transverse diameter measurements. Under a stereo microscope, H & E-stained sections were aligned vertically by means of the reference holes and digitized. A schematic diagram of the electrode array was placed on the digitized sections and aligned with fiducial marks, accounting for tissue shrinkage due to fixation (typically 35%). On each section, fiber direction was assessed by a semiautomated method at 36 regularly spaced array electrodes (Fig. 78).

3. Results

3.1. BBRs induced by premature stimulation applied in the RV.

In figure 40 are shown stimulated beats at long coupling intervals through three test sites in the RV (two epicardial and one endocardial) and the corresponding sinus beat of the experiment 11.

Stimulated beats at long coupling intervals and sinus beat.

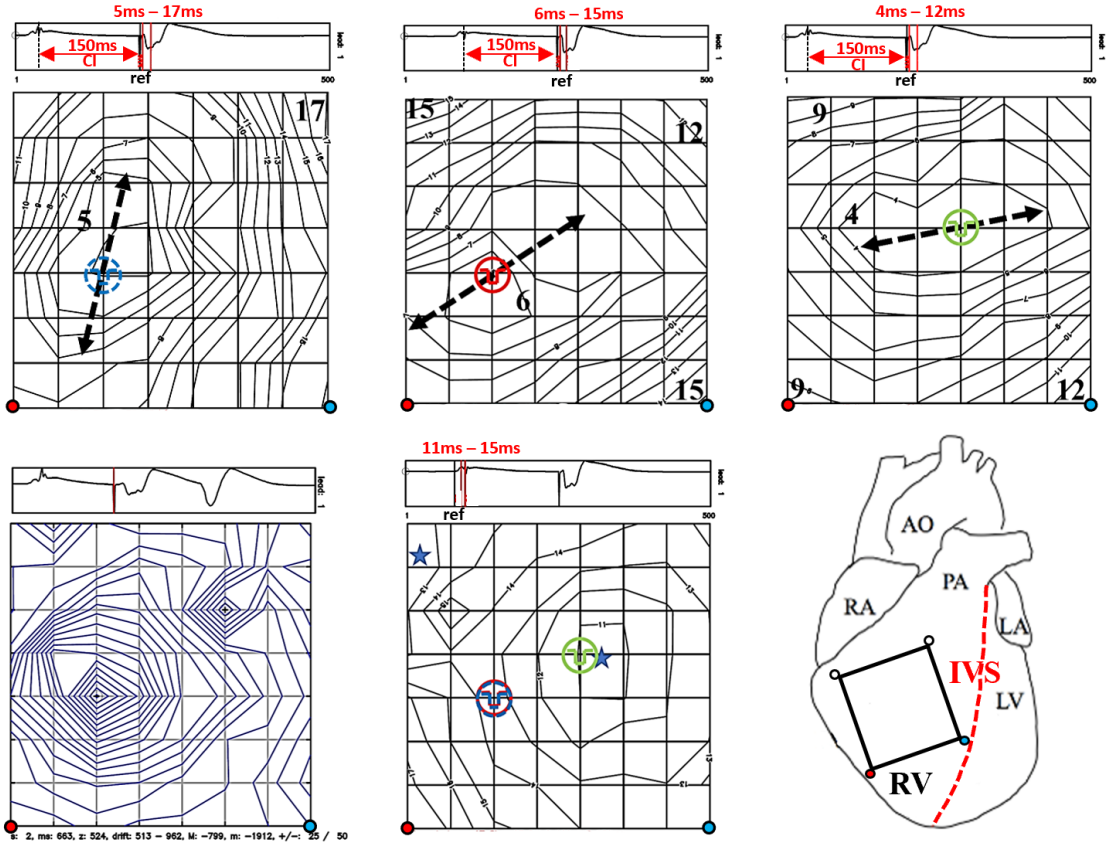

Figure 40: Upper left panel: activation isochrone map of diastolic premature stimulation (S: 400 µA, I: 150 ms) through endocardial electrode corresponding to epicardial electrode 27.
Upper central panel: activation isochrone map of diastolic premature stimulation (S: 100 µA, I: 150 ms) through epicardial electrode 27 of the grid corresponding to endocardial electrode.
Upper right panel: activation isochrone map of diastolic premature stimulation (S: 200 µA, I: 150 ms) through electrode 37 of the grid.
Lower left panel: isopotential map 1 msec after the instant of endocardial stimulation.
Lower central panel: activation isochrone map of sinus beat with reported positions of the three test sites.
Lower right panel: representation of the position of the electrode array on the ventricular epicardium: AO, aorta; RA, right atrium; LA, left atrium; LV, left ventricle; RV, right ventricle; IVS, interventricular septum.

The activation map of the endocardial test site (upper left panel of figure 40) shows an epicardial source proximal to the stimulation point (indicated by the dotted line blue symbol) with low response latency (4 msec) and anisotropic propagation with higher velocity along an intermediate direction between endocardial and epicardial fiber directions (indicated by the double arrowed dotted black line). The entire region mapped by the grid was found to be activated in 13 msec. The stimulation point was localized in the RV between the two BTPs of sinus beat.

The correspondent isopotential map obtained for the instant of stimulation (lower left panel of figure 40) indicates the position of the endocardial test site which coincides with the position of the epicardial potential minimum.

The activation map of the epicardial test site c27 (upper central panel of figure 40) shows a source localized all around the stimulation point (indicated by red symbol) with low response latency (5 msec) and anisotropic propagation in accordance with the direction of the epicardial fibers (indicated by the double arrowed dotted black line). Note that epicardial fibers are rotated clockwise compared to the endocardial fibers, in accordance with the different direction of the major axis of the ellipses in the two activation maps obtained through the two test sites.

The activation map of the epicardial test site c37 (upper right panel of figure 40) shows a source localized all around the stimulation point (indicated by green symbol) with low response latency (4 msec) and anisotropic propagation in accordance with the direction of the epicardial fibers (indicated by double arrowed dotted black line).

In accordance with the sinus beat activation map (lower central panel), in this experiment, the grid resulted positioned on part of the anterior surface of the RV; in fact, two BTPs of the RV (indicated by the blue stars) are visible. The collision at the IVS level is not visible and it is localized externally to the right of the matrix.

Activation during the sinus beat was extremely rapid with the entire region mapped by the grid completing its activation in just 6 ms.

Figure 41 shows S-I planes of the three test sites used in the RV in the experiment 11.

S-I planes.

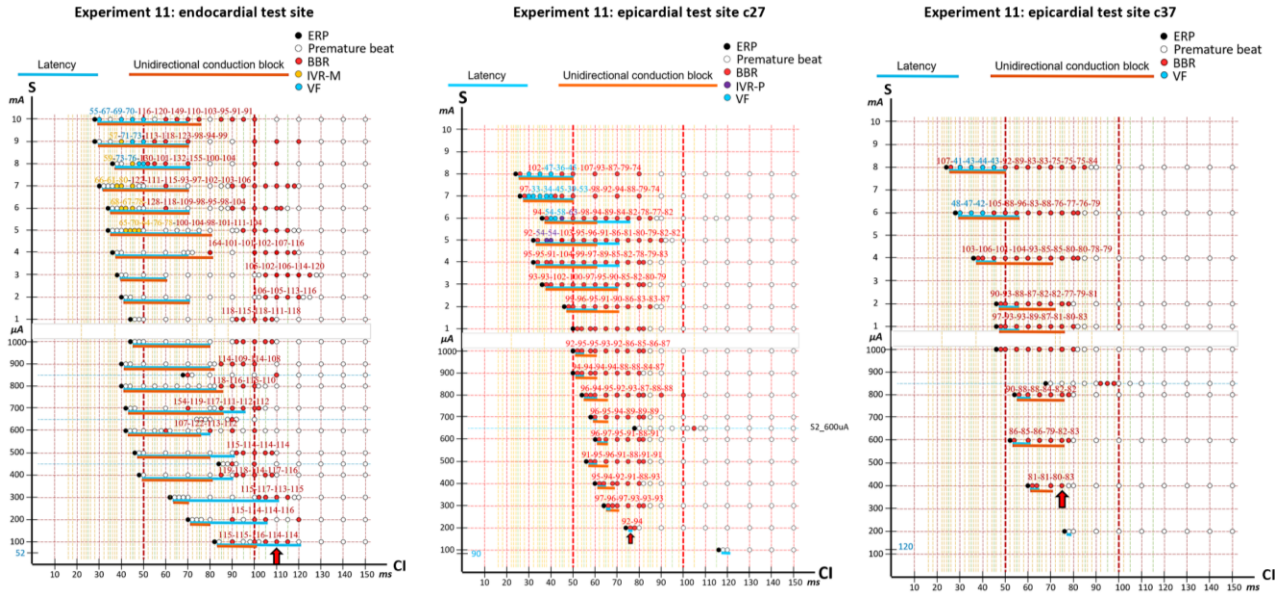

Figure 41: left panel: S-I plane of endocardial test site, central panel: S-I plane of epicardial c27 test site), right panel: S-I plane of epicardial c37 test site of the experiment 11.

Left panel: with the endocardial test site, BBRs were obtained from 100 μA to 10 mA of stimulation strength.

Central panel: with the correspondent epicardial test site, electrode 27 of the grid, BBRs were obtained from 200 μA to 8 mA of stimulation strength.

Right panel: with epicardial test site, electrode 37 of the grid, BBRs were obtained from 400 μA to 8mA of stimulation strength.

Red arrows indicate premature beats and BBRs whose activation maps will be reported in the present work.

In particular, will be shown activation isochrone maps and unipolar EGs of:

- BBR induced by premature stimulation through endocardial test site (S: 100 μA, I: 110 ms), figure 42.
- BBR induced by premature stimulation through epicardial test site c27 (S: 200 μA, I: 76 ms), figure 43.
- BBR induced by premature stimulation through epicardial test site c37 (S: 400 μA, I: 75 ms), figure 44.

BBR triggered by premature stimulation (S: 100 µA, I:110 ms) through endocardial test site.

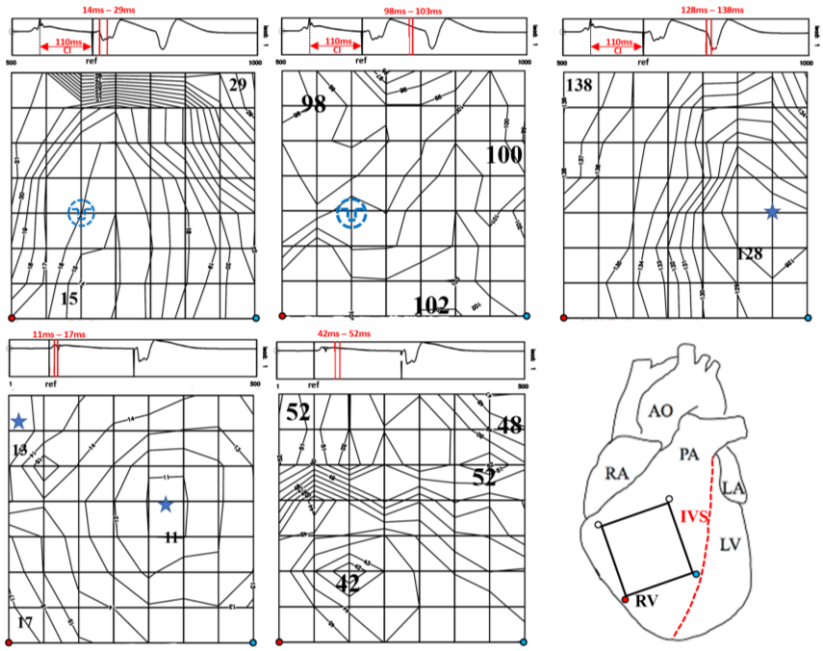

Figure 42: upper left panel: activation isochrone map of premature beat (S: 100 µA, I: 110 ms) of endocardial test site.
Upper central panel: recovery isochrone map of premature beat (S: 100 µA, I: 110 ms) of endocardial test site.
Upper right panel: activation isochrone map of the first induced BBR.
Lower left panel: activation isochrone map of the sinus beat.
Lower central panel: recovery isochrone map of the sinus beat.
Lower right panel: representation of the position of the electrode array on the ventricular epicardium: AO, aorta; RA, right atrium; LA, left atrium; LV, left ventricle; RV, right ventricle; IVS, interventricular septum.

The activation pattern (upper left panel of fig. 42) of the premature beat (S: 100 µA, I: 110 ms) of the endocardial test site shows that source resulted characterized by slight asymmetry and response latency increased to 15 ms (compared to the 5 ms shown in fig. 40, upper left panel). Orientation of major elliptical axis of activation isochrones is rotated toward endocardial fiber direction around pacing site.

The recovery pattern of the premature beat (upper central panel of fig. 42) shows a uniform distribution of RTs. This element suggests that the induced reentry should not be of IVR-M type.

The activation pattern of the first induced BBR (upper right panel of fig. 42) shows that it resulted characterized by a BTP localized in a similar position compared to one of the two BTPs observed in the sinus beat (lower left panel) and emerging at the epicardial level after 128 ms from the instant of stimulation.

AT1-AT2 interval of this BBR resulted equal to 113 ms.

The recovery pattern of sinus beat (lower central panel) shows that RT distribution had no enhanced recovery gradient.

BBR triggered by premature stimulation (S: 200 µA, I:76 ms) through epicardial test site c27.

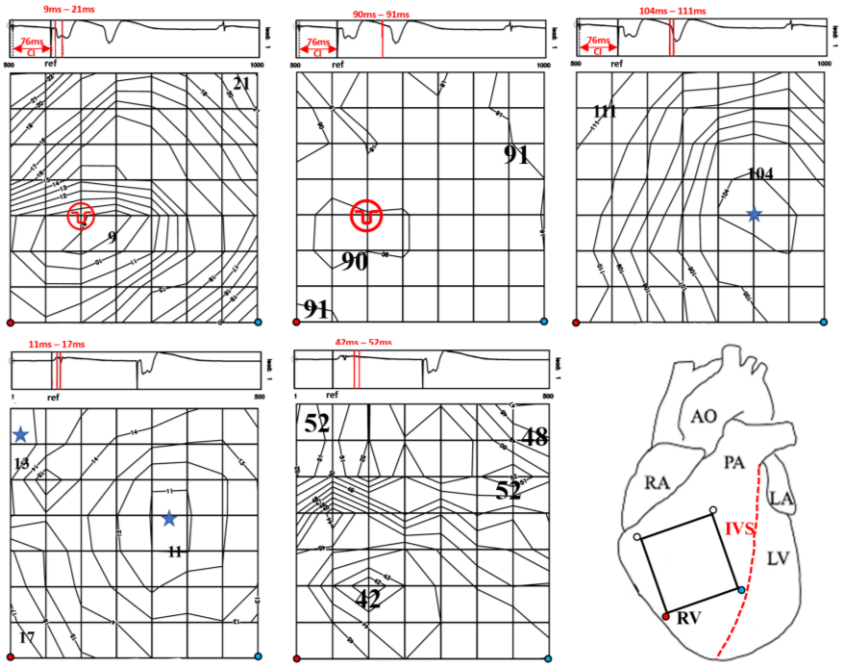

Figure 43: upper left panel: activation isochrone map of premature beat (S: 200 µA, I: 76 ms) of epicardial test site 27.
Upper central panel: recovery isochrone map of premature beat (S: 200 µA, I: 76 ms) of epicardial test site 27.
Upper right panel: activation isochrone map of the induced BBR.
Lower left panel: activation isochrone map of the sinus beat.
Lower central panel: recovery isochrone map of the sinus beat.
Lower right panel: representation of the position of the electrode array on the ventricular epicardium: AO, aorta; RA, right atrium; LA, left atrium; LV, left ventricle; RV, right ventricle; IVS, interventricular septum.

The activation pattern (upper left panel of figure 43) of the premature beat (S: 200 µA, I: 76 ms), of the epicardial test site 27, shows that source resulted localized around the stimulation point and response latency increased to 9 ms (compared to the 6 ms shown in fig. 40, upper central panel, S: 200 µA, I: 150 ms). No UCB is visible in this map at the epicardium level. Orientation of major elliptical axis of activation isochrones is parallel to epicardial fiber direction.

The recovery pattern of the premature beat (upper central panel of fig. 43) shows a uniform distribution of RTs. This element suggests that the induced reentry should not be of the IVR-M type.

The activation pattern of the first BBR (upper right panel of figure 43) shows a BTP localized at one of the two BTPs observed in the sinus beat (lower left panel) and emerging at the epicardial level after 104 ms from the instant of stimulation. Note that the activation pattern of this BBR is identical to the activation pattern of the BBR induced by the endocardial premature beat (Fig. 42, upper right panel).

BBR triggered by premature stimulation (S: 400 µA, I: 75 ms) through epicardial test site c37.

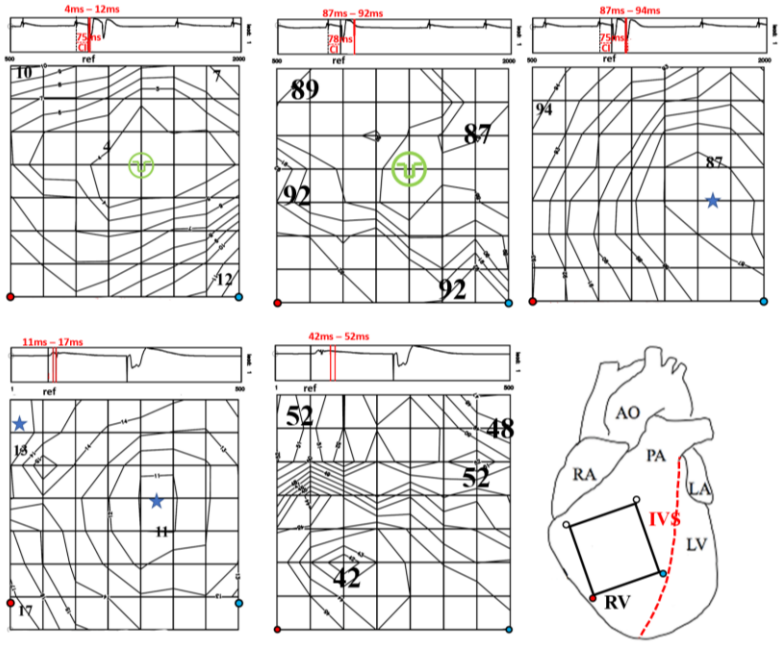

Figure 44: upper left panel: activation isochrone map of premature beat (S: 400 µA, I: 75 ms) of epicardial test site 37. Upper right panel: activation isochrone map of the induced BBR.
Upper central panel: recovery isochrone map of premature beat (S: 400 µA, I: 78 ms) of epicardial test site 37.
Lower left panel: activation isochrone map of the sinus beat.
Lower central panel: recovery isochrone map of the sinus beat.
Lower right panel: representation of the position of the electrode array on the ventricular epicardium: AO, aorta; RA, right atrium; LA, left atrium; LV, left ventricle; RV, right ventricle; IVS, interventricular septum.

The activation pattern (upper left panel of figure 44) of the premature beat (S: 400 µA, I: 75 ms), of the epicardial test site c37, shows that source resulted localized all around the stimulation point with a response latency of 4 ms.

The recovery pattern (upper central panel of fig. 44) was computed for a premature beat at 3 ms longer coupling interval (78 ms instead of 75 ms) because it was not followed by reentry. We assume that the RT distributions of the two premature beats are similar. The uniform distribution of the RTs suggests that the reentry induced at 75 ms coupling interval should not be of IVR-M type.

The activation pattern of the induced BBR (upper right panel of fig. 44) was characterized by a BTP similar to one of the two BTPs observed in the sinus beat (lower left panel) 87 ms from the instant of stimulation. Note that the activation pattern of this BBR is identical to those displayed in Fig. 42 and 43 (upper right panels).

AT1-AT2 interval of this BBR resulted equal to 83 ms.

Note that all the BBRs shown above were obtained from premature beats without a visible UCB at the epicardium and were characterized by a BTP localized in the same point.

Overall, BBRs were induced through 32 of the 33 test sites in the RV and resulted almost always characterized by LBBB pattern as in the examples above reported. In these cases BTPs of BBRs resulted always localized in correspondence of one of the BTPs of the sinus beat in the RV.

Much more rarely, BBRs with RBBB or BBRs with left posterior fascicular block were obtained and the correspondent BTPs resulted always localized in correspondence of one (or more) BTPs of the sinus beat.

Mean AT1-AT2 of BBRs induced through premature stimulation in the RV resulted equal to 96,6 ms (SE = 3.14).

BBRs were induced through all the 22 epicardial test sites in the RV and their mean AT1-AT2 interval resulted equal to 97,85 ms (SE = 4.1).

BBRs where induced through 10 of the 11 endocardial test sites in the RV and their mean AT1-AT2 interval resulted equal to 95,2 ms (SE = 3.7).

3.2. BBRs induced by premature stimulation applied in the LV.

In figure 45 are shown activation isochrone maps of sinus beat and stimulated beats at long coupling intervals at low (100 µA) and high (6 mA) stimulation strength through the endocardial test site in the LV of the experiment 3.

Sinus beat and stimulated beats at long coupling intervals.

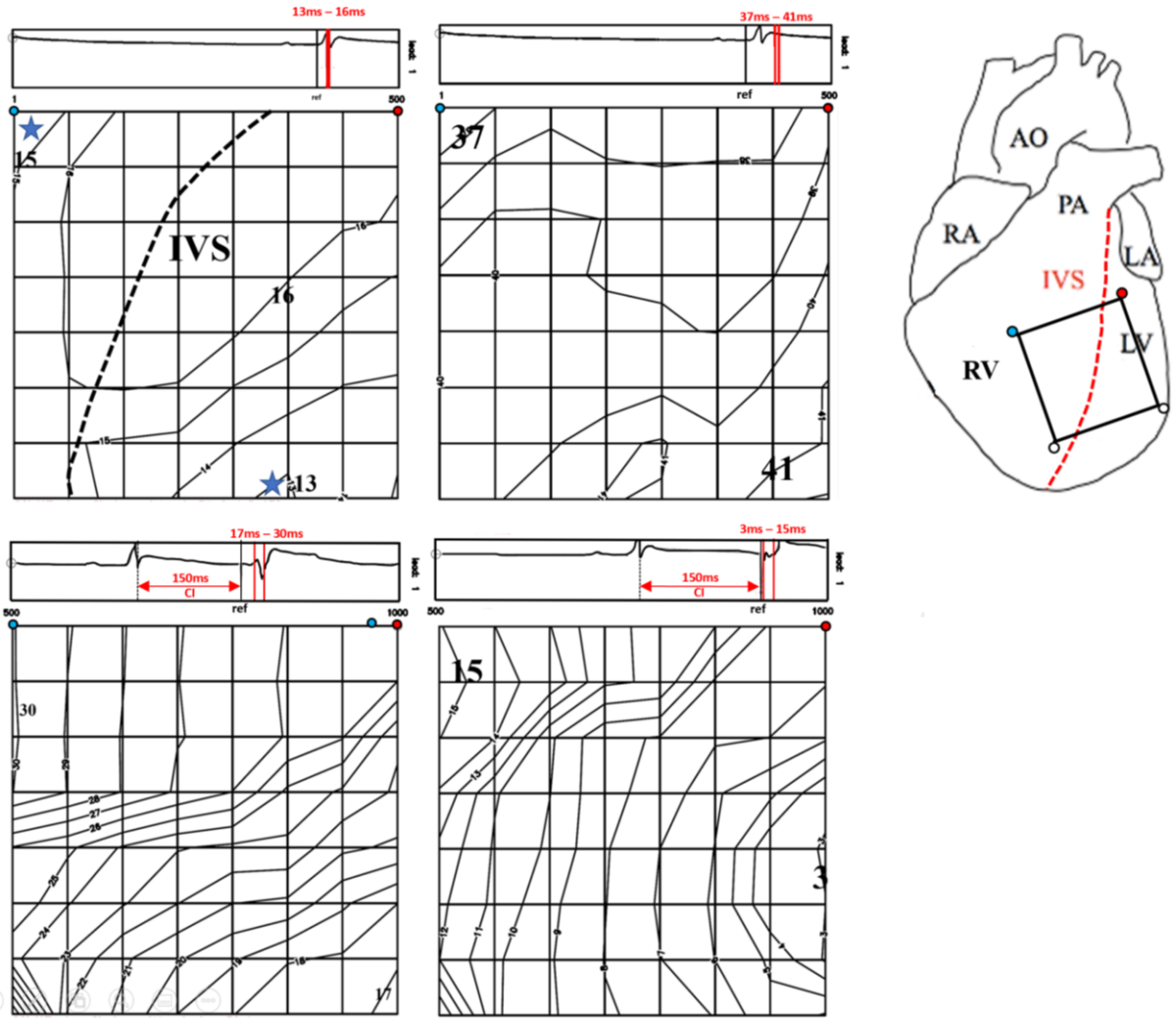

Figure 45. Upper left panel: activation isochrone map of sinus beat.
Upper central panel: recovery isochrone map of sinus beat.
Upper right panel: representation of the position of the electrode array on the ventricular epicardium: AO, aorta; RA, right atrium; LA, left atrium; LV, left ventricle; RV, right ventricle; IVS, interventricular septum.
Lower left panel: activation isochrone map of stimulated beat (S: 100 µA, I: 150 ms).
Lower right panel: activation isochrone map of stimulated beat (S: 6 mA, I: 150 ms).

In accordance with the sinus beat activation map (upper left panel of figure 45), in this experiment the grid resulted positioned on part of the anterior face of the LV and on a smaller portion of the RV. Two wave fronts from RV and LV activation onset (blue stars) collide in the region of the epicardial projection of septum (dashed line). One of the BTP of the LV (lower blue star) and the collision at the IVS level are clearly visible, while the BTP of the RV (higher blue star) is localized at the boundary of the grid and hence it is not well defined. The entire region mapped by the grid was activated in just 3 ms.

The recovery time map of the sinus beat (upper central panel of figure 45) shows gradual increase of RT from RV (37 ms) to LV (41 ms).

According to the activation pattern of the premature beat (lower left panel of figure 45) at low stimulation strength (100 µA), the endocardial test site is localized externally to the grid in the free wall of the LV. A wavefront from the LV crosses the lower left corner of electrode grid at 17 ms. Activation of the entire region mapped by the grid was completed in 13 ms.

The activation pattern of the premature beat (lower right panel of figure 45) at high stimulation strength (6 mA) shows an early wave front crossing the left side of the grid (3 ms. vs 17 ms). The time-space different activation patterns are likely due to the higher stimulation strength (6 mA vs 100 µA).

The S-I plane of the endocardial test site in the LV (figure 46) shows that ERP (black points) decreased progressively with increasing the stimulation strength, with a value of 78 ms at 100 μA and a value of 24 ms at 10 mA.

Three main typologies of BBR were obtained through this test site, which were reported in the S-I plane with three different colours: red points indicate BBR with anterograde conduction occurring in the RV (and therefore characterized by left bundle branch block), orange points indicate BBR with anterograde conduction occurring in the LV (and therefore characterized by right bundle branch block) and brown points indicate BBR with anterograde conduction occurring in both LV and RV.

BBRs with anterograde conduction in the RV were obtained from the stimulation strength of 1 mA.

BBRs with anterograde conduction in the LV were obtained from 2 mA of stimulation strength.

BBRs with anterograde conduction in both LV and RV were obtained from 5 mA.

Note that from 5 mA, BBRs with anterograde conduction in the RV were obtained at the extremes of the vulnerability window of arrhythmias, while the other two types of BBRs occupy the central portion of such vulnerability window. Also note that, for each stimulation strength, the BBRs with antegrade conduction in the RV are characterized by greater AT1-AT2 intervals than the other two types of BBRs.

Short run VT were obtained at 6 mA and 7 mA of stimulation strength.

Red arrows indicate premature beats and re-entries whose activation maps will be reported in the present work.

In particular, registrations through single EG and activation isochrone maps of the following BBRs and VT will be shown:

- BBR induced by premature stimulation (S: 6 mA, I: 70 ms) and characterized by BTPs in both ventricles and BBR induced by premature stimulation (S: 6 mA, I: 70 ms) and characterized by BTP only in the RV (thus resulting in LBBB activation pattern), figures 47 and 48.
- BBR induced by premature stimulation (S: 6 mA, I: 68 ms) and characterized by BTPs in both ventricles and BBR induced by premature stimulation (S: 6 mA, I: 68 ms) and characterized by BTP only in LV (thus resulting in RBBB activation pattern), figures 49 and 50.

S-I plane.

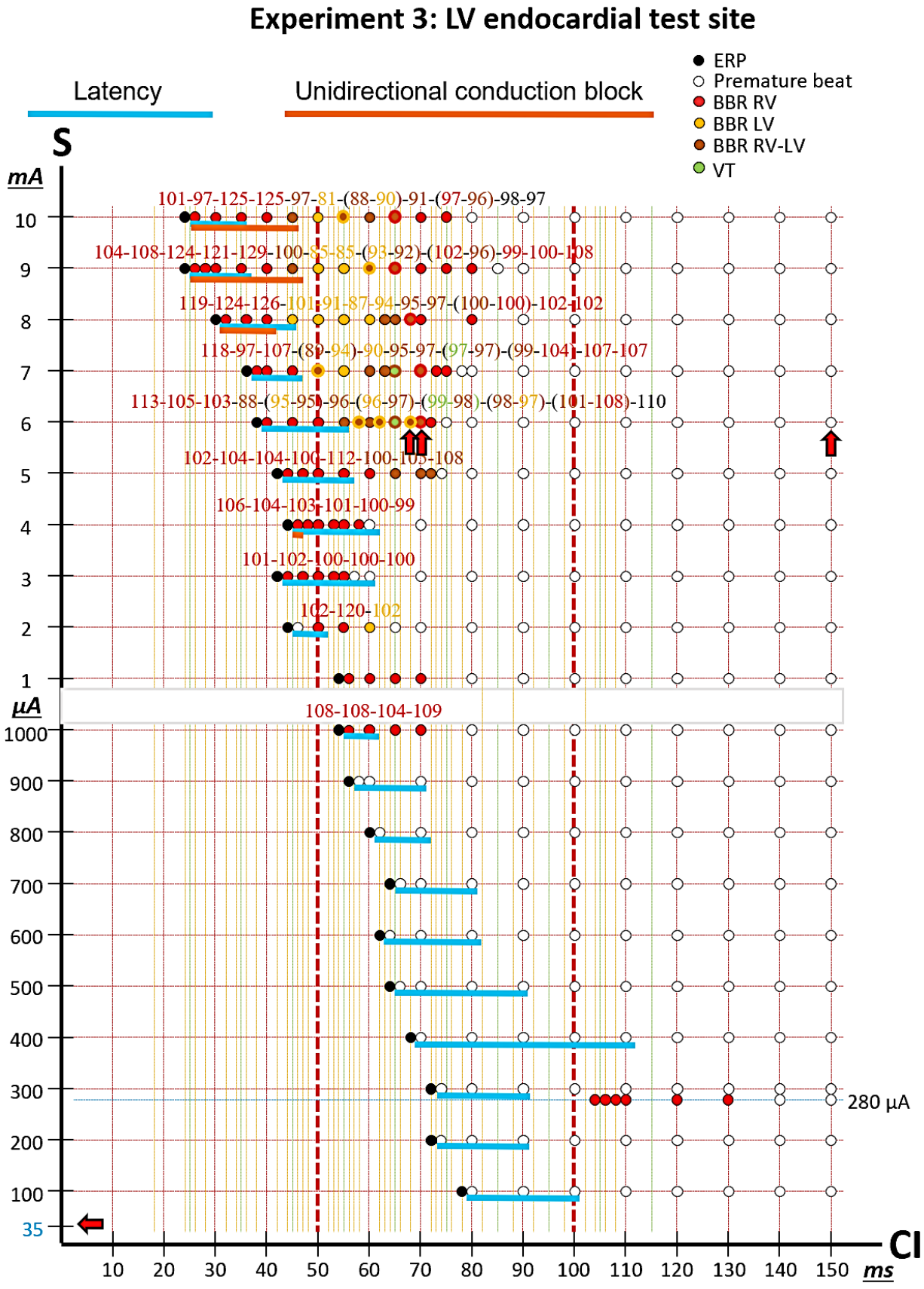

Figure 46: S-I plane of endocardial test site in the LV of the experiment 3.

Premature stimulation (S: 6 mA, I: 70 ms).

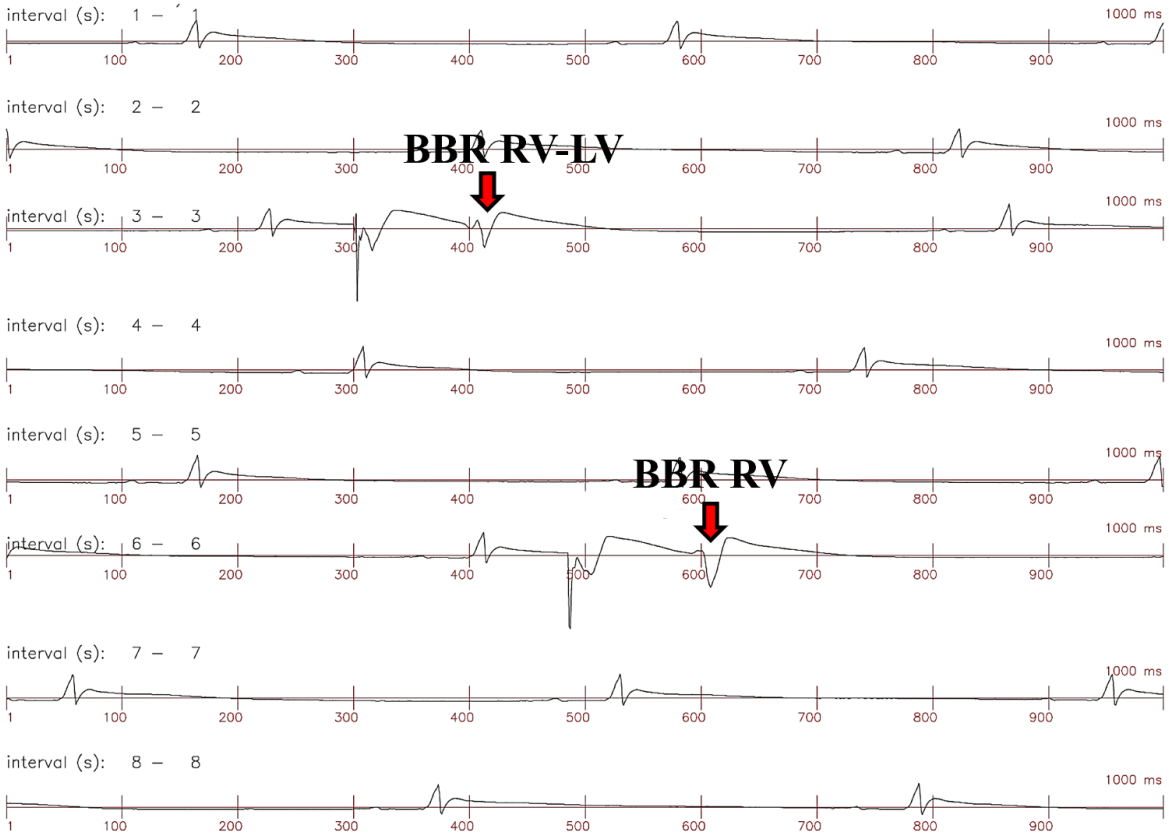

Figure 47: registration of premature stimulation applied with a stimulation strength of 6 mA and a coupling interval of 70 ms. Each line contains 1 second of registration.
The first red arrow (second 3) indicates the BBR characterized by antegrade conduction in LV and RV.
The second red arrow (second 6) indicates the BBR with anterograde conduction in RV.

Premature stimulation through endocardial test site in the LV with a stimulation strength of 6 mA and a coupling interval of 70 ms was able to induce both BBR with anterograde conduction in LV and RV (third second of the registration) and BBR with anterograde conduction in RV (sixth second of registration).

Red arrows of fig. 47 indicate premature beats and BBRs of which activation will be reported in the present work.

BBRs triggered by premature stimulation (S: 6mA, I: 70 ms).

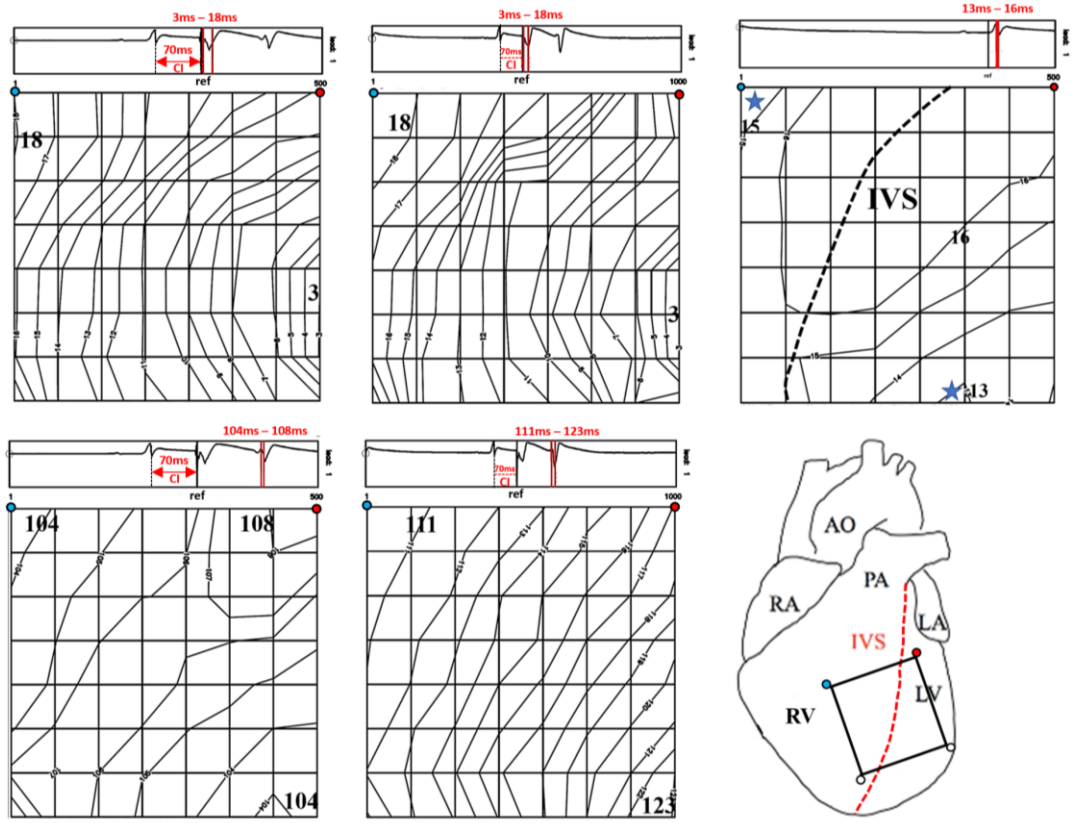

Figure 48: activation isochrone map of premature beat (S: 6 mA and I: 70 ms) upper left panel (third second of registration showed in fig. 47) and upper central panel (sixth second of registration showed in fig. 47).
Upper right panel: sinus beat activation map.
Lower left panel: activation isochrone map of BBR with anterograde conduction in RV and LV.
Lower central panel: activation isochrone map of BBR with anterograde conduction in RV.
Lower right panel: representation of the position of the electrode array on the ventricular epicardium: AO, aorta; RA, right atrium; LA, left atrium; LV, left ventricle; RV, right ventricle; IVS, interventricular septum.

Activation patterns of the premature beats triggered by a stimulation with a strength of 6 mA and a coupling interval of 70 ms are shown in upper left and central panels of fig. 48. In both cases response latency resulted of 3 ms, no UCB is visible in the portion of epicardium mapped by the grid and the entire region resulted activated in 15 ms. Note that these activation patterns are similar to the activation pattern of the stimulated beat (S: 6 mA, I: 150 ms) showed previously in fig. 45. The increase in conduction time is caused by the higher prematurity of the stimulus.

The activation pattern of the BBR with anterograde conduction through RBB and left anterior fascicle is shown in lower left panel of fig. 48. The activation pattern is similar to the activation pattern of sinus beat (upper right panel). However, the collision of RV and LV wave fronts is slightly shifted towards LV.

The activation pattern of the BBR with anterograde conduction through RBB (lower central panel of fig. 48) is characterized by a LBBB sinus beat activation pattern. Note that S-AT2 interval of this BBR is longer than BBR shown in the lower left panel (111 ms vs 104 ms).

Premature stimulation (S: 6 mA, I: 68 ms).

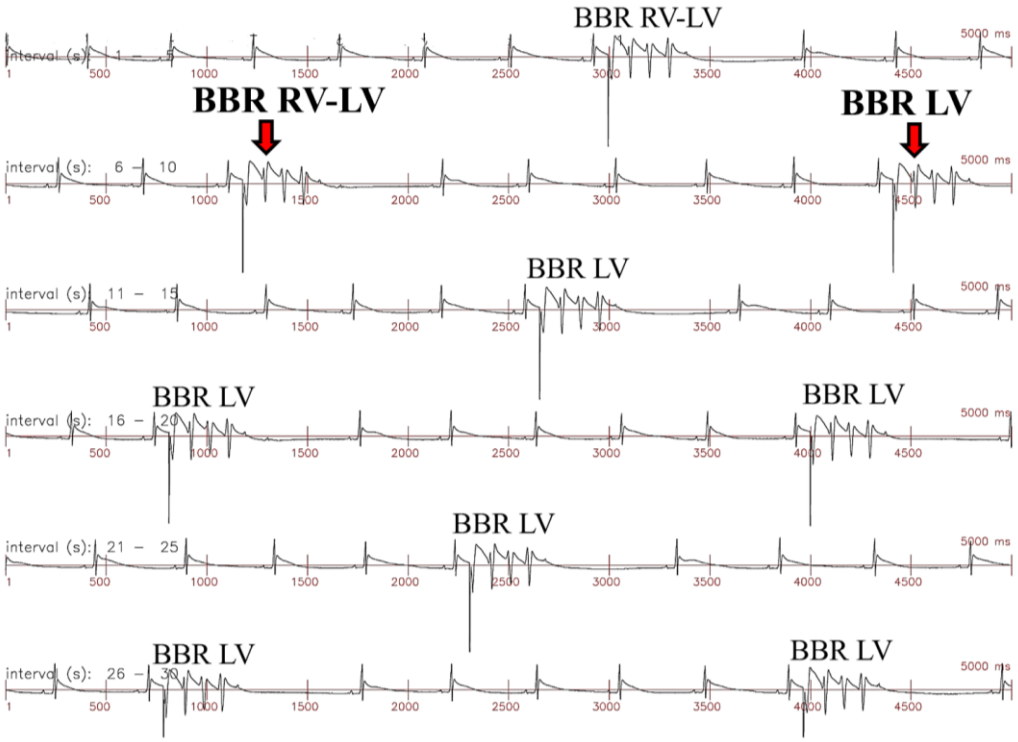

Figure 49: registration of premature stimulations applied with a stimulation strength of 6 mA and a CI of 68 ms. Each line contains 5 second of registration.
The first red arrow (second 7) indicates the BBR characterized by antegrade conduction in LV and RV.
The second red arrow (second 10) indicates the BBR with anterograde conduction in LV.

Premature stimulation through endocardial test site in the LV with a stimulation strength of 6 mA and a coupling interval of 68 ms was able to induce both BBR with anterograde conduction in LV and RV and BBR with anterograde conduction in RV.

Red arrows of fig. 49 indicate premature beats and BBRs of which activation will be reported in the present work.

BBRs triggered by premature stimulation (S: 6mA, I: 68 ms).

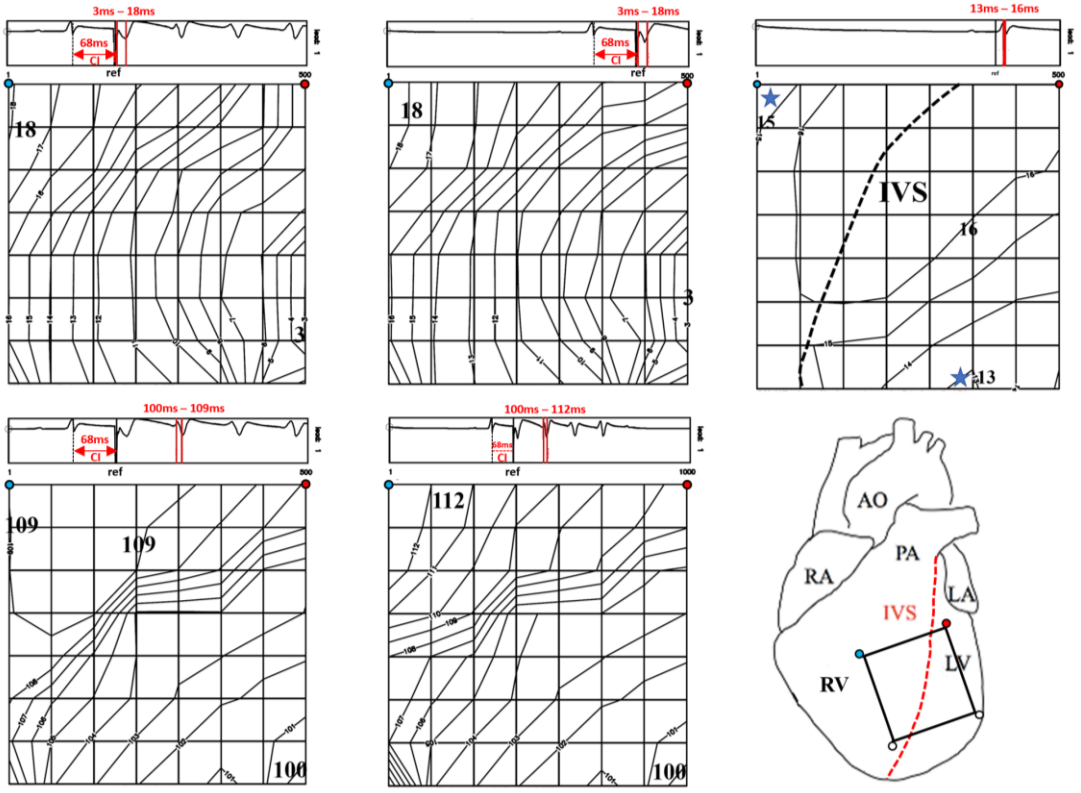

Figure 50. Upper left and central panels: activation isochrone map of premature beats (S: 6 mA, I: 68 ms). Upper right panel: activation isochrone map of sinus beat. Lower left panel: activation isochrone map of BBR with anterograde conduction in RV and LV. Lower central panel: activation isochrone map of BBR with anterograde conduction in LV. Lower right panel: representation of the position of the electrode array on the ventricular epicardium: AO, aorta; RA, right atrium; LA, left atrium; LV, left ventricle; RV, right ventricle; IVS, interventricular septum.

The activation patterns of the premature beats triggered by a stimulation with a strength of 6 mA and a coupling interval of 68 ms are shown in upper left and central panels of fig. 50. In both cases response latency resulted of 3 ms, no UCB is visible in the portion of epicardium mapped by the grid and the entire region mapped by the grid resulted activated in 15 ms. Note that these activation patterns are almost identical to the activation pattern of the stimulated beat (S: 6 mA, I: 70 ms) showed previously in fig. 48.

The activation pattern of the BBR with anterograde conduction through RBB and left anterior fascicle (lower left panel of fig. 50) is very similar to the activation pattern of sinus beat (upper right panel) and to the other BBR with anterograde conduction through RBB and left anterior fascicle showed in fig. 48 (lower left panel); the only difference is the position of the collision of right and left wave fronts.

The activation pattern of the BBR with anterograde conduction through anterior fascicle of LBB (lower central panel of figure 48) shows an activation pattern that reflects a sinus beat

with a RBBB. Note that the S-AT2 intervals of the two BBRs here reported are identical (100 ms).

Overall, BBRs were induced through 7 of the 13 test sites in the LV and resulted characterized by three possible patterns (LBBB, RBBB and left posterior fascicle block) as in the examples above reported. When visible in the matrix, BTPs of BBRs resulted always localized in correspondence of one (or more) of the BTPs of the sinus beat.

Mean AT1-AT2 of BBRs induced through premature stimulation in the LV resulted equal to 94,7 ms.

BBRs were induced through 3 of the 6 epicardial test sites in the LV and their mean AT1-AT2 interval resulted equal to 96,8 ms (SE = 13.6).

BBRs where induced through 4 of the 7 endocardial test sites in the LV and their mean AT1-AT2 interval resulted equal to 92,5 ms (SE = 5.5).

Note that in all the experiments performed, considering both the test site in the RV and the test site in the LV, in no case did a BBR degenerate into VF. This result indicates that the BBRs in the normal heart are benign phenomena.

3.3. **IVR-P, and IVR-M induced by premature stimulation in the RV.**

In figure 51 are shown activation isochrone maps and EGs maps of sinus beat and stimulated beat at low stimulation strength (S: 100 µA, I: 150 ms) through the epicardial test site in the RV of the experiment 2.

Sinus beat and stimulated beat at diastolic threshold.

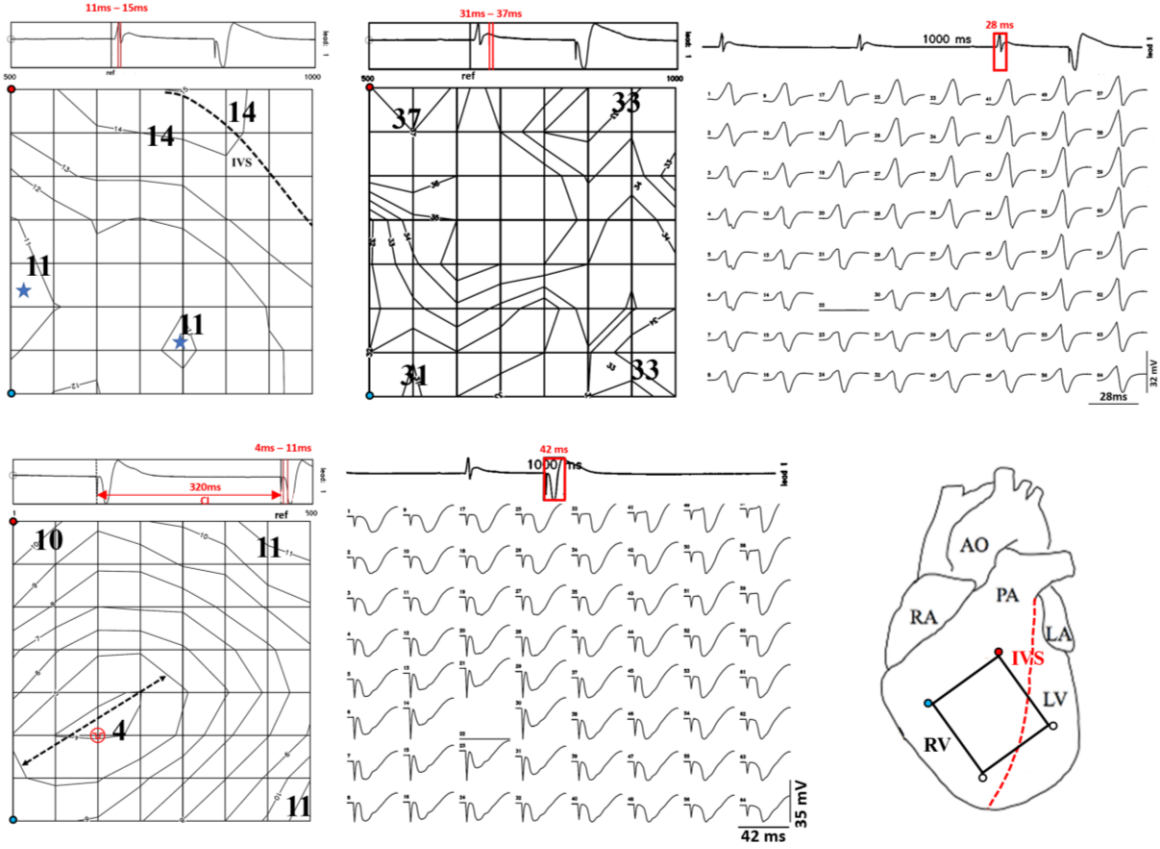

Figure 51. Upper left panel: sinus beat activation isochrone map.
Upper central panel: sinus beat recovery isochrone map.
Upper right panel: sinus beat EGs map.
Lower left panel: stimulated beat (S: 100 µA, I: 150 ms) activation isochrone map.
Lower central panel: stimulated beat (S: 100 µA, I: 150 ms) EGs map.
Lower right panel: representation of the position of the electrode array on the ventricular epicardium: AO, aorta; RA, right atrium; LA, left atrium; LV, left ventricle; RV, right ventricle; IVS, interventricular septum.

As the sinus beat activation map shows (upper left panel of fig. 51), in this experiment, the grid was positioned on part of the anterior face of the RV and on a smaller part of the LV. Two RV breakthrough points (BTPs), one on the anterior surface and the other outside the left side of the grid (blue stars), give rise to a large wave front that collides with a wave front from the LV in the region of the epicardial projection of septum (dashed line). The entire region mapped by the grid completed its activation in just 4 ms.

The recovery map of sinus beat (upper central panel) shows a gradual RT distribution without enhanced gradient.

The unipolar EGs of sinus beat (upper right panel) show steep intrinsic deflections at each grid electrode, thus indicating normal epicardial activation.

Activation onset during the stimulated beat (S: 100 μA, I: 150 ms, lower left panel) initiated all around the stimulation point (electrode 22 of the grid, indicated by the red symbol) with 4 ms latency. Major axis of elliptical activation isochrones was parallel to epicardial fiber direction at the pacing site (black double arrowed dashed line). The entire region mapped by the grid was activated in 11 ms.

The stimulation point was in the RV region between the two BTPs of sinus beat.

The unipolar EGs of stimulated beat at diastolic threshold strength (lower central panel) show steep intrinsic deflections at each grid electrode, indicating uniform anisotropic conduction.

S-I plane of the epicardial test site 22 of the experiment 2.

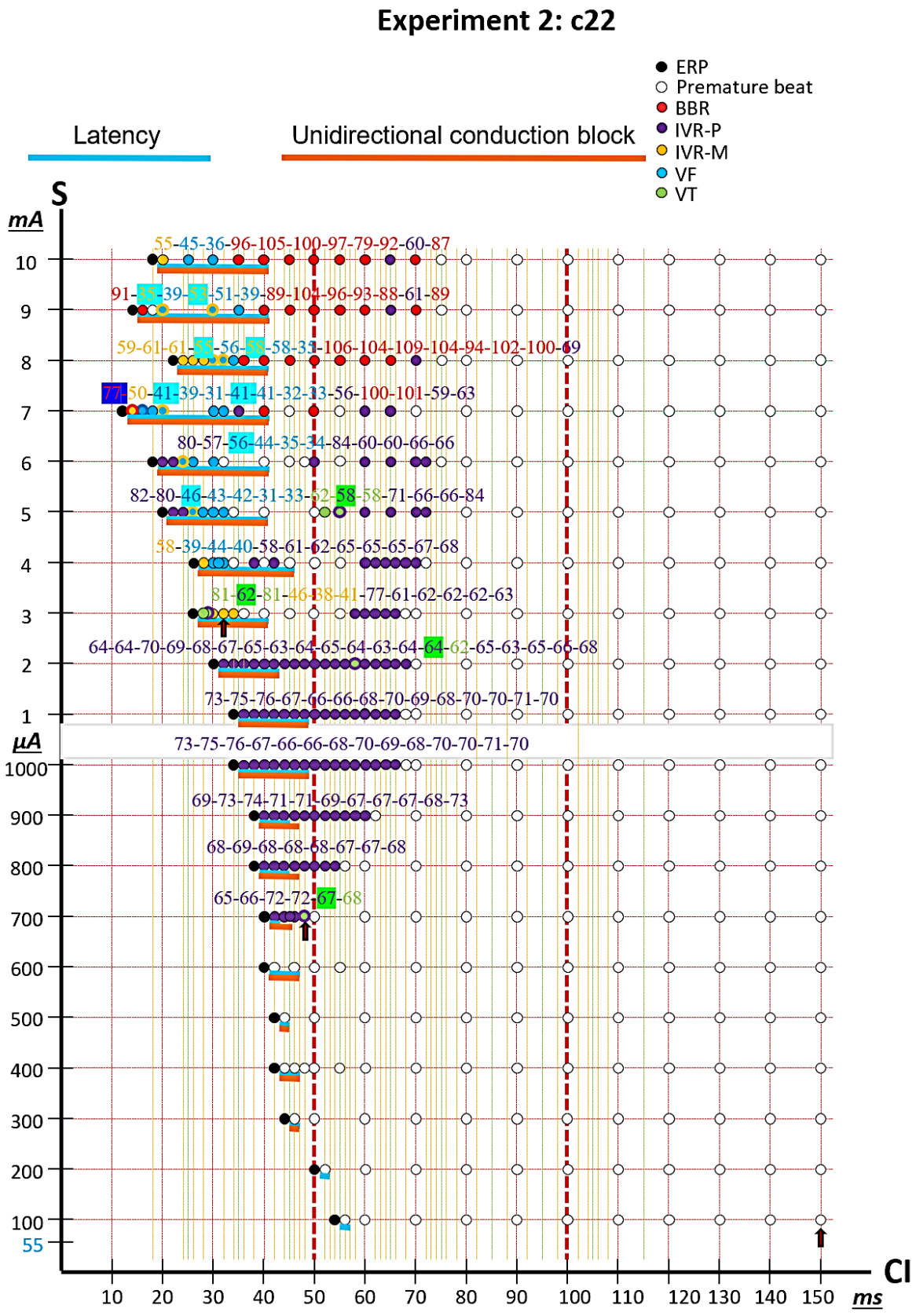

Figure 52: S-I plane of test site 22 of the grid of the experiment 2.

As it is visible from the S-I plane, with the test site considered, the ERP (black points) progressively decreased with increasing stimulation strength, with a longest value of 54 ms at 100 µA and a shortest value of 12 ms at 7 mA. No arrhythmia occurred below 700 µA stimulus strength.

The first IVR-Ps (indicated by purple points) and the first VT (indicated by green points) were obtained with the stimulation strength of 700 µA.

Starting from 3 mA, the first IVR-Ms were obtained (indicated by yellow points).

Starting from 4 mA, such figure 8 reentries degenerated into VFs (indicated by cyan points).

Starting from 7 mA, the first BBRs were obtained (indicated by red points).

By increasing the stimulation strength, the vulnerability window to all the different occurring arrhythmias increased both at shorter and longer coupling intervals.

Above 8 mA, BBRs almost completely replaced IVR-Ps.

Red arrows indicate premature stimulations of which activation and EGs described below.

In particular, will be shown the activation isochrone maps and the unipolar EGs of:

- IVR-P triggered by premature stimulation applied at short coupling interval (S: 700 µA, I: 48 ms), figures 53 and 54.
- IVR-M triggered by premature stimulation (S: 3mA, I: 32 ms), figures 55 and 56.

In addition, AT1-AT2 interval graphs for the stimulation strength of 8 mA will be shown.

Premature stimulation (S: 700 µA, I: 48 ms).

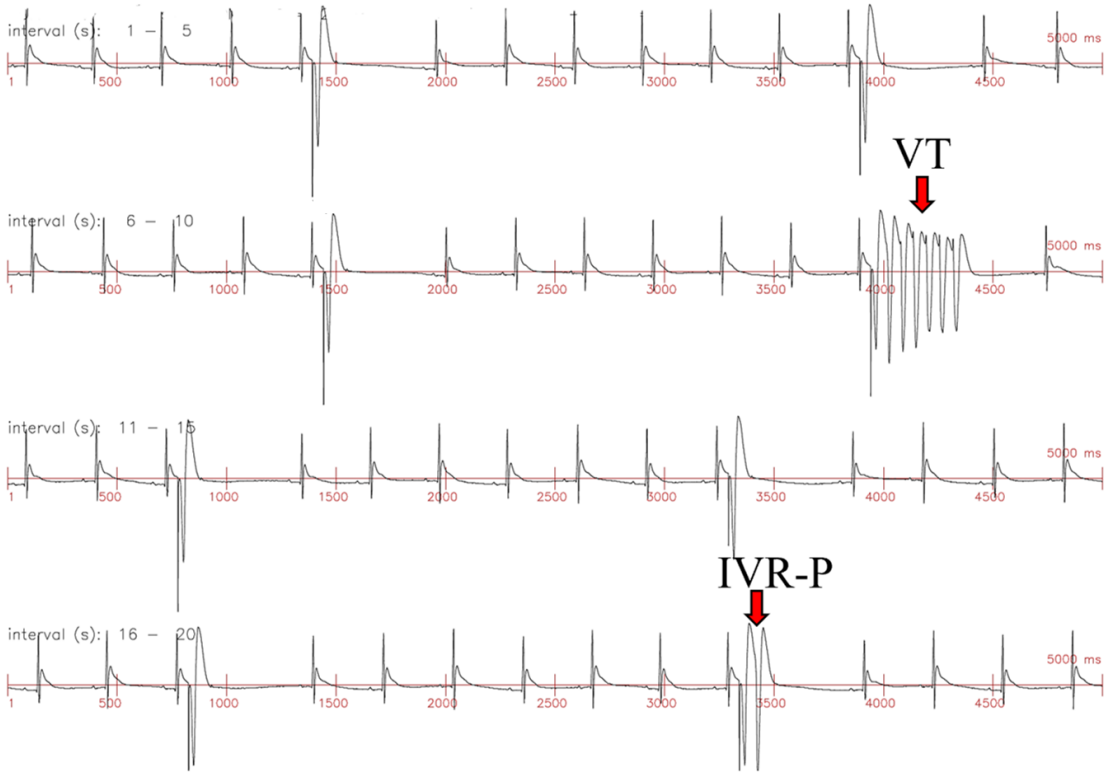

Figure 53: example of short run VT and of IVR-P. Registration of premature stimulations applied at 700 µA of stimulation strength and 48 ms of coupling interval during sinus rhythm. In each line five seconds are reported. The first arrow (second 10) indicates the induced VT. The second arrow (second 19) indicates the single IVR-P.

As it is visible, in the registration reported (fig. 53), some of the premature stimulations were able to induce IVR-P and short run VT (a sequence of IVR-P), while other premature beats were not followed by arrhythmias.

IVR-P triggered by premature stimulation (S: 700 µA, I: 48 ms).

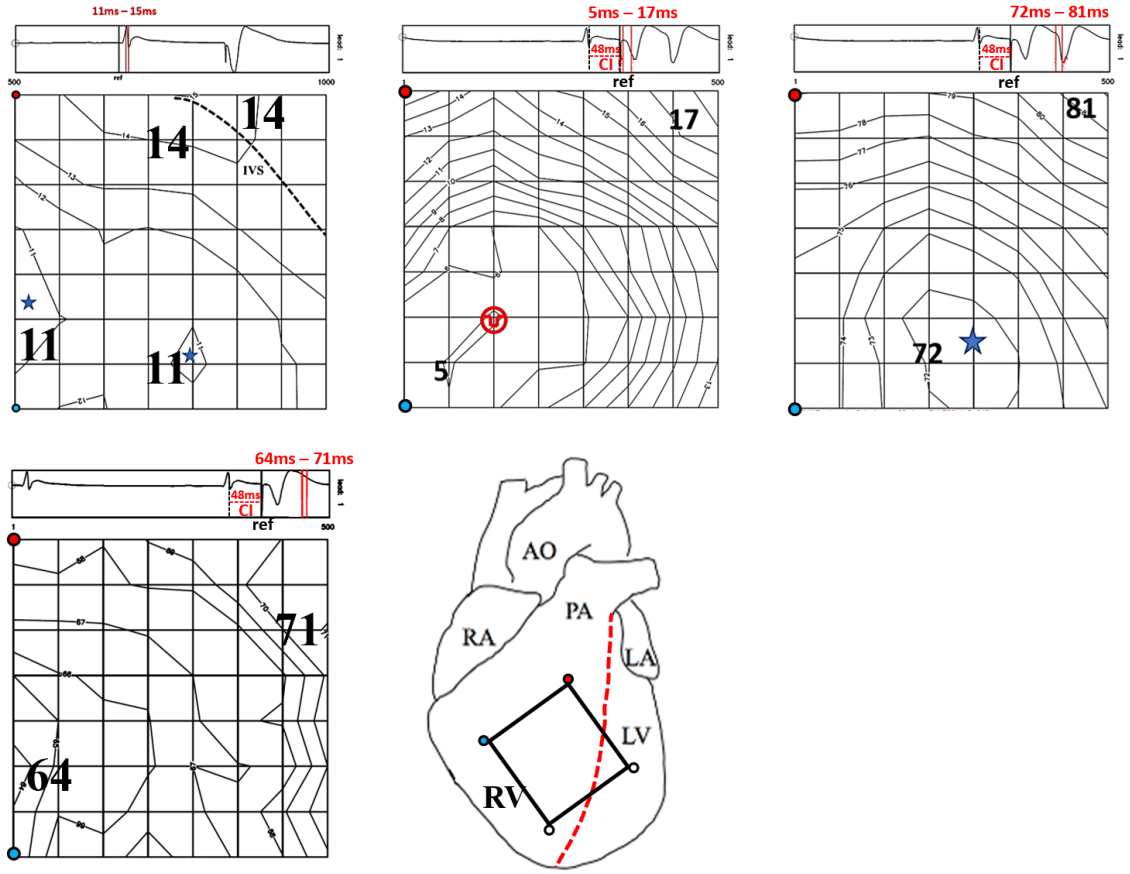

Figure 54: Upper panels: activation isochrone maps of sinus beat, premature beat and reentry of the IVR-P (showed in fig. 53, second 19) induced by premature stimulation applied at 700 µA and 48 ms of coupling interval during sinus rhythm. Blue stars indicate BTPs, red symbol indicates the test site.
Lower left panel: recovery isochrone maps of premature beat (S: 700 µA, I: 48 ms).
Lower central panel: representation of the position of the electrode array on the ventricular epicardium: AO, aorta; RA, right atrium; LA, left atrium; LV, left ventricle; RV, right ventricle; IVS, interventricular septum.

IVR-P (upper right panel) resulted characterized by a BTP localized in the same position of one of the two BTPs of sinus beat (upper left panel).

Premature beat activation map (upper central panel) shows a source localized around the test site with 5 ms response latency. Propagation occurred in all directions from the pacing site with reduced velocity due to the short coupling interval.

Premature beat recovery map (lower central map) was computed for a premature beat occurring at the same strength and coupling interval that was not followed by re-entry. RT map shows a gradual increase of RTs with a recovery pattern that follows the premature activation pattern (upper central panel). The first region to depolarize is the first region to repolarize. The absence of an enhanced RT gradient suggests that the induced reentry is not due to an IVR-M.

Premature and re-entry beats show activation patterns with no evident UCB at the epicardium.

These findings and the short AT1-AT2 interval (67 ms) between premature and re-entry beats suggest the occurrence of a reentry pathway through the terminal Purkinje system of the stimulated ventricle (IVR-P).

Premature stimulation (S: 3 mA, I: 32 ms).

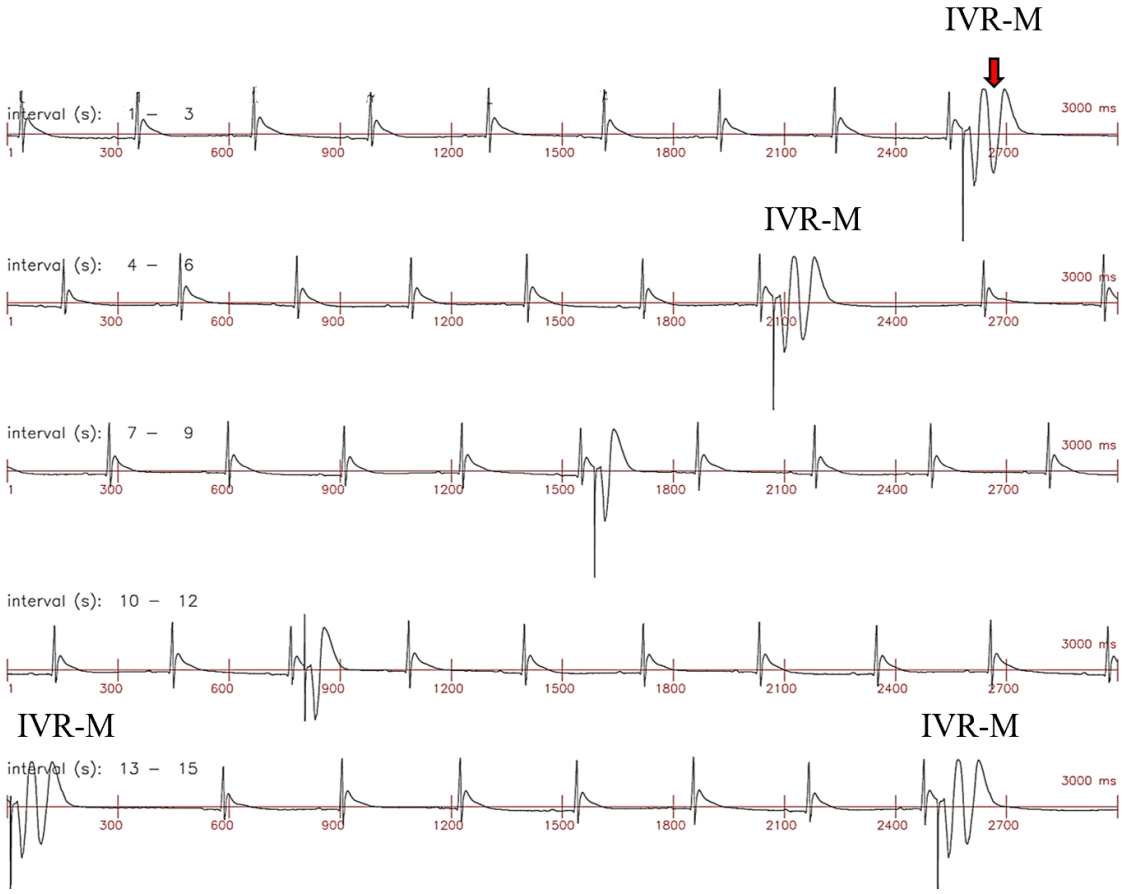

Figure 55: examples of IVR-Ms. Registration of premature stimulations applied at 3 mA of stimulation strength and 32 ms of coupling interval during sinus rhythm. In each line three seconds are reported. Red arrow (second 3) indicates the induced IVR-M.

As shown in figure 55, premature stimulation applied with a stimulation strength of 3 mA and a coupling interval of 32 ms was able to induce IVR-Ms consistently.

Red arrow indicates premature beat and IVR-M of which activation maps and EG maps will be reported in the present work.

IVR-M triggered by premature stimulation (S: 3 mA, I: 32 ms).

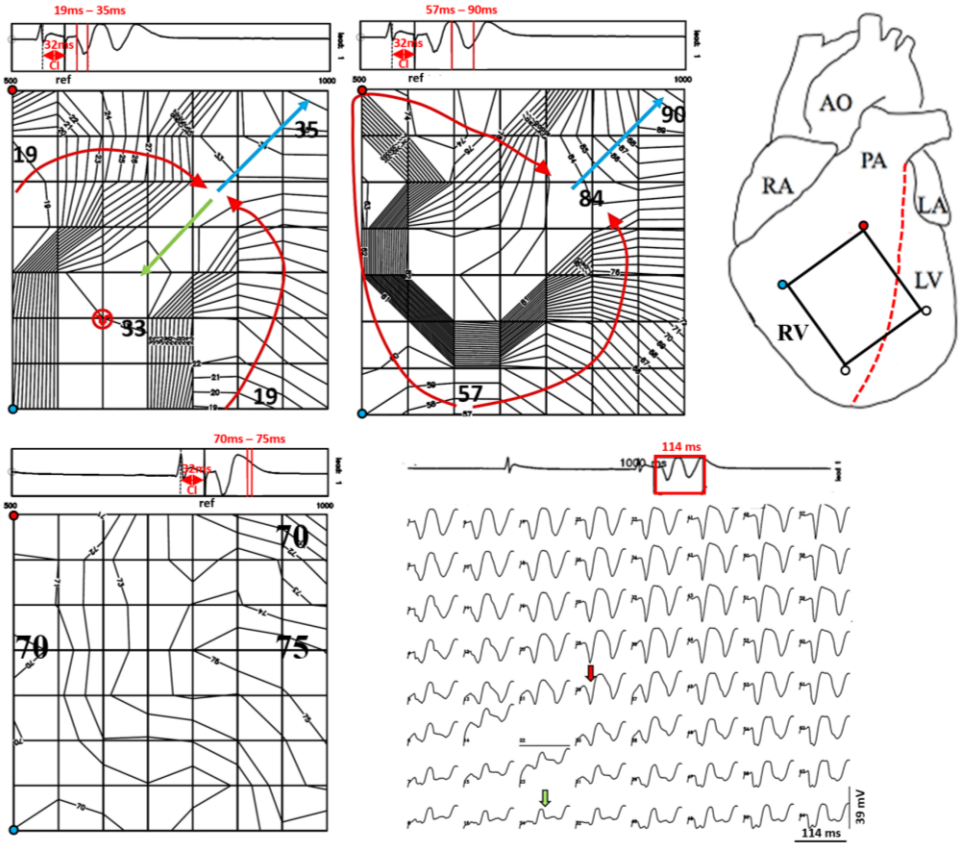

Figure 56: example of UCB in the premature beat followed by figure 8 reentry. Upper left panel: activation isochrone map of premature beat.
Upper central panel: activation isochrone map of IVR-M.
Upper right panel: representation of the position of the electrode array on the ventricular epicardium: AO, aorta; RA, right atrium; LA, left atrium; LV, left ventricle; RV, right ventricle; IVS, interventricular septum.
Lower left panel: recovery isochrone map of premature beat.
Lower right panel: EGs map of premature beat and IVR-M.

Premature beat activation map at very short coupling interval (32 ms, upper left panel of fig. 56) resulted characterized by an external source localized several millimetres away from the test site in the RV, outside the grid, thus indicating the occurrence of graded responses. An arch of UCB is visible in the epicardium in the activation map. From the external source two wavefronts (red arrows) turned around the arch of UCB, collided and merged at 33 ms after the premature stimulation. Of the two wave fronts that originated, one activated the LV (blue arrow) while the other (green arrow) re-entered through the distal side of the UCB (IVR-M). Note the increased response latency, 19 ms, compared to the previously reported premature beat, 5 ms, shown in figure 46 (S: 700 μA, I: 48 ms).

Premature beat recovery map (lower left panel of fig. 56) was computed for a premature beat occurring at the same strength and coupling interval that was not followed by re-entry. Premature beat recovery map shows lower RT values in the RV compared to LV, with the recovery pattern that follows the activation pattern. Note that absolute RT values of the points around pacing site characterized by weak intrinsic deflection in the EGs map are affected by the influence of far-field potentials.

IVR-M activation map (upper central panel of fig. 56) shows the occurrence of an external source giving rise to a wave front the entered the lower side of the electrode array 57 ms after (the instant of the premature stimulation). The wave front from the external source divides into two new wave fronts that surround the area of block (red arrows), collide and merge at 84 ms giving rise to a wave front that propagates toward LV (blue arrow).

Note that re-entry beat source activation originated in the region where premature beat graded response occurred.

The EGs map (lower right panel of fig. 56) of premature and IVR-M beats shows that there is no evident sign of graded conduction in the EGs across the region of re-entry (red and green arrows).

Overall, IVRs were induced through 29 of the 33 test sites in the RV and resulted always characterized by LBBB pattern as in the examples above reported. Their BTP resulted often localized in proximity of the test site in correspondence of the region in which graded response occurred in the premature beat or in correspondence of the source of the premature beat. With less frequency, their BTP resulted localized in the same position of one of the BTPs of the sinus beat in the RV.

Mean AT1-AT2 of IVRs induced through premature stimulation in the RV resulted equal to 61,2 ms (SE = 1.7).

IVRs were induced through 19 of the 22 epicardial test sites in the RV and their mean AT1-AT2 interval resulted equal to 59,76 ms (SE = 2.2).

IVRs where induced through 10 of the 11 endocardial test sites in the RV and their mean AT1-AT2 interval resulted equal to 63 ms (SE = 2.3).

IVRs were induced through 9 of the 13 test sites in the LV and resulted characterized by RBBB pattern as in the examples above reported. Their BTP resulted often localized in proximity of the test site in correspondence of the region in which graded response occurred in the premature beat or in correspondence of the source of the premature beat. With less

frequency, their BTP resulted localized in the same position of one of the BTPs of the sinus beat in the LV.

Mean AT1-AT2 of IVRs induced through premature stimulation in the LV resulted equal to 65,3 ms (SE = 3.8).

IVRs were induced through 3 of the 6 epicardial test sites in the LV and their mean AT1-AT2 interval resulted equal to 58,9 ms (SE = 6).

IVRs where induced through 6 of the 7 endocardial test sites in the LV and their mean AT1-AT2 interval resulted equal to 71,65 ms (SE = 3.5).

AT1-AT2 interval graph, 8 mA.

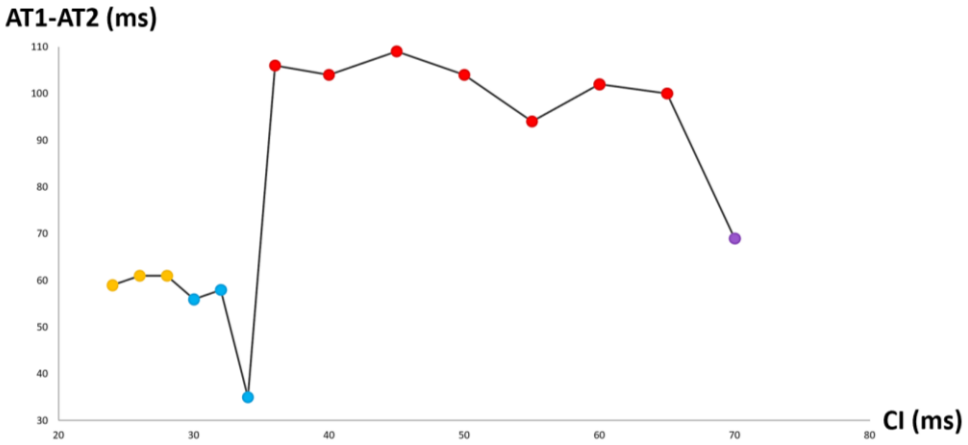

Figure 57: AT1-AT2 interval graph for premature stimulations applied at 8 mA.
Red points indicate BBRs, purple point indicates IVR-P, yellow points indicate IVR-Ms and cyan points indicate VFs.

Figure 57 shows the AT1-AT2 interval graph obtained for this test site with premature stimulation applied at 8 mA of stimulation strength.

Note that AT1-AT2 intervals of BBRs are longer than AT1-AT2 intervals of IVR-P (~ 30 ms) and much longer (~ 40 ms) than AT1-AT2 intervals of VFs and IVR-Ms.

Note that the pattern of the AT1-AT2 graph of the example shown above (fig. 49) was confirmed in all the test sites and in all the stimulation strengths in which the three types of arrhythmias (VFs, IVRs and BBRs) were induced.

In other words, when all the three typologies of arrhythmias were induced, IVRs have always been characterized by longer AT1-AT2 intervals compared to VFs and by shorter AT1-AT2 intervals compared to BBRs.

3.4. Focal and figure 8 VFs induced by premature stimulation in the RV.

In figure 58 are shown activation isochrone maps of sinus beat and stimulated beat at long coupling interval (S: 100 µA, I: 150 ms) through the epicardial test site c27 in the RV of the experiment 11.

Sinus beat and stimulated beat (S: 100 µA, I: 150 ms).

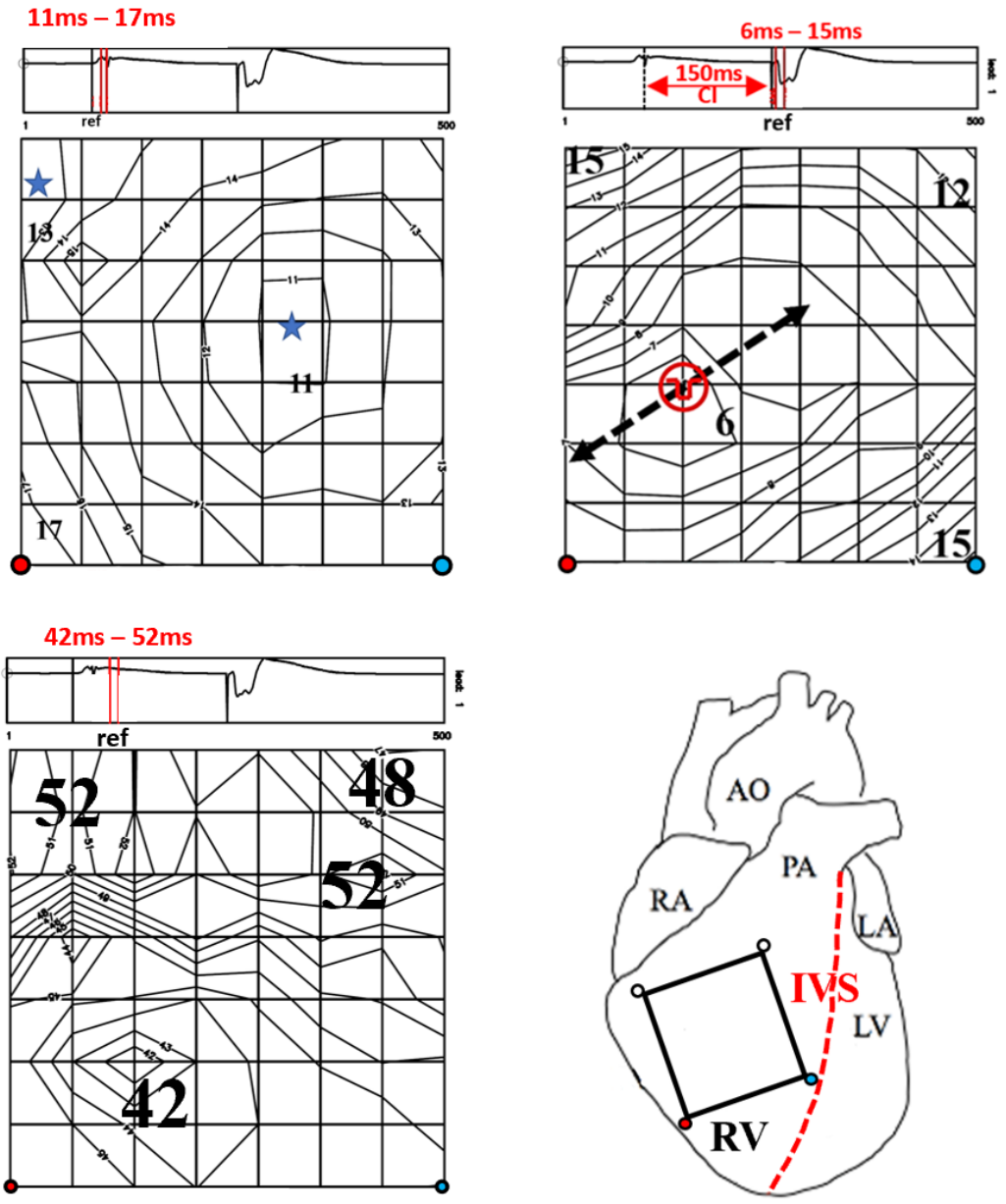

Figure 58: upper left panel: activation isochrone map of sinus beat.
Upper right panel: activation isochrone map of stimulated beat (S: 100 µA, I: 150 ms) through epicardial test site c27 of the experiment 11.
Lower left panel: recovery isochrone map of sinus beat.
Lower right panel: representation of the position of the electrode array on the ventricular epicardium: AO, aorta; RA, right atrium; LA, left atrium; LV, left ventricle; RV, right ventricle; IVS, interventricular septum.

In accordance with the sinus beat activation map (upper left panel), in this experiment the grid resulted positioned on part of the anterior surface of the RV; in fact, two BTPs of the RV (indicated by the blue stars) are visible. The collision at the IVS level is not visible and is localized outside the upper right corner of the matrix.

Activation during the sinus beat was extremely rapid with the entire region mapped by the grid completing its activation in just 6 ms.

The activation map of the stimulated beat (upper right panel) shows a source localized all around the stimulation point (indicated by red symbol) with short latency response (5 ms) and anisotropic propagation in accordance with the direction of the epicardial fibers (indicated by the black arrows).

The recovery pattern of sinus beat (lower left panel) shows that RT minimum resulted localized in the RV, 1 mm lower compared to the epicardial test site. Overall, RTs resulted uniform without a significant gradient.

S-I plane.

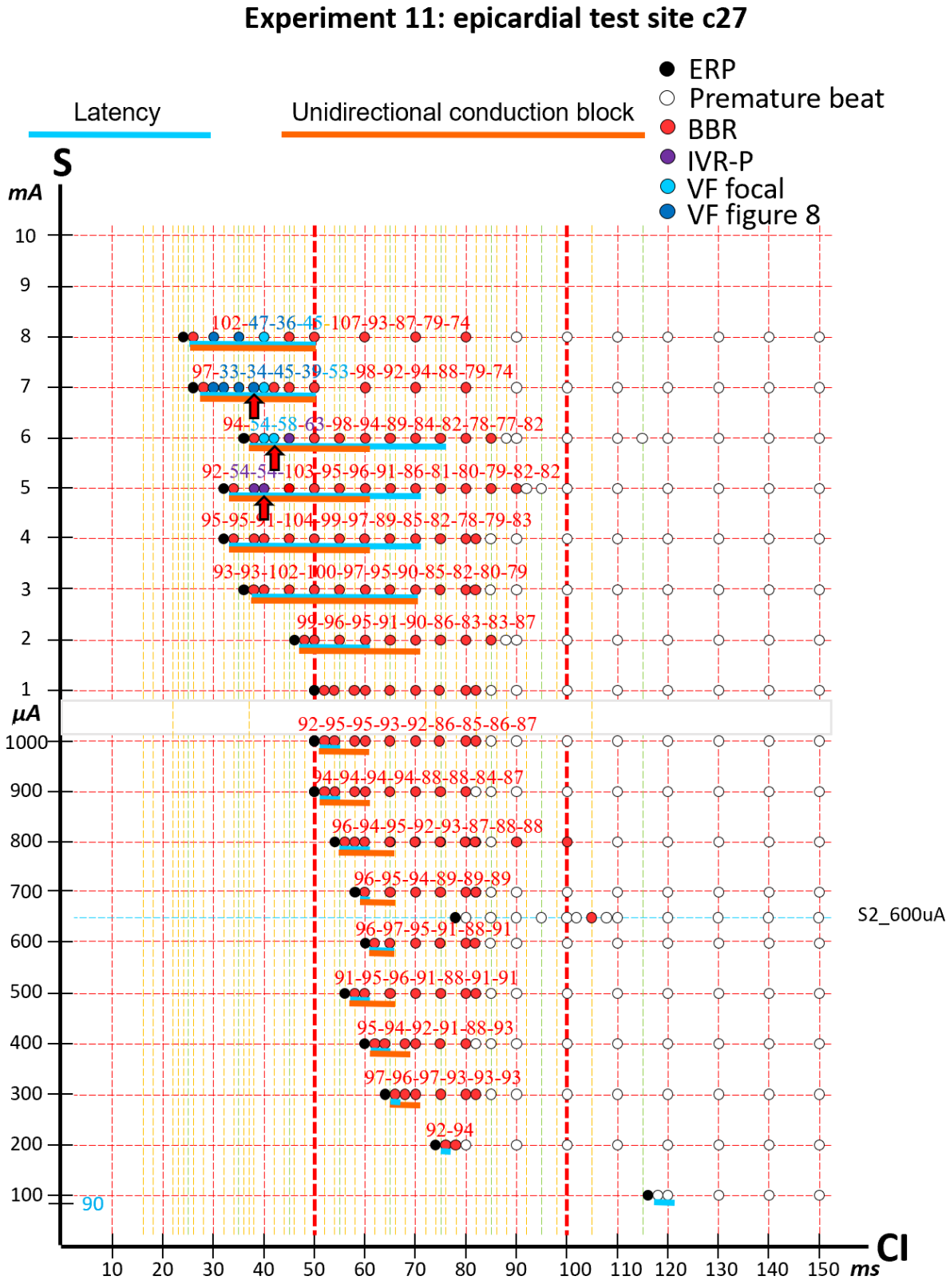

Figure 59: S-I plane of epicardial test site (electrode 27 of the grid) in the RV of the experiment 11.

The S-I plane of the epicardial test site, electrode 27 of the grid, in the RV (fig. 59) shows that ERP (black points) decreased progressively increasing the stimulation strength, with a value of 116 ms at 100 µA and a value of 24 ms at 8 mA.

BBRs were obtained from 200 µA of stimulation strength and have already been described earlier in this work (subparagraph 3.1).

IVR-Ps were obtained from 5 mA of stimulation strength.

VFs were obtained from 6 mA of stimulation strength; because the first reentry of VFs resulted characterized by two main activation patterns, one focal and the other more similar to the classic figure 8 reentry, two different colours were used to indicate the two "typologies" of VFs.

Red arrows indicate premature beats and re-entries of which activation maps will be reported in the present work.

In particular, will be shown activation isochrone maps, recovery isochrone maps and unipolar EGs of:

- VF with first reentry characterized by focal activation pattern triggered by premature stimulation (S: 6 mA, I: 42 ms), figures 60, 61 and 62.
- VF with first reentry characterized by figure 8 reentry pattern triggered by premature stimulation (S: 7 mA, I: 38 ms), figures 63, 64 and 65.

Premature stimulation (S: 6 mA, I: 42 ms).

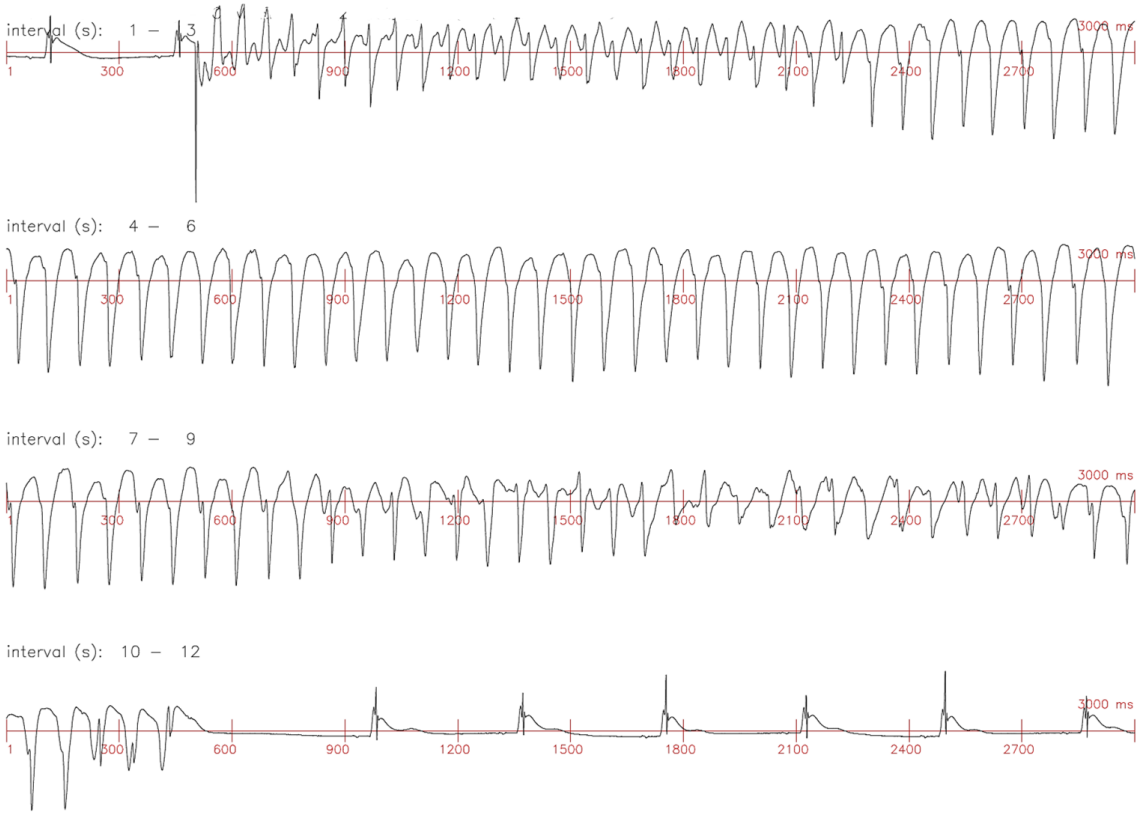

Figure 60: registration of VF triggered by premature stimulation applied with a stimulation strength of 6 mA and a coupling interval of 42 ms. Each line contains 3 seconds of registration.

Fig. 60 shows the registration of the VF triggered by premature stimulation applied during sinus rhythm with a stimulation strength of 6 mA and a coupling interval of 42 ms.
Each line contains 3 seconds.

VF triggered by premature stimulation (S: 6mA, I: 42 ms) characterized by focal pattern.

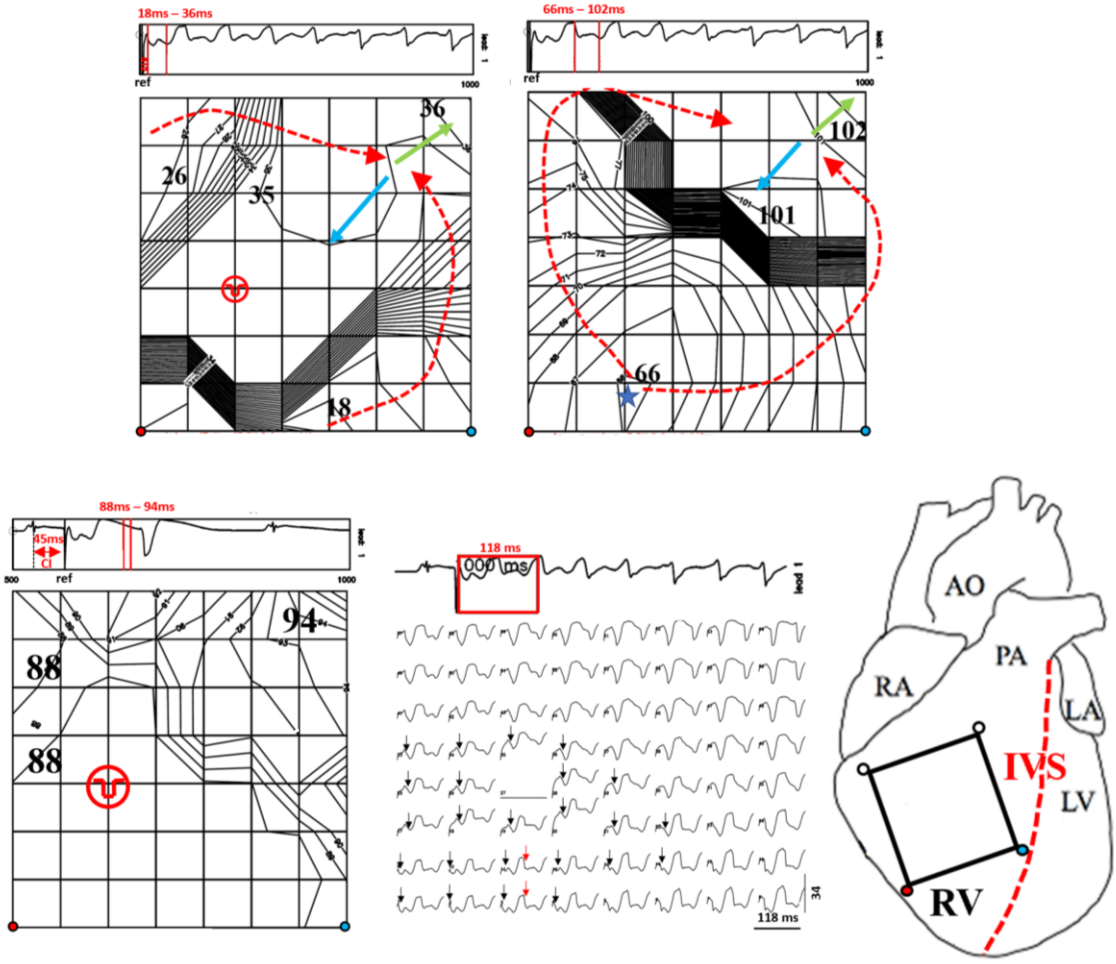

Figure 61: example of VF triggered by premature stimulation (S: 6 mA, I: 42 ms).
Upper left panel: activation isochrone map of premature beat.
Upper right panel: activation isochrone map of first reentry of VF.
Lower left panel: recovery isochrone map of premature beat (S: 5 mA, I: 45 ms).
Lower central panel: EGs map of the time interval comprising the premature beat and of the first reentry of VF.
Lower right panel: representation of the position of the electrode array on the ventricular epicardium: AO, aorta; RA, right atrium; LA, left atrium; LV, left ventricle; RV, right ventricle; IVS, interventricular septum.

The activation pattern of the premature beat (upper left panel of fig. 61) triggered by premature stimulation (S: 6 mA, I: 42 ms) shows a source localized away from the test site, outside the grid, indicating the occurrence of a graded response. UCB is clearly visible at the epicardium. From the source (not visible in the activation map), two wavefronts (red arrows) turn around the region of UCB, collide and merge after 35 ms from the instant of stimulation, activating the rest of the heart (green arrow) and not re-entering through the distal side of the block (blue arrow).

The activation pattern of the first reentry of the VF (upper right panel of fig. 61) shows a focal source in the region where UCB occurred in the activation map of the premature beat.

From the focal source (blue star), two wavefronts (red arrows) originate and turn around a region of UCB upward shifted from the pacing site. The two wavefronts collide and merge after 100 ms from the instant of stimulation and then complete the activation of the ventricles (green arrow) not re-entering through the distal portion of the UCB (blue arrow).

The recovery map (lower left panel of fig. 61) was computed for a premature beat (S: 5 mA, I: 45 ms instead of S: 6 mA, I: 42 ms) that was not followed by a short coupled reentry that induced VF. However, we assume that the premature beat (5 mA, I: 45 ms) has a similar RT distribution of the premature beat (S: 6 mA, I: 42 ms) that induced VF. The recovery map shows RTs of the same value (88 ms) in the region where block occurred in the premature beat. Around this region RTs gradually increased. Note that 88 ms RT value is likely due to the influence of far field potentials surrounding the region of graded response.

The EGs map (lower central panel of fig. 61) of time interval comprising premature beat and ~~of~~ first reentry of the VF shows that activation re-entry onset (red arrows) occurs in the region of UCB (black arrows).

UCB is characterized by EGs with slow rate of change of the intrinsic deflection.

Note that, at the epicardial level, no evident impulse reentry conduction occurs across the region of block suggesting that VF is more likely due to IVR-P rather than IVR-M.

VF triggered by premature stimulation (S: 6mA, I: 42 ms).

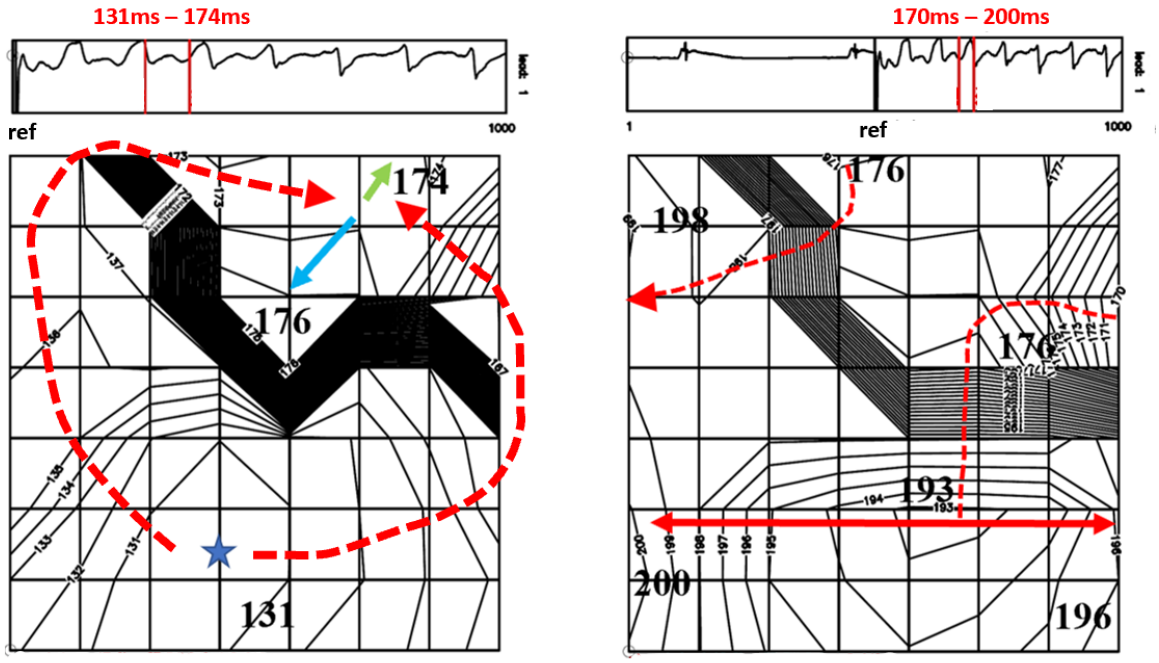

Figure 62: activation maps of second (left panel) and third (right panel) reentries of the VF triggered by premature stimulation (S: 6 mA, I: 42 ms).

The activation pattern (left panel of fig. 62) of the second reentry of the VF (triggered by premature stimulation, S: 6 mA, I: 42 ms) shows a focal source localized in the same position of the focal source of the first reentry (fig. 61 upper right panel). From the focal source (blue star), two wavefronts (red arrowed dotted arrows) have origin and then turn around another UCB. The two wavefronts collide after 173 ms from the instant of stimulation and then complete the activation of the heart (green arrow) and try to re-enter through the distal portion of the UCB (blue arrow).

The activation map of the third reentry (right panel of fig. 62) shows that the figure 8 reentry attempt, seen in the left panel, is successful. Thus, right panel of fig. 62 shows the end of the second reentry and the beginning of the third reentry of the VF.

Hence, maps shown above suggest that IVR-Ps may act as further premature stimuli (first and second reentries would correspond, in this case, to S2 and S3) and favour the development of figure 8 reentries and of VF.

Premature stimulation (S: 7mA, I: 38 ms).

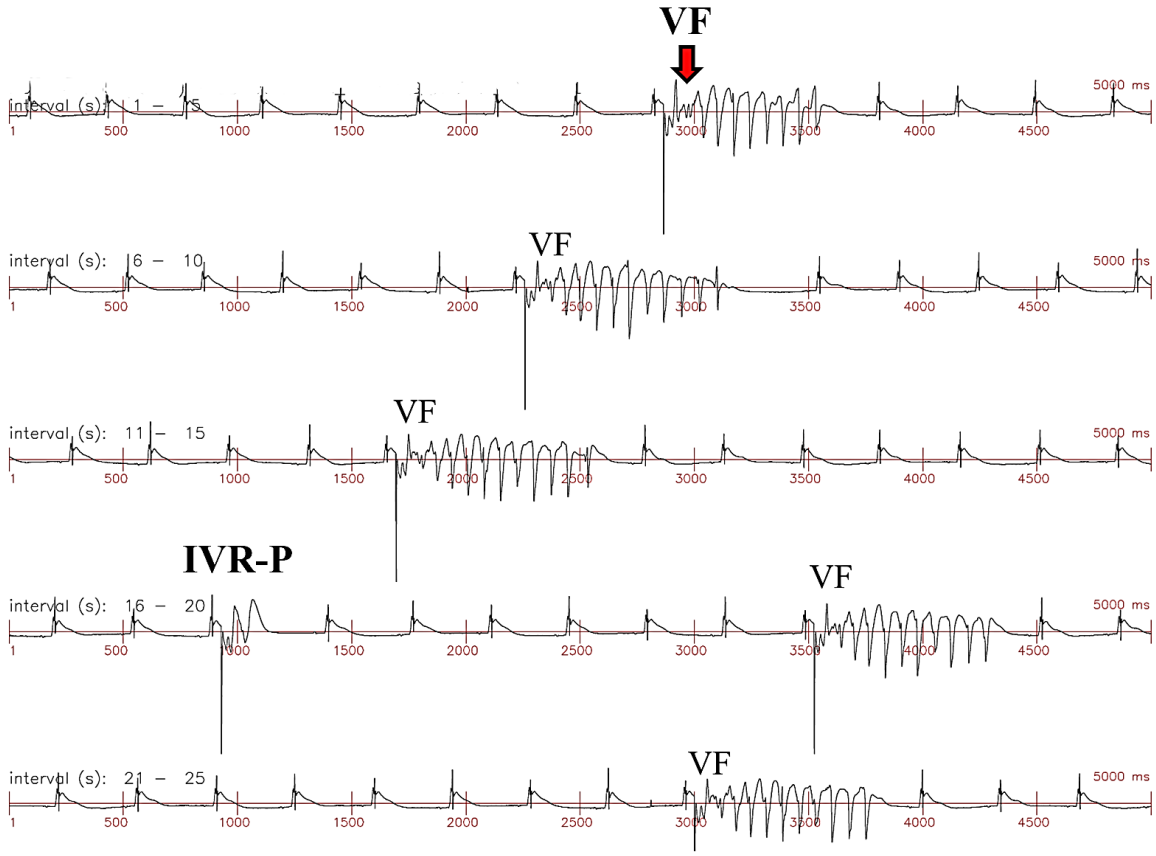

Figure 63: registration of VFs and IVR-P triggered by premature stimulations applied with a stimulation strength of 7 mA and a coupling interval of 38 ms. Each line contains 5 seconds of registration.

Fig. 63 shows the arrhythmias induced by premature stimulations applied through epicardial test site c27 in the RV with a stimulation strength of 7 mA and a coupling interval of 38 ms; VFs and IVR-P arrhythmias were induced.

Red arrow of fig. 63 indicate premature beat and VF re-entries of which activation maps and EGs map will be reported in the present work.

VF triggered by premature stimulation (S: 7mA, I: 38 ms) characterized by figure 8 pattern.

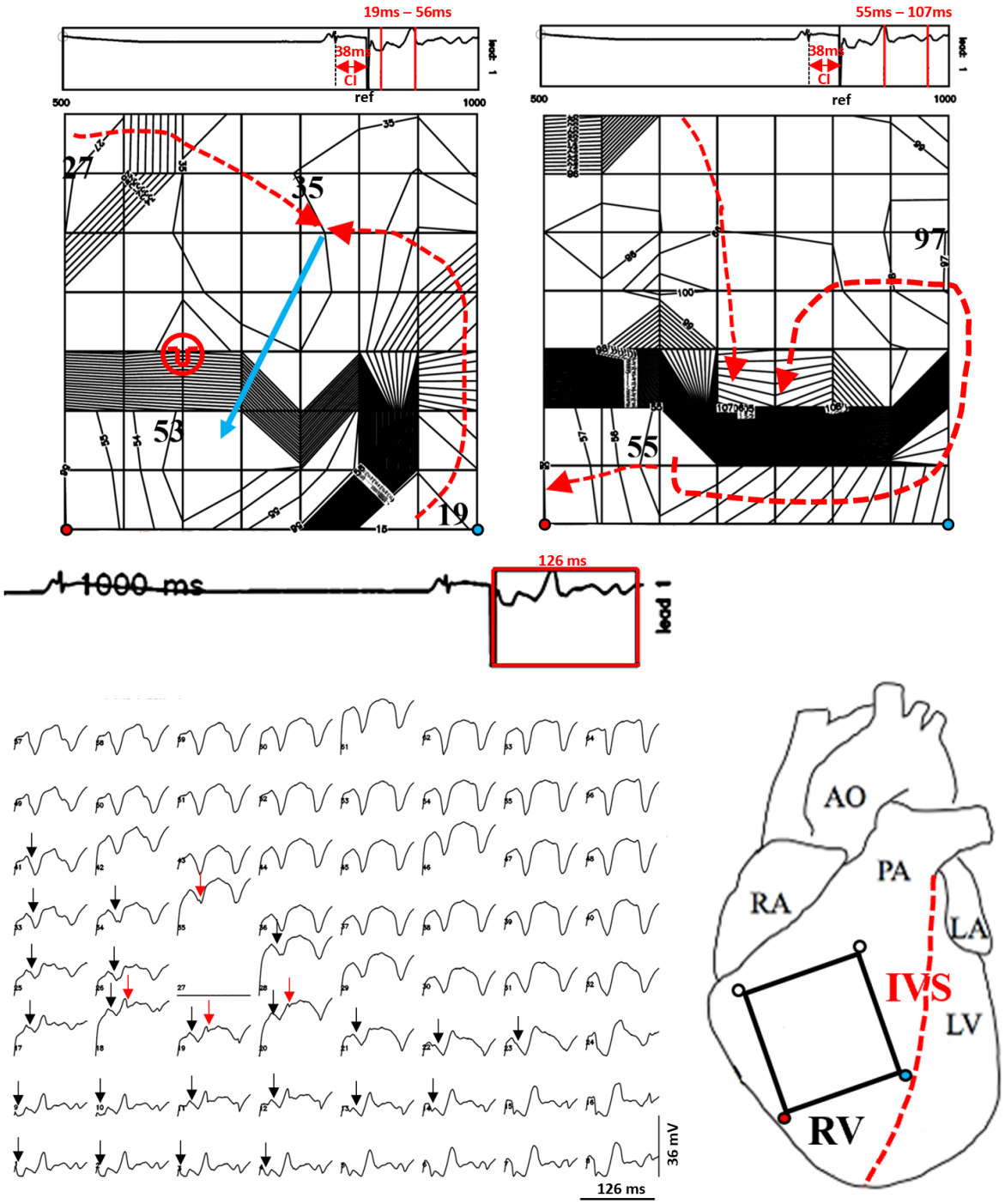

Figure 64: example of VF triggered by premature stimulation (S: 7 mA, I: 38 ms).
Upper left panel: activation isochrone map of premature beat.
Upper right panel: activation isochrone map of first reentry of VF.
Lower left panel: EGs map of premature beat and of first reentry of VF.
Lower right panel: representation of the position of the electrode array on the ventricular epicardium: AO, aorta; RA, right atrium; LA, left atrium; LV, left ventricle; RV, right ventricle; IVS, interventricular septum.

The activation pattern of the premature beat (upper left panel of fig. 64) triggered by premature stimulation (S: 7 mA, I: 38 ms) shows a source localized away from the test site, outside the grid, indicating the development of the graded response. UCB is clearly visible in the epicardium. From the source (not visible in the activation map), two wavefronts (red arrows) turn around the UCB, collide after 35 ms from the instant of stimulation and then attempt to re-enter through the distal side of the UCB (blue arrow). Figure 8 reentry is successful, and it is completed after 53 ms from the instant of stimulation. Note that figure 8 reentry is completed in the same position in which in the VF previously shown (fig. 62, right panel) there was the focal source of its first reentry.

Note that figure 8 reentry is completed more quickly than the IVR-P (53 ms vs 66 ms) shown above (fig. 62).

The activation pattern of the first reentry of the VF (upper right panel of fig. 64) is almost identical to the premature beat.

The EGs map (lower left panel of fig. 64) of premature beat and of the first reentry of the VF shows all the elements of a figure 8 reentry occurring at the epicardial level. Particularly, black arrows indicate the points of the tissue which resulted refractory (blocked) during the premature beat activation (EGs with weak intrinsic deflection), while red arrow at the electrode 35 indicates the last activation at the level of the distal side of the UCB and red arrows at electrodes 18, 19 and 20 indicate the first re-activations of the proximal side of the UCB.

Note that the graded conduction clearly visible in this EGs map is completely absent in the EGs map of the VF obtained at lower intensity (6 mA vs 7 mA) and previously shown (fig. 61, lower central panel).

Hence, the example just reported shows how IVR-P is able to lower the VF threshold compared to IVR-M.

VF triggered by premature stimulation (S: 7mA, I: 38 ms).

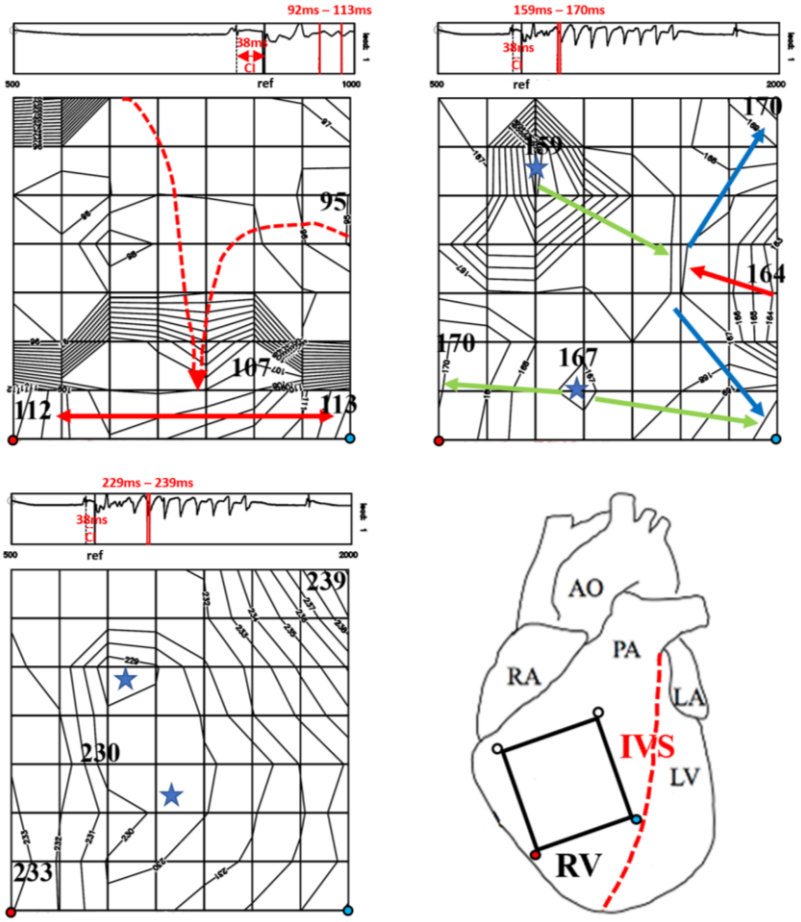

Figure 65: activation maps of second (upper left panel), third (upper right panel) and fourth (lower left panel) reentries of the VF triggered by premature stimulation (S: 7 mA, I: 38 ms).
Lower right panel: representation of the position of the electrode array on the ventricular epicardium: AO, aorta; RA, right atrium; LA, left atrium; LV, left ventricle; RV, right ventricle; IVS, interventricular septum.

The activation map (upper left panel of fig. 65) shows the final part of the first reentry of the VF, whose initial part was shown in fig. 64 (upper right panel).

The activation map of the second reentry of the VF (upper right panel of fig. 65) shows a wavefront (red arrow) entering in the grid, after 164 ms from the instant of stimulation, which likely is the continuation of the wavefront leaving the grid, after 113 ms from stimulation instant, in the upper left panel. Two BTPs are also visible (blue stars), arising after 159 ms and 167 ms from the instant of stimulation.

The activation map of the third reentry of the VF (lower left panel of fig. 65) shows two BTPs (blue stars) visible at the centre of the grid. Note that these two BTPs are almost in the same position of the two BTPs visible in the upper right panel.

BTPs of second and third reentries may therefore indicate a role of the Purkinje system in the maintenance of VF.

3.5. VFs induced by endocardial premature stimulation applied in the RV.

In figure 66 are shown activation isochrone map and recovery isochrone map of sinus beat, activation isochrone map of stimulated beat at long coupling interval (S: 600 µA, I: 150 ms) and isopotential map of stimulated beat (S: 100 µA, I: 150 ms) through the endocardial test site in the RV of the experiment 15.

Sinus beat and stimulated beat (S: 100 µA, I: 150 ms).

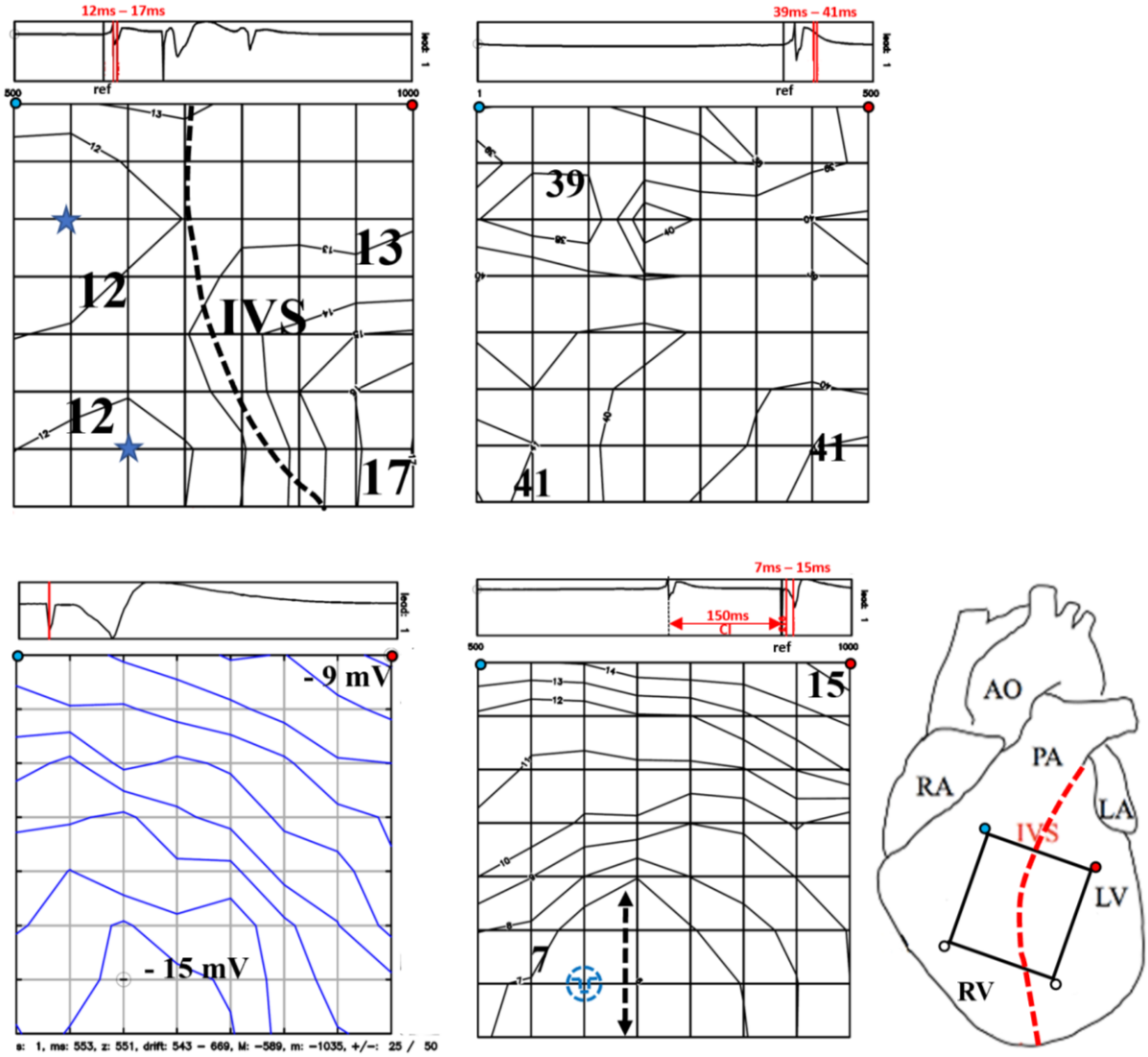

Figure 66. Upper panel: activation isochrone map (left panel) and recovery isochrone map (right panel) of sinus beat of the experiment 15.
Lower left panel: isopotential map of endocardial stimulus artifact (S: 100 µA, I: 150 ms).
Lower central panel: activation isochrone map of diastolic premature stimulation (S: 600 µA, I: 150 ms) through endocardial electrode.
Lower right panel: representation of the position of the electrode array on the ventricular epicardium: AO, aorta; RA, right atrium; LA, left atrium; LV, left ventricle; RV, right ventricle; IVS, interventricular septum.

In experiment 15 the grid is positioned on part of the anterior surface of the RV and of the LV. Two BTPs of the RV (blue stars) and activation from the LV are visible in the sinus beat activation map (fig. 66, upper left panel). The wave fronts progressing from RV and LV collide in the region of the epicardial projection of septum (dashed line).

Activation during the sinus beat was completed in 5 ms.

The sinus beat recovery time map (fig. 66, upper right panel), shows absence of enhanced RT gradient (39-41 ms).

The isopotential map (lower left panel of fig. 66) of endocardial stimulus artifact identifies on the epicardial surface the position of the endocardial test site corresponding with the position of potential minimum. Hence, the endocardial test site is localized close to lower RV BTP of the sinus beat.

The activation isochrone map of the premature beat (lower central panel of fig. 66) shows a source localized all around the endocardial test side (blue symbol) with low response latency (7 ms) and anisotropic propagation in accordance with the direction of the endocardial fibers (indicated by the black arrows). The entire region mapped by the grid is activated in 8 ms.

S-I plane.

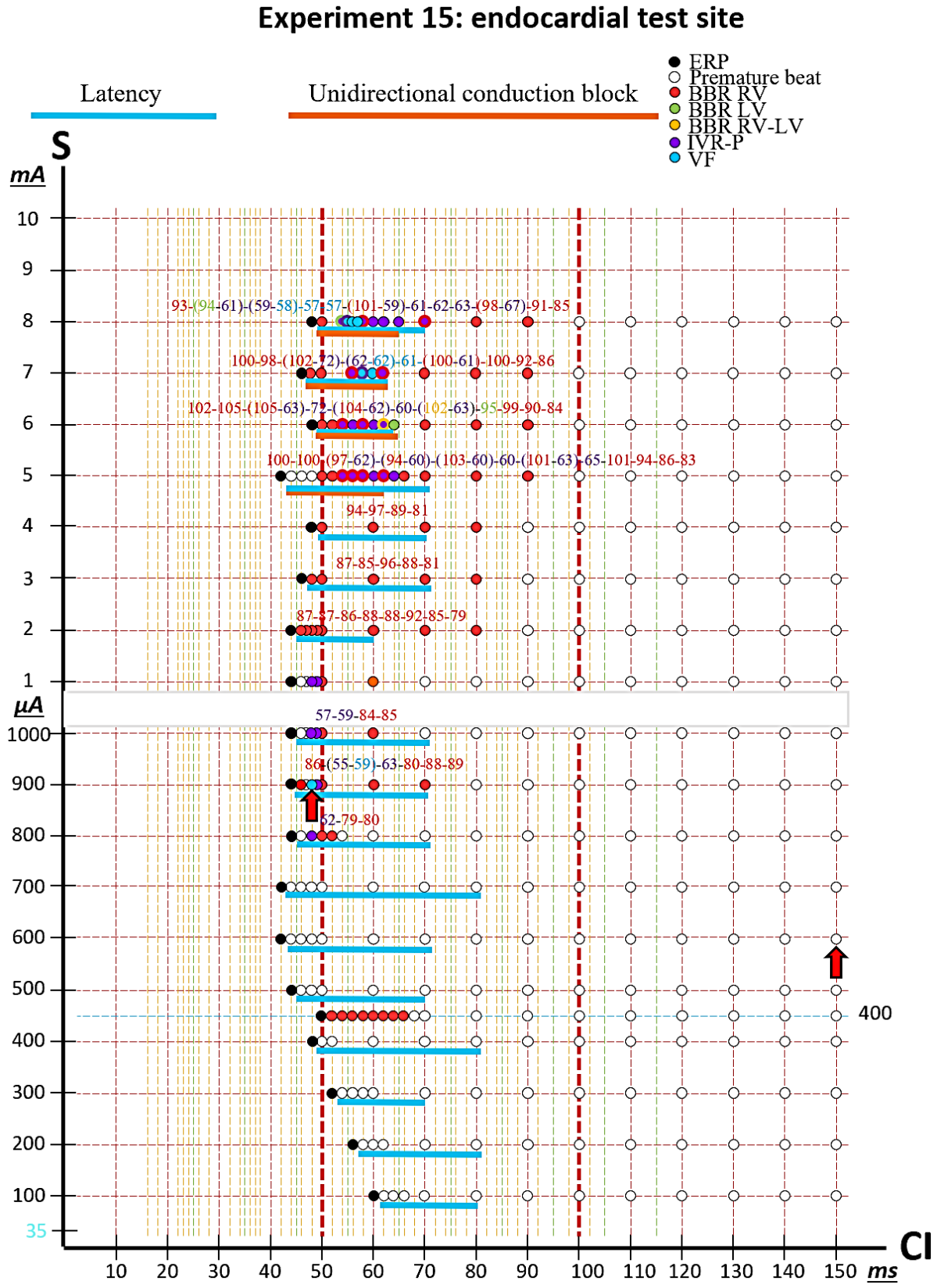

Figure 67: S-I plane of the endocardial test site in the RV of the experiment 15.

The S-I plane of the endocardial test site in the RV (fig. 67) shows that ERPs (black points) were almost constant with the increase of the stimulation strength, with a longest value of 60 ms at 100 µA and a thresholds value of 42 ms at 600 µA, 700 µA and 5 mA.

BBRs initially occurred at 800 µA of stimulation strength and consistently occurred at all higher stimulation strengths. Most of them were BBR with anterograde conduction in the RV (LBBB pattern) and are indicated by red points. More rarely, from 6 mA of stimulation strength, BBR with anterograde conduction in the LV (RBBB pattern, indicated by green points) and BBR with anterograde conduction in both LV and RV (indicated by yellow point and consistently repeated at this coupling interval) were also obtained.

IVR-Ps were initially obtained at 800 µA of stimulation strength. Note that IVR-Ps did not occur from 2 mA to 4 mA, while they occurred again initiating at 5 mA but, as it will be shown, with a different activation pattern.

VFs occurred only once at 900 µA and then occurred again initiating at 7 mA of stimulation strength.

Red arrows indicate premature beats and re-entries of which activation maps, recovery maps and EGs maps will be reported in the present work.

In particular, activation isochrone maps and unipolar EGs of the VF induced at low stimulation strength (S: 900 µA, I: 48 ms), will be shown in figures 68 and 69.

Premature stimulation (S: 900 µA, I: 48 ms).

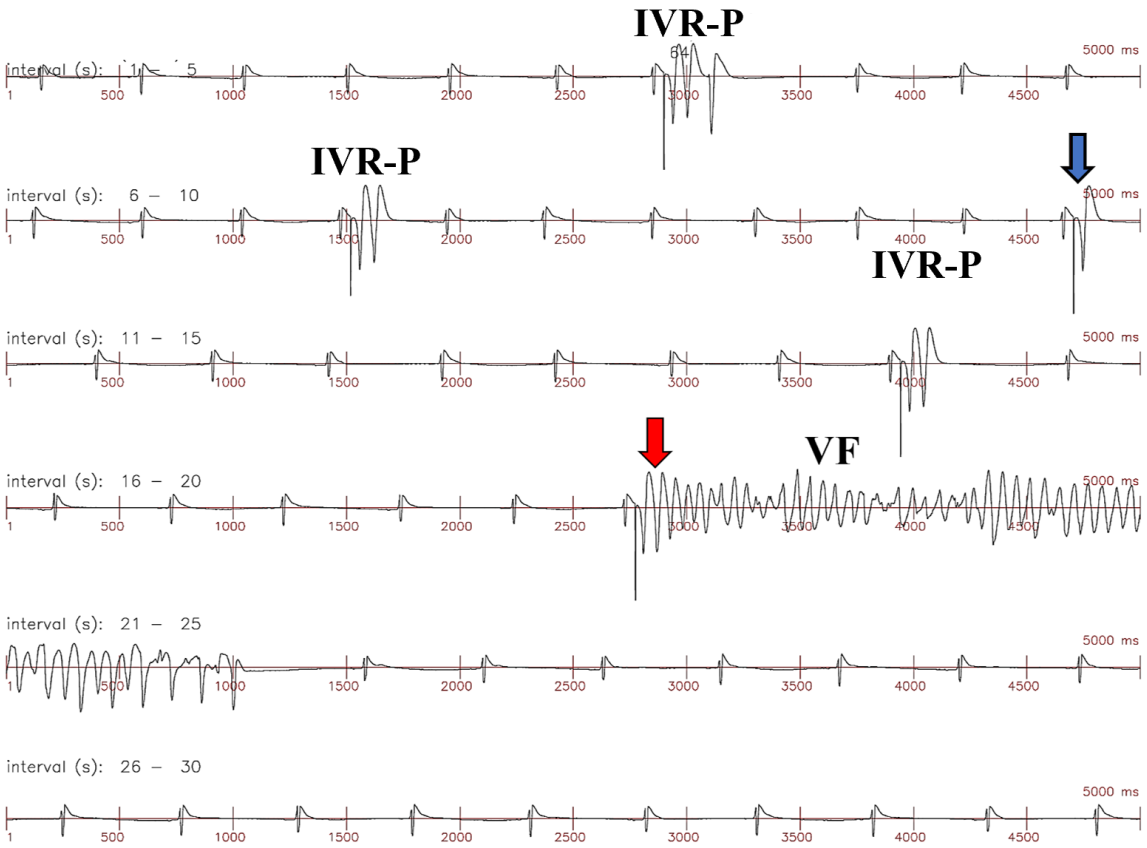

Figure 68: registration of IVR-Ps and VF triggered by premature stimulations applied with a stimulation strength of 900 µA and a coupling interval of 48 ms. Each line contains 5 seconds of registration.

Red arrows of fig. 68 indicate premature beats, IVR-P and first reentries of VF whose activation and recovery maps will be reported in the present work.

Note that only one premature stimulation (tenth second of the registration) failed to induce arrhythmias.

Premature stimulations with these parameters (S: 900 µA, I: 48 ms) were successively applied again for over 30 seconds and while IVR-Ps were successfully induced again with consistency, no other VFs were induced again.

These results suggest that IVR-Ps in critical circumstances may degenerate into VF and lower the threshold for its occurrence.

IVR-P and VF triggered by premature stimulation (S: 900 µA, I: 48 ms).

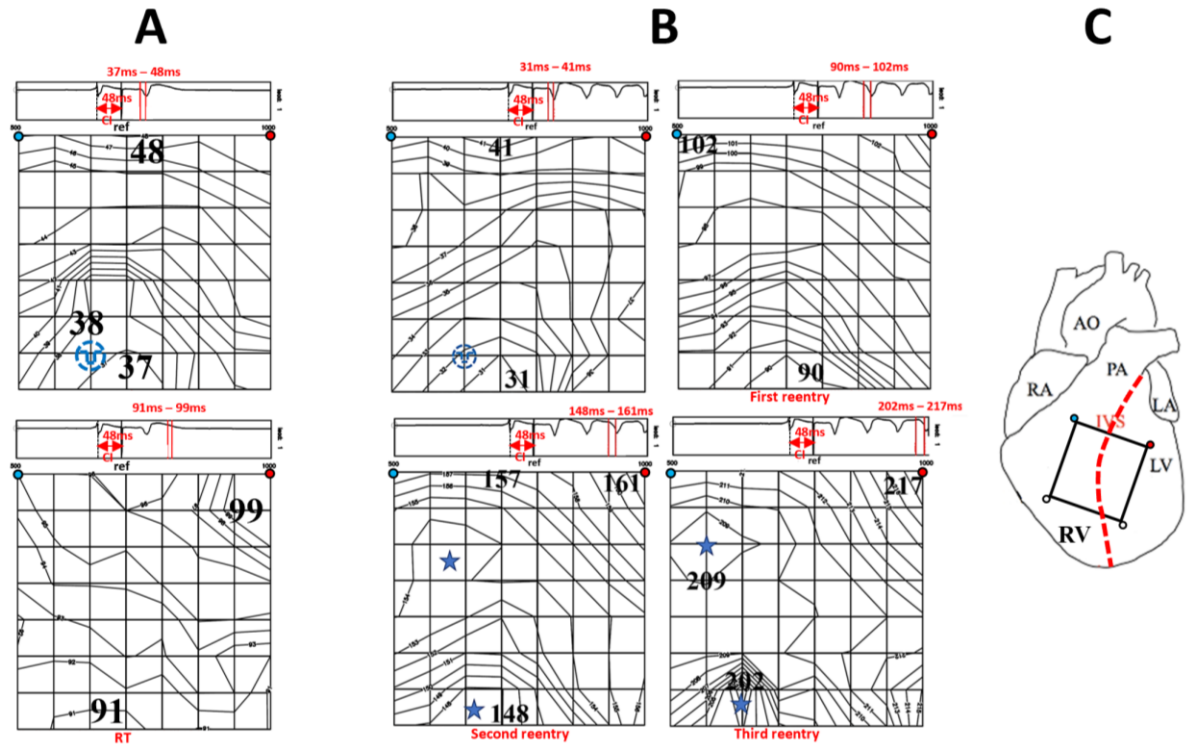

Figure 69.
A. Upper panel: activation isochrone map of endocardial RV premature beat not followed by re-entry (S: 900 µA, I: 48 ms, blue arrow in fig 68). Lower panel: recovery isochrone map of endocardial RV premature beat not followed by re-entry (S: 900 µA, I: 48 ms)
B. Upper left panel: activation isochrone map of endocardial RV premature beat followed by re-entry and VF (S: 900 µA, I: 48 ms, red arrow in fig. 68). Upper right panel: activation isochrone map of the first reentry of VF. Lower left panel: activation isochrone map of the second reentry of VF. Lower right panel: activation isochrone map of the third reentry of VF.
C. Representation of the position of the electrode array on the ventricular epicardium: AO, aorta; RA, right atrium; LA, left atrium; LV, left ventricle; RV, right ventricle; IVS, interventricular septum.

The activation pattern of endocardial RV premature beat not followed by re-entry in Fig. 69 A, upper panel (S: 900 µA, I: 48 ms, blue arrow in Fig. 68) shows a wave front crossing at 37 ms the lower grid side, close to the epicardial projection of the endocardial pacing site (blue dashed symbol). The long activation latency of 37 ms suggests the occurrence of graded response around the endocardial pacing site before onset of activation at distance from the pacing site. Earlier activation at 38 ms near the center of the grid is likely due to activation from the underlying conducting system. The entire region mapped by the grid was activated in 11 ms. In addition, no region of conduction block is present at the epicardium during activation.

Fig. 69 A, lower panel, shows the RT distribution of the endocardial RV premature beat not followed by re-entry (upper panel). Earliest RT occurs at 91 ms, at the region of earliest activation, where the activation-recovery interval is 54 ms. Hence, the recovery pattern is

similar to the activation pattern with no enhanced RT gradient in the region of the electrode array.

The activation pattern of endocardial RV premature beat followed by reentry and VF displayed in Fig. 69 B, upper left panel (S: 900 μA, I: 48 ms, red arrow in Fig. 68) shows a wave front crossing at 31 ms the lower grid side, close to the epicardial projection of the endocardial pacing site (blue dashed symbol). Interestingly, 31 ms activation latency, that occurred only once, is, however, 6 ms shorter than activation latency induced by numerous repetitive premature stimulations at the same (48 ms) or shorter (46 ms) coupling intervals (S-I plane in fig. 67, S: 900 μA). The entire region mapped by the grid was activated within 10 ms with no evident sign of conduction block at the epicardium. The premature beat was followed by multiple re-entries and VF.

The activation pattern of the first reentry beat (Fig. 69 B, upper right panel) shows a wave front entering the grid after 90 ms from the instant of stimulation, where earliest activation occurred for the premature beat. The activation pattern of the first reentry is very similar to that of the premature beat. If we assume that the activation-recovery interval of the premature beat at the early site of activation is 54 ms, as for the premature beat in Fig. 69 A, then the AT1-AT2 interval of 59 ms is consistent with an early reactivation at the same site from a PMJ of a terminal Purkinje fiber (IVR-P).

The activation pattern of the second reentry (Fig. 69 B, lower left panel) shows two BTPs (blue stars) localized in the same region of the two sinus BTPs in the RV (Fig. 67). The earliest BTP occurs at 148 ms while the second at 154 ms from the stimulus. The AT2-AT3 activation interval was 58 ms at the site of earliest activation.

The activation pattern of the third reentry (Fig. 69 B, lower right panel) shows two BTPs localized in a similar position of the two BTPs of the second reentry. The earliest BTP occurs at 202 ms, while the other at 209 ms from the instant of stimulation. The AT3-AT4 activation interval was 55 ms.

These findings suggest that activation latency of 31 ms represents a critical value for inducing multiple reentries of the IVR-P type followed by VF (Fig. 68). The critical value occurred only once in the vulnerable domain of the S-I plane comprised by S=800-1000 μA and I=46-48 ms (Fig. 67) All other stimulations in this vulnerable domain were followed only by one or multiple reentries.

Hence, it can be speculated that, in some instances, the initial reentry beats act like "premature stimulus equivalents" (i.e. S2, S3, S4) aiding the emergence of sustained ventricular tachyarrhythmias.

Overall, VFs were induced through 31 of the 33 test sites in the RV.
Mean AT1-AT2 of VFs induced through premature stimulation in the RV resulted equal to 54,4 ms (SE = 1.7).
VFs were induced through 22 of the 22 epicardial test sites in the RV and their mean AT1-AT2 interval resulted equal to 50,5 ms (SE = 1.9).
VFs were induced through 9 of the 11 endocardial test sites in the RV and their mean AT1-AT2 interval resulted equal to 56,4 ms (SE = 3.3).
Note that the two endocardial test sites which did not succeed to trigger VF were positioned in the RV free wall, externally to the portion mapped by the grid, while all the endocardial test sites positioned in the portion of RV below the grid were able to induce VF.
VFs were induced through 5 of the 13 test sites in the LV.
Mean AT1-AT2 of VFs induced through premature stimulation in the LV resulted equal to 59,5 ms (SE = 9.1).
VFs were induced through 3 of the 6 epicardial test sites in the LV and their mean AT1-AT2 interval resulted equal to 45,1 ms (SE = 5.2).
VFs were induced through 2 of the 7 endocardial test sites in the LV and their mean AT1-AT2 interval resulted equal to 73,9 ms (SE = 15.9).
VFs resulted characterized by a first reentry with two possible patterns: focal pattern and figure 8 reentry pattern. VFs with focal pattern were consistently the first to be induced with each test site and were replaced by VFs with figure 8 reentry pattern at higher stimulation strength for the same test site.
This result suggests that IVR-P is able to lower VF threshold, compared to IVR-M.
At the same time IVR-Ms are characterized by circuits with shorter AT1-AT2. Hence, when the IVR-M circuit becomes available (higher stimulation strength) it anticipates the IVR-P and for this reason at higher stimulation strength VFs with figure 8 reentry pattern were typically obtained.
VFs resulted characterized by slightly lower mean value of AT1-AT2 interval (54,4 ms vs 61,2 ms for the RV, 59,5 ms vs 65,3 ms). This result seems to suggest that when IVRs become extremely short coupled, they can degenerate in VF.

3.6. Statistical results.

This paragraph presents assessment of ventricular arrhythmia vulnerability by quantitative evaluation of critical stimulation parameters, identified by stimulus strength and coupling interval coordinates, in the strength-interval plane of all test sites.

Premature stimulation applied during sinus rhythm in normal rat hearts induced repetitive ventricular responses and tachyarrhythmias. In particular, the mean values of critical stimulation parameters are computed for stimuli that induce repetitive ventricular responses (BBRs, IVRs) and tachyarrhythmias (VFs) as well as for stimuli that create conditions favouring arrhythmia induction, such as local stimulus response latency, UCB and AT1-AT2 intervals. In essence, critical stimulation parameters define the lower limit, or threshold, of vulnerability for the induction of the corresponding event.

All test sites are divided into eight groups:

a. epicardial in the RV, b. endocardial in the RV, c. epicardial in the LV, d. endocardial in the LV, e. RV total (which includes all the test sites in the RV), f. LV total (which includes all the test sites in the LV), g. Epi total (which includes all the epicardial test sites), h. Endo total (which includes all the endocardial test sites).

Overall, in the 17 experiments, considered test sites are: 22 epicardial in the RV, 11 endocardial in the RV, 6 epicardial in the LV and 7 endocardial in the LV.

Repetitive ventricular responses that occurred in the present study include BBRs and IVRs:

- BBRs are non-sustained reentry arrhythmias whose circuit comprehends the branches of conducting system and myocardium of both ventricles whose epicardial activation patterns are characterized by BTPs in the same position of sinus BTPs.
- IVRs are non-sustained reentry circuits that occur in the same ventricle and are characterized by focal (IVR-P) or figure 8 (IVR-M) activation patterns.

  IVR-P, displaying BTPs often localized in positions different from sinus BTPs, is likely characterized by a reentry circuit comprising terminal Purkinje system and myocardium of the stimulated ventricle.

  IVR-M is characterized by a reentry circuit comprising local myocardium of the stimulated ventricle.

Premature beats followed by tachyarrhythmias (VFs) were characterized by a first reentry with two possible activation patterns (focal or figure 8) due to different intraventricular (IVR) reentry circuits. Precisely:

- VF with first focal reentry, likely due to a reentry circuit comprising terminal Purkinje system and myocardium of the stimulated ventricle, characterized by activation patterns with BTPs often localized in positions different from sinus BTPs.
- VF with first figure 8 reentry, due to a reentry circuit comprising local myocardium of the stimulated ventricle.

1) BBR induction thresholds.

In the RV, BBRs were induced in 22 of the 22 epicardial test sites with threshold stimuli characterized by strength = 2,050 µA (SE = 687.1) and coupling interval = 84 ms (SE = 3.3). BBRs were induced at 10 of the 11 endocardial test sites with threshold stimuli characterized by strength = 790 µA (SE = 402.9) and coupling interval = 100 ms (SE = 4).

In the LV, BBRs were induced at 3 of the 6 epicardial test sites with threshold stimuli characterized by strength = 4,825 µA (SE = 1731.3) and coupling interval = 84 ms (SE = 18.75).

BBRs were induced through 4 of the 7 endocardial test sites in the LV and the mean threshold stimulation strength for their induction was found to be equal to 3080 µA (SE = 993.2); the mean longest RW-S coupling interval capable of inducing BBRs resulted equal to 79 ms (SE = 12.9).

Mean stimulation strength and coupling interval thresholds for BBRs induction will be shown in figure 70.

Mean BBRs induction thresholds.

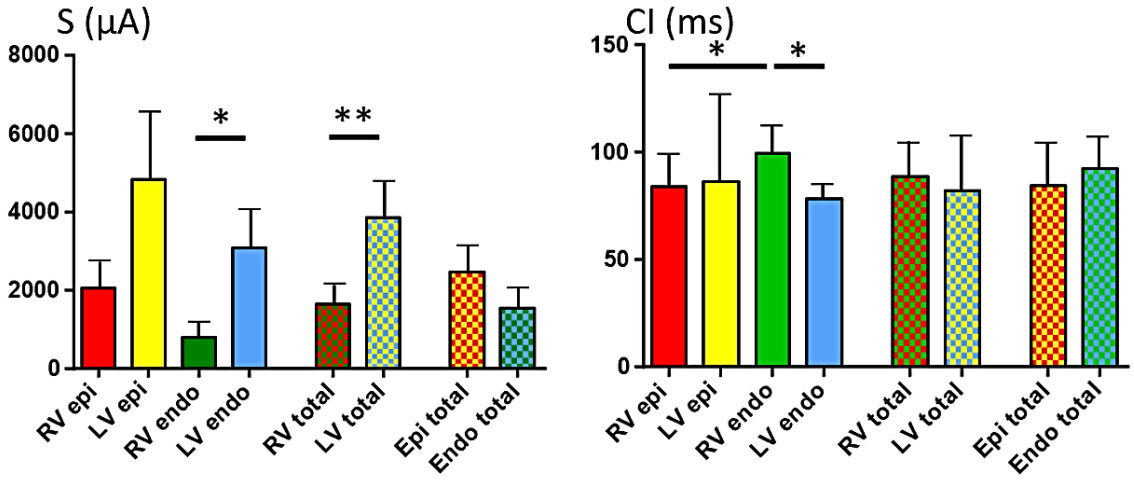

Figure 70. Left panel: mean stimulation strength thresholds for BBRs induction. Right panel: mean coupling interval thresholds for BBRs induction.

Endocardial test sites in the RV resulted characterized by a significant (p.<0,05) lower mean stimulation threshold compared to endocardial test sites in the LV.

Test sites in the RV showed a significant (p.<0,01) lower mean stimulation threshold compared to test sites in the LV.

Epicardial test sites in the RV resulted characterized by a significant (p.<0,05) lower mean coupling interval threshold compared to endocardial test sites in the RV.

Endocardial test sites in the LV resulted characterized by a significant (p.<0,05) lower mean coupling interval threshold compared to endocardial test sites in the RV.

2) IVR induction thresholds.

IVRs were induced through 19 of the 22 epicardial test sites in the RV and the mean threshold stimulation strength for their induction was found to be equal to 4271 µA (SE = 442.8); the mean longest RW-S coupling interval capable of inducing IVRs resulted equal to 59 ms (SE = 2.8).

IVRs were induced through 10 of the 11 endocardial test sites in the RV and the mean threshold stimulation strength for their induction was found to be equal to 2420 µA (SE = 506.35); the mean longest RW-S coupling interval capable of inducing IVRs resulted equal to 62 ms (SE = 3.9).

IVRs were induced through 3 of the 6 epicardial test sites in the LV and the mean threshold stimulation strength for their induction was found to be equal to 6333 µA (SE = 1666.7); the mean longest RW-S coupling interval capable of inducing IVRs resulted equal to 47 ms (SE = 7.7).

IVRs were induced through 6 of the 7 endocardial test sites in the LV and the mean threshold stimulation strength for their induction was found to be equal to 6333 µA (SE = 1054.1); the mean longest RW-S coupling interval capable of inducing IVRs resulted equal to 67 ms (SE = 3.65).

Mean stimulation strength and coupling interval thresholds for IVRs induction will be shown in figure 71.

Mean IVRs induction thresholds.

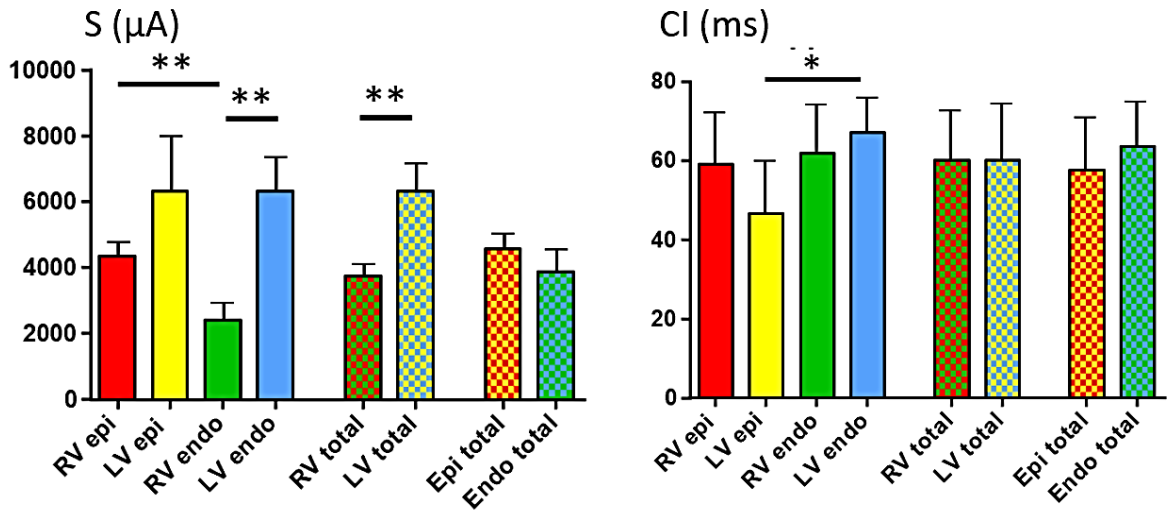

Figure 71. Left panel: mean stimulation strength thresholds for IVR induction.
Right panel: mean coupling interval thresholds for IVR induction.

Endocardial test sites in the RV resulted characterized by a significant (p.<0,01) lower mean stimulation strength threshold compared to endocardial test sites in the LV and to epicardial test sites in the RV.

Test sites in the RV showed a significant (p.<0,01) lower mean stimulation strength threshold compared to test sites in the LV.

Epicardial test sites in the LV resulted characterized by a significant (p.<0,05) lower mean coupling interval threshold compared to endocardial test sites in the LV.

3) VFs induction thresholds.

VFs were induced through all 22 epicardial test sites in the RV and the mean threshold stimulation strength for their induction was found to be equal to 5000 µA (SE = 354.3); the mean longest RW-S coupling interval capable of inducing VFs resulted equal to 51 ms (SE = 2.7).

VFs were induced through 9 of the 11 endocardial test sites in the RV and the mean threshold stimulation strength for their induction was found to be equal to 4544 µA (SE = 949.7); the mean longest RW-S coupling interval capable of inducing VFs resulted equal to 54 ms (SE = 2.8).

Note that VF was not induced through the two endocardial test sites localized in the RV free wall, while all the 9 endocardial test sites localized in the RV anterior face were able to induce VF.

VFs were induced through 3 of the 6 epicardial test sites in the LV and the mean threshold stimulation strength for their induction was found to be equal to 8333 µA (SE = 881.9); the mean longest RW-S coupling interval capable of inducing VFs resulted equal to 33 ms (SE = 3.7).

VFs were induced through 2 of the 7 endocardial test sites in the LV and the mean threshold stimulation strength for their induction was found to be equal to 8500 µA (SE = 2121.3); the mean longest RW-S coupling interval capable of inducing VFs resulted equal to 72 ms (SE = 12).

Mean stimulation strength and coupling interval thresholds for VFs induction will be shown in figure 72.

Mean VFs induction thresholds

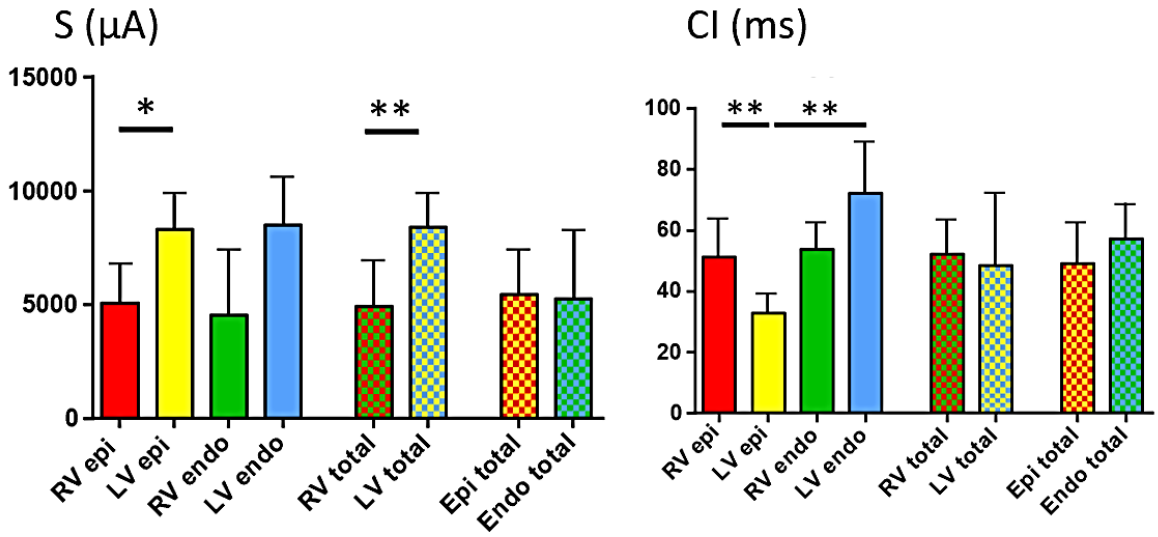

Figure 72. Left panel: mean stimulation strength thresholds for VFs induction. Right panel: mean coupling interval thresholds for VFs induction.

Epicardial test sites in the RV resulted characterized by a significant (p.<0,05) lower mean stimulation strength threshold compared to epicardial test sites in the LV.

Test sites in the RV resulted characterized by a significant (p.<0,01) lower mean stimulation strength threshold compared to test sites in the LV.

Epicardial test sites in the LV resulted characterized by a significant (p.<0,01) lower mean CI threshold compared to epicardial test sites in the RV and to endocardial test sites in the LV.

Mean stimulation strength thresholds for the induction of the three main categories of arrhythmias above discussed were statistically compared in RV and LV, as shown in figure 73.

Mean stimulation strength for arrhythmias induction.

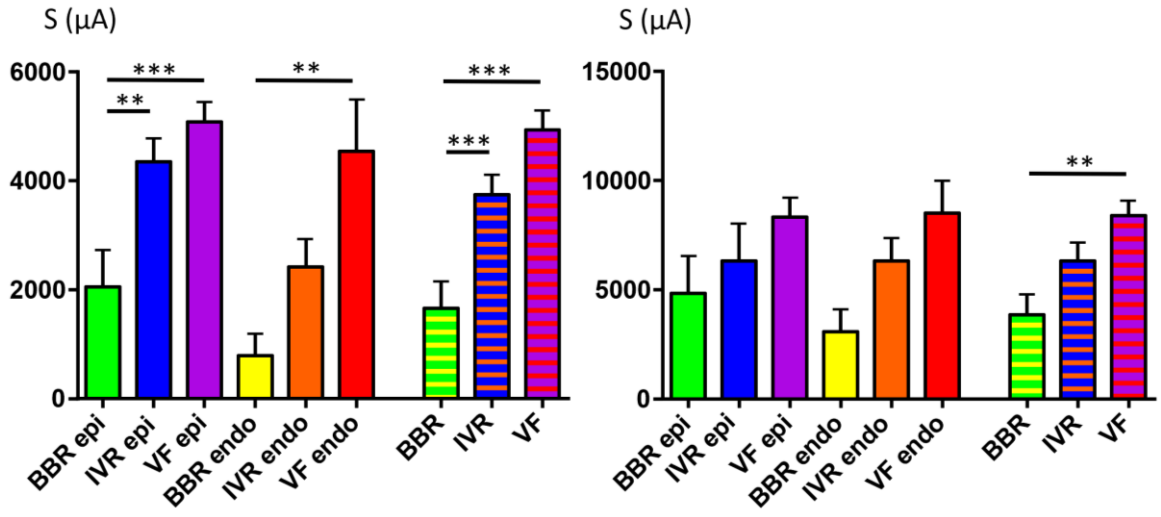

Figure 73. Left panel: mean stimulation strength thresholds for arrhythmias induction in the RV. Right panel: mean stimulation strength thresholds for arrhythmias induction in the LV.

Regarding to epicardial stimulation applied in the RV:

- BBRs resulted characterized by a significant ($p<0,01$) lower mean stimulation strength threshold compared to IVRs.
- BBRs resulted characterized by a significant ($p<0,001$) lower mean stimulation strength threshold compared to VFs.

Regarding to endocardial stimulation applied in the RV:

- BBRs resulted characterized by a significant ($p<0,01$) lower mean stimulation strength threshold compared to VFs.

Considering all the stimulations applied in the RV:

- BBRs resulted characterized by a significant ($p<0,001$) lower mean stimulation strength threshold compared to IVRs and to VFs.

Regarding to all the stimulation applied in the LV:

- BBRs resulted characterized by a significant ($p<0,01$) lower mean stimulation strength threshold compared to VFs.

Mean premature stimulation coupling interval thresholds for the induction of the three main categories of arrhythmias above discussed were statistically compared in RV and LV, as shown in figure 74.

Mean CI thresholds for arrhythmias induction

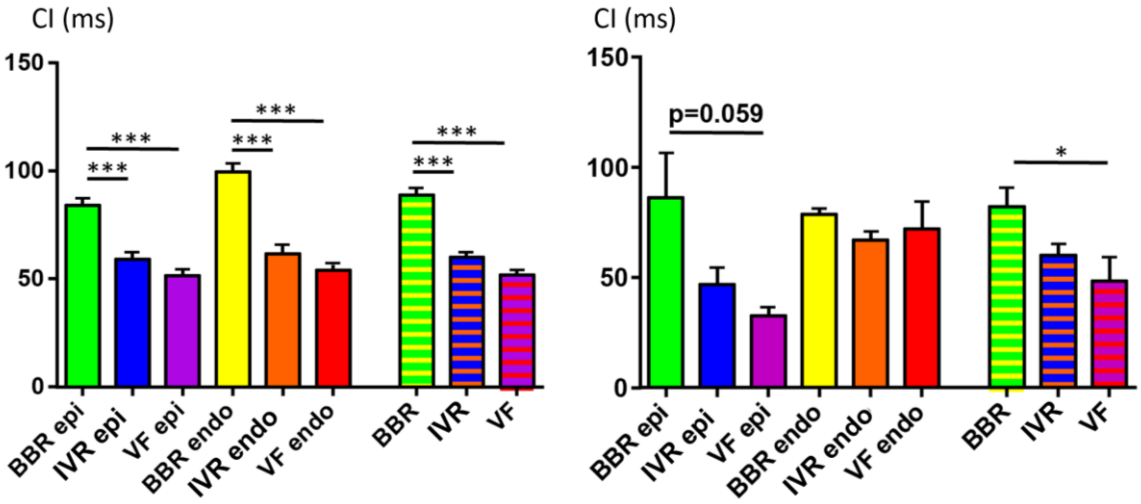

Figure 74. Left panel: mean CI thresholds for arrhythmias induction in the RV. Right panel: mean CI thresholds for arrhythmias induction in the LV.

Regarding to epicardial stimulation applied in the RV:

- BBRs resulted characterized by a significant ($p<0,001$) longer mean premature stimulation CI threshold compared to IVRs and to VFs.

Regarding to endocardial stimulation applied in the RV:

- BBRs resulted characterized by a significant ($p<0,001$) longer mean premature stimulation CI threshold compared to IVRs and to VFs.

Considering all the stimulations applied in the RV:

- BBRs resulted characterized by a significant ($p<0,001$) longer mean premature stimulation CI threshold compared to IVRs and to VFs.

Regarding to all the stimulation applied in the LV:

- BBRs resulted characterized by a significant ($p<0,05$) longer mean premature stimulation CI threshold compared to VFs.

For the epicardial stimulations in the RV, the stimulation strength threshold for the occurrence of response latency resulted equal to 136 µA (SE = 10.5); the mean longest RW-S coupling interval, for stimulations applied at strength equal or higher to 1 mA, at which response latency occurred resulted equal to 69 ms (SE = 3.2).

For the endocardial stimulations in the RV, the stimulation strength threshold for the occurrence of response latency resulted equal to 154 µA (SE = 40); the mean longest RW-S coupling interval, for stimulations applied at strength equal or higher to 1 mA, at which response latency occurred resulted equal to 70 ms (SE = 3.3).

For the epicardial stimulations in the LV, the stimulation strength threshold for the occurrence of response latency resulted equal to 200 µA (SE = 70.7); the mean longest RW-S coupling interval, for stimulations applied at strength equal or higher to 1 mA, at which response latency occurred resulted equal to 68 ms (SE = 10.7).

For the endocardial stimulations in the LV, the stimulation strength threshold for the occurrence of response latency resulted equal to 136 µA (SE = 14.3); the mean longest RW-S coupling interval, for stimulations applied at strength equal or higher to 1 mA, at which response latency occurred resulted equal to 83 ms (SE = 5.65).

For the epicardial stimulations in the RV, the stimulation strength threshold for the occurrence of UCB resulted equal to 345 µA (SE = 54.9); the mean longest RW-S coupling interval, for stimulations applied at strength equal or higher to 1 mA, at which UCB occurred resulted equal to 71 ms (SE = 2.85).

For the endocardial stimulations in the RV, the stimulation strength threshold for the occurrence of UCB resulted equal to 970 µA (SE = 482.6); the mean longest RW-S coupling interval, for stimulations applied at strength equal or higher to 1 mA, at which UCB occurred resulted equal to 67 ms (SE = 2.72).

For the epicardial stimulations in the LV, the stimulation strength threshold for the occurrence of UCB resulted equal to 1100 µA (SE = 384.7); the mean longest RW-S coupling interval, for stimulations applied at strength equal or higher to 1 mA, at which UCB occurred resulted equal to 68 ms (SE = 10.68).

For the endocardial stimulations in the LV, the stimulation strength threshold for the occurrence of UCB resulted equal to 1957 µA (SE = 1047.2); the mean longest RW-S coupling interval, for stimulations applied at strength equal or higher to 1 mA, at which UCB occurred resulted equal to 70 ms (SE = 5.8).

Mean stimulation strength and coupling interval thresholds for UCB occurrence will be shown in figure 75.

Mean unidirectional conduction block occurrence thresholds.

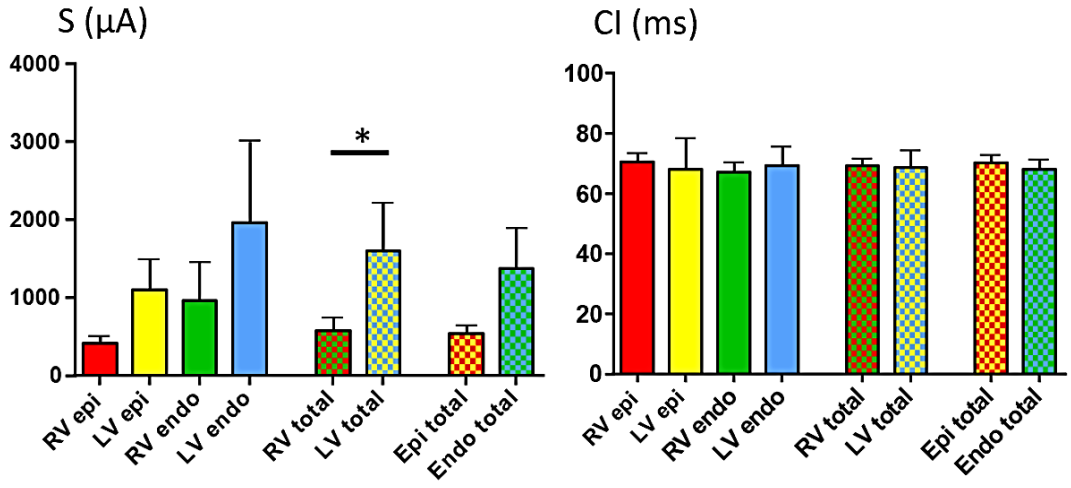

Figure 75. Left panel: mean stimulation strength thresholds for UCB occurrence. Right panel: mean coupling interval thresholds for UCB occurrence.

Test sites in the RV resulted characterized by a significant (p.<0,05) lower mean stimulation strength threshold compared to test sites in the LV.

For the epicardial stimulations in the RV, the mean AT1-AT2 interval of BBRs resulted equal to 97,85 ms, the mean interval AT1-AT2 interval of IVRs resulted equal to 59,8 ms and the mean interval AT1-AT2 interval of VFs resulted equal to 50,5 ms.

For the endocardial stimulations in the RV, the mean AT1-AT2 interval of BBRs resulted equal to 95,2 ms, the mean interval AT1-AT2 interval of IVRs resulted equal to 63 ms and the mean interval AT1-AT2 interval of VFs resulted equal to 56,4 ms.

For the epicardial stimulations in the LV, the mean AT1-AT2 interval of BBRs resulted equal to 96,8 ms, the mean interval AT1-AT2 interval of IVRs resulted equal to 58,9 ms and the mean interval AT1-AT2 interval of VFs resulted equal to 45,1 ms.

For the endocardial stimulations in the LV, the mean AT1-AT2 interval of BBRs resulted equal to 92,5 ms, the mean interval AT1-AT2 interval of IVRs resulted equal to 71,65 ms and the mean interval AT1-AT2 interval of VFs resulted equal to 73,9 ms.

Mean AT1-AT2 intervals of BBRs, IVRs and VFs for premature stimulations applied in RV and LV will be shown in figure 76.

Mean AT1-AT2 intervals of arrhythmias.

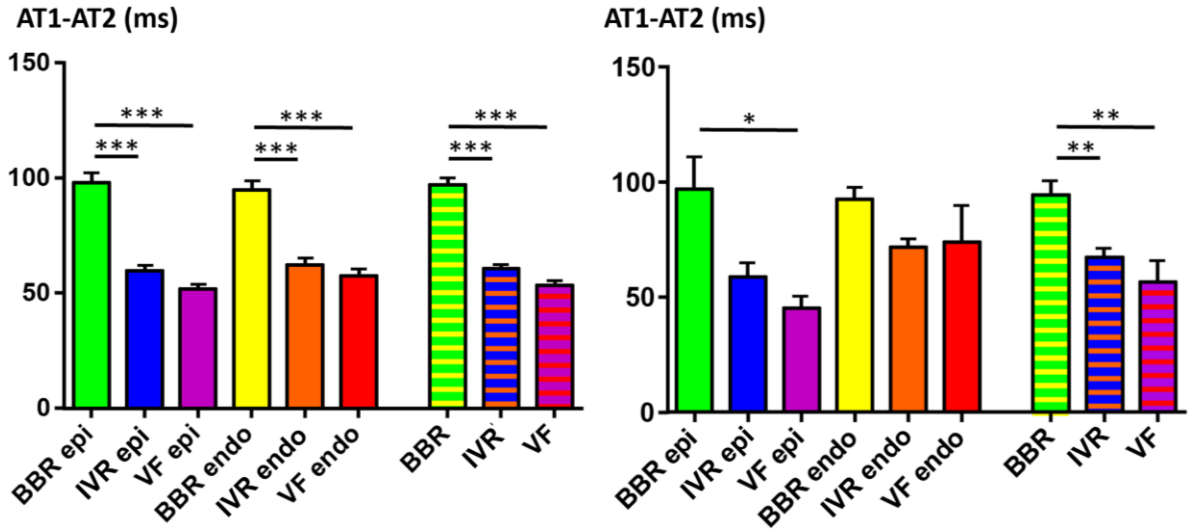

Figure 76. Left panel: mean AT1-AT2 intervals of BBRs, IVRs and VFs in RV. . Right panel: mean AT1-AT2 intervals of BBRs, IVRs and VFs in LV.

Regarding to epicardial stimulations applied in the RV:

- BBRs resulted characterized by a significant ($p<0,001$) longer mean AT1-AT2 interval compared to IVRs and to VFs.

Regarding to endocardial stimulations applied in the RV:

- BBRs resulted characterized by a significant ($p<0,001$) longer mean AT1-AT2 interval compared to IVRs and to VFs.

Considering all the stimulations applied in the RV:

- BBRs resulted characterized by a significant ($p<0,001$) longer mean AT1-AT2 interval compared to IVRs and to VFs.

Regarding to epicardial stimulations applied in the LV:

- BBRs resulted characterized by a significant ($p<0,05$) longer mean AT1-AT2 interval compared to VFs.

Considering all the stimulations applied in the LV:

- BBRs resulted characterized by a significant ($p<0,01$) longer mean AT1-AT2 interval compared to IVRs and to VFs.

The comparison between ERP values measured with RW-S and S1-S2 at the same stimulation strength (8x the diastolic threshold) was performed with 18 test sites.

The same 18 test sites and the corresponding measured ERPs were subsequently divided into four main groups (epicardial test sites in the RV, epicardial test sites in the LV, endocardial test sites in the RV, endocardial test sites in the LV) to compare their mean refractoriness. The four main groups were then grouped following different principles to perform further comparisons (total test sites in the RV, LV total test sites in the LV, total epicardial test sites and total endocardial total test sites).

All the comparisons are shown in figure 77.

ERP mean values.

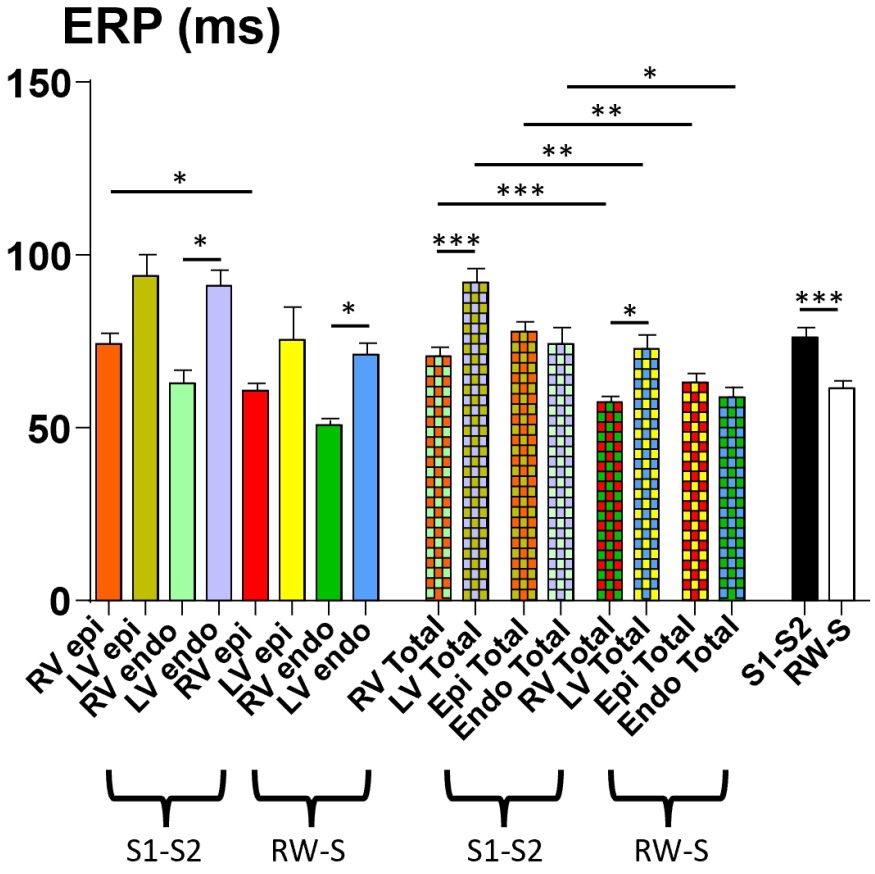

Figure 77. ERP mean values measured through S1-S2 and RW-S at a stimulation strength equal to 8x the diastolic threshold.

Regarding to the four main groups:

- Mean ERP measured through S1-S2 protocol in epicardial test sites in the RV resulted significantly longer ($p<0,05$) than mean ERP measured through RW-S protocol in the same test sites.
- Mean ERP measured through S1-S2 protocol in endocardial test sites in the LV resulted significantly longer ($p<0,05$) than mean ERP measured through S1-S2 protocol in epicardial test sites in the LV.
- Mean ERP measured through RW-S protocol in endocardial test sites in the LV resulted significantly longer ($p<0,05$) than mean ERP measured through RW-S protocol in endocardial test sites in the RV.

Regarding to the four grouped groups:

- Mean ERP measured through S1-S2 protocol in all the test sites in the RV resulted significantly longer ($p<0,001$) than mean ERP measured through RW-S protocol in the same test sites.
- Mean ERP measured through S1-S2 protocol in all the test sites in the LV resulted significantly longer ($p<0,001$) than mean ERP measured through S1-S2 protocol in all the test sites in the RV.
- Mean ERP measured through S1-S2 protocol in all the test sites in the LV resulted significantly longer ($p<0,01$) than mean ERP measured through RW-S protocol in the same test sites.
- Mean ERP measured through S1-S2 protocol in all the test epicardial sites resulted significantly longer ($p<0,01$) than mean ERP measured through RW-S protocol in the same test sites.
- Mean ERP measured through S1-S2 protocol in all the endocardial test sites resulted significantly longer ($p<0,05$) than mean ERP measured through RW-S protocol in the same test sites.

Overall, considering all the test sites, mean ERP measured through S1-S2 protocol resulted significantly longer ($p<0,001$) than mean ERP measured through RW-S protocol.

3.7. Preliminary histological results.

Histological analysis was performed to identify fiber direction at different ventricular wall depths (Fig. 78) and to localize the positions of endocardial test sites. The entire procedure has been completed for three of the seventeen experiments.

Histological analysis obtained for the heart of experiment 16 are displayed in Fig. 78 A and B. Fig 78 A shows two histological sections, one at 64 µm depth representing RV subepicardial tissue (upper panel) and the other at 296 µm depth comprising RV subendocardial tissue and transmural interventricular septum (lower panel). Myocardial fiber direction is identified by the white segments centered at each electrode site over the tissue. Fig. 78 B displays magnifications of the areas comprised within square dashed lines in A. Interestingly, in Fig.78 B, lower panel, the black circle identifies the position of the RV endocardial pacing site represented by the cross section of the 50 µm diameter silver wire barb inserted into the subendocardial layer (see Methods). Hence, histological analysis for the heart of this experiment reveals over 90° counterclockwise (from epicardium to endocardium) fiber rotation across RV wall.

Isochrone maps obtained by premature epicardial and endocardial stimulation during sinus rhythm (S=100 µA, I=150 ms) at electrode sites in Fig 78 B are shown in Fig. 78 C, upper and lower panels, respectively. Briefly, during the experiment, endocardial stimulation allowed real time identification of endocardial pacing site by the position of the potential minimum displayed in the equipotential map of stimulus artefact. Successively, the electrode of the epicardial array corresponding to the same position of the potential minimum previously displayed was stimulated with the same pacing protocol. Epicardial isochrones maps refer to epicardial (Fig. 78 C, upper panel) and endocardial (Fig. 78 C, lower panel) stimulation at corresponding sites indicate by the symbols.

Rotation of major axis of elliptical isochrones (not displayed) is correspondingly influenced by epi-endo counterclockwise fiber direction rotation across the RV wall (double headed arrow dashed lines).

Fibers direction at different ventricular wall depths in the RV.

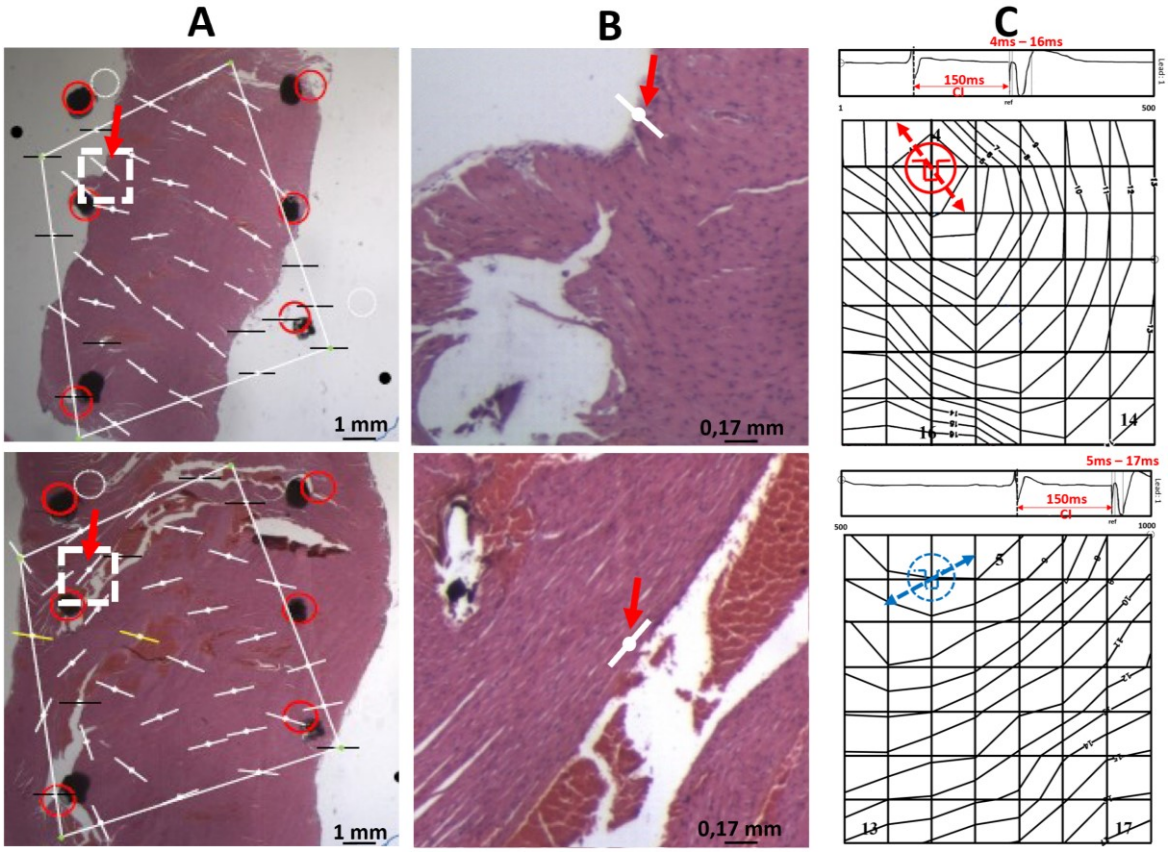

Figure 78.
A. Histological sections at 64 µm (epicardial, upper panel) and 296 µm (endocardial, lower panel) depth from the top of the paraffin block embedding excised ventricular wall; white perimeter and dots: schematic representation of superimposed electrode array; white segments: fiber directions at corresponding electrodes; red dotted circular lines and black circles: markers superimposed on needle track reference holes.
B. Epicardial (upper panel) and endocardial (lower panel) magnifications of the areas comprised within square dashed lines in corresponding panels in A.
C. Isochrones after epicardial (upper panel) and endocardial (lower panel) stimulation at pacing sites identified by symbols.

Discussion.

4.1. RW-S and S1-S2 protocols, considerations.

In human electrophysiological studies, the most commonly used programmed electrical stimulation is the S1-S2 method, which consists of a series of basal stimuli (S1) given at a fixed rate slightly higher than sinus rate that are followed by one premature stimulus (S2). In this protocol, S1 and S2 are usually applied in the same test site. Programmed stimulation in clinical electrophysiological studies is mainly used to re-induce previous arrhythmias that spontaneously developed in the same patients with the aim to identify possible arrhythmogenic substrates for ablation. When the S1-S2 protocol is not sufficient to induce arrhythmias, further premature stimuli (S3 and possibly S4) can be applied after S2 to increase dispersion of refractoriness and facilitate the induction of arrhythmias.

In the present work, we mainly used the RW-S stimulation protocol, which consists in the application of a single premature stimulus during sinus rhythm.

The RW-S protocol was mainly used for two reasons. Firstly, it is that it is a much less stressful protocol on the heart, because only a single premature stimulus is applied during normal sinus rhythm and compared to the S1-S2 protocol, the number of stimulations is reduced by a factor of 10. Accordingly, the RW-S protocol has allowed to perform the numerous stimulations required for the construction of a detailed S-I plane for each test site. In particular, it was possible to study a maximum of five different test sites in a single experiment and to evaluate differences in arrhythmia vulnerability in different regions of the same heart. Therefore, for example, it was possible to evaluate differences in arrhythmia vulnerability for i) an epicardial test site and the corresponding endocardial test site in the RV (two test sites that are less than 0.5 mm apart); ii) a test site in the RV and a test site in the LV. iii) an epicardial test site located at a sinus BTP and an epicardial test site in a region distant from sinus BTP. The possibility of building detailed S-I planes, with very fine changes in the stimulation parameters (shortening the coupling interval by 10 ms in the less interesting areas and shortening the coupling interval by 2 ms in the more critical and arrhythmogenic areas, as well as the gradual increase of the stimulation strength by only 100 µA) allowed to observe in detail how a premature beat, initially benign (low response latency, symmetrical source around the stimulation point, bidirectional conduction), becomes progressively aberrant and arrhythmogenic (increase in response latency, distancing and asymmetry of the source from the point of stimulation and development of UCB).

The same detailed procedure would not have been possible using the S1-S2 protocol which is instead a much more stressful protocol and therefore would have led to more rapid heart exhaustion.

Secondly, the RW-S protocol simulates much better the spontaneous extrasystole which obviously develops during sinus rhythm and not after a series of stimulated beats. From this point of view, the RW-S protocol is a much more useful tool to understand how the spontaneous extrasystole is able to trigger IVF.

It must be emphasized that the two stimulation protocols involve a different activation sequence of the specialized conducting system. In particular, with the RW-S protocol, during the sinus beat, earlier anterograde activation of the conducting system (and therefore of the Purkinje fibers) is followed by the activation of the ventricular myocardium; while at the onset of the premature stimulus, the earlier activation of the ventricular muscle is followed by the retrograde activation of the conducting system. With the S1-S2 protocol, on the other hand, during both basal beats S1 and premature beat S2, the activation of the ventricular muscle is followed by retrograde activation of the conducting system.

In addition, at the same stimulation strength, the two protocols measure different ERP values, with the RW-S protocol which on average measures a shorter value of ERP of about 20 milliseconds in the rat heart; this result is due to the different electrotonic modulation of repolarization with the two protocols. In fact, with the S1-S2 protocol, during the basal beats (S1) the source is localized around the stimulation point and from the source the activation front propagates in all directions; for this reason, the source region will receive an electrotonic current which slows down the repolarization from all the neighbouring points which are activated subsequently during the activation pattern.

With the RW-S protocol, on the other hand, the basal beat is the sinus beat and therefore at no point does a situation similar to that which occurs in the S1 beat occurs; in other words, during the sinus beat, no point will receive an electrotonic current that slows repolarization from all directions and for this reason the same test site will complete earlier its repolarization and therefore will be characterized by a shorter ERP than during the S1-S2 protocol.

4.2. ERP measurement, considerations.

While during experiments the ERP of a test site at a given strength was measured as the longest coupling interval not followed by a propagated response in the myocardium, in the present work, it was considered as “real” ERP the shortest coupling interval followed by a propagated response in the myocardium with a source localized around the stimulation point and with low response latency. The previous consideration has been made because, starting from the occurrence of response latency or of removal of the source from the stimulation point, although the myocardium continues to respond to the premature stimulus, it is no longer the stimulated point that gives rise to a propagating action potential; instead, electrotonic and graded response phenomena develop and allow the development of a propagating action potential in a point different from the stimulated one (which is instead refractory). What has typically been observed is that between the “real” ERP and the experimentally measured ERP, as the coupling interval is shortened, the response in the premature beat becomes progressively aberrant; initially an increase response latency occurs but the source remains localized around the stimulation point. Then, by further shortening the coupling interval, an asymmetrical response is first observed, with the source located near the stimulation point but only at one side, and then a distancing of the source from the stimulation electrode occurs (due to graded responses occurrence). It is generally in this range of coupling intervals, between the "real" ERP and the experimentally measured ERP, that the UCB developed and most IVR-Ps, IVR-Ms and VFs were obtained.

4.3 Greater vulnerability to arrhythmias for RV than for LV.

The results obtained in the present work indicate a greater vulnerability to arrhythmias for RV compared to LV, both for benign arrhythmias such as BBRs and for more dangerous arrhythmias such as IVR-Ps, IVR-Ms and VFs. In fact, not only stimulation strength thresholds for arrhythmias induction resulted lower in the RV but these arrhythmias were also obtained with greater frequency and consistency in the RV than in the LV.

As for the greater vulnerability to BBRs, this should be due to the fact that RBB is characterized by a longer refractoriness than LBB[45]; consequently, the retrograde conduction following the premature beat should be more favoured in the LBB. The consequence of this situation is that with premature stimulation in the RV and retrograde conduction in the LBB a longer circuit is determined than with premature stimulation in the LV and retrograde conduction in the LBB; the longer circuit favours the development of the reentry since the length of the circuit must be greater than the wavelength (conduction speed x ERP of the region proximal to the UCB) for reentry occurrence.

The greater vulnerability to VF, on the other hand, seems to be due to the source-load mismatch presents between RV and IVS combined with the longer refractoriness of IVS compared to RV. The maps of the RTs during the sinus beat typically show higher RTs values in the IVS than in the RV; this situation in combination with the fact that the wall of the septum is much thicker than that of the RV (source-load mismatch) favours the development of the UCB, a necessary condition for the development of the figure 8 reentry. Premature stimulation in the LV eliminates the question of source-sink mismatch (because the front passes from the thicker IVS to the thinner RV) and so the development of a UCB sufficiently critical to favour the development of reentry becomes more difficult.

The lower thickness of the RV could also explain its greater vulnerability to IVRs, as latent PMJs and even quiescent PMJs may be able, in the presence of a partially refractory RV (reduced load), to activate the muscle more easily than at the level of the LV, where the wall is much thicker and therefore resulting in a much greater load that could prevent the delivery of the impulse from the junctions not well coupled to the muscle.

4.4. BBRs.

BBRs were consistently induced in 41 of the 45 test sites, through RW-S protocol.

Since in the present work no measurements of the activity of the His bundle and of the two bundle branches (right and left) were performed, the BBRs were identified on the basis of their epicardial activation pattern and the latency interval from the premature beat. In fact, since the BBRs are reentries that require antegrade conduction through one of the two bundle branches (RBB in the case of BBR with LBBB pattern and LBB in the case of BBR with RBBB pattern), their activation pattern should be very similar to that of the sinus beat in the activated ventricle. Namely, in the case of a BBR with antegrade conduction through the RBB, the corresponding activation pattern displays RV activation pattern of the sinus beat with absence of sinus beat activation in the LV. In the case of a BBR with antegrade conduction in the LBB, the corresponding activation pattern displays LV activation pattern of the sinus beat, with absence of sinus beat activation in the RV.

The AT1-AT2 interval was used to distinguish BBRs from IVR-Ps characterized by activation patterns similar to the sinus beat. In fact, since the BBRs have a longer circuit, as the participation of the conducting system of both ventricles is required (retrograde conduction through one of the two branches and anterograde conduction through the other branch), their AT1-AT2 interval should be substantially longer than that of IVR-Ps (in which only the conducting system of the paced ventricle is involved in the IVR).

In our experiments BBRs were consistently induced with lower mean vulnerability thresholds in the RV than in the LV (fig. 70); in addition, the domains of vulnerability for BBR in the S-I plane were more extensive for stimulations in the RV than in the LV. This finding is likely due the longer action potential duration and refractoriness in RBB than in LBB measured in the dog heart[45]. The shorter proximal LBB action potential duration and refractory period was interpreted as due to the proximity of the low ohmic resistance Purkinje fiber-muscle junctions on the left septal surface, effecting electrotonic foreshortening of these proximal left bundle branch parameters. In fact, with the stimulation in the RV, RBBB is obtained at longer RW-S coupling intervals than LBBB with the stimulation in the LV. Since UCB is a necessary condition for the occurrence of reentry circuit arrhythmias, if RBBB occurs earlier than LBBB with premature stimulations, the development of a reentry arrhythmia through the RBB should be favoured. In addition, since ERP is shorter in the LBB than in the RBB, retrograde conduction through LBB should be favoured.

In most cases, premature stimulation in the RV resulted in the development of BBR with LBBB pattern characterized by retrograde conduction through LBB and antegrade conduction through RBB (for example: fig. 42). However, more rarely, a few BBRs with RBBB patterns have been obtained during the stimulations applied in the RV. In addition, BBRs with an activation pattern similar to that of the sinus beat were also obtained, suggesting antegrade conduction through both branches; in these cases, LV activation should have occurred with retrograde conduction through the posterior fascicle and antegrade conduction through the anterior fascicle of the LBB.

With the premature stimulations applied in the LV, both BBR with RBBB pattern (example: fig. 50) and with LBBB pattern (example: fig. 48) were obtained (without preference in terms of frequency of these events). More rarely, BBRs with sinus beat activation pattern have been also obtained suggesting antegrade conduction through the RBB and the anterior fascicle of the LBB (example: fig. 50). In particular, as LV activation is concerned, since the LBB has a shorter ERP than the RBB, the retrograde conduction should have occurred through the left posterior fascicle of the LBB and antegrade conduction through the anterior fascicle of the LBB. The occurrence of a similar result has been reported by Mehdirad et al during LV free wall extra-stimulation in only one patient[44].

In our experiments, the S1-S2 protocol at each test site was performed at only one stimulation strength, 8 times diastolic threshold. The S1-S2 protocol more efficiently induced BBRs usually at lower stimulation strength and larger coupling interval than the RW-S protocol. Differences in BBR vulnerability threshold with the two protocols are likely due to differences in the wavelength of the conducting impulse (conduction velocity × refractory period) that must be shorter than the path length of the complex reentry circuit comprising ventricular myocardium and conducting system. Although the BBR reentry circuit path length coincides for the two protocols, nevertheless the wavelength of the conducting impulse depends on the premature beat that encounters differences in i) activation pattern, time sequence and frequency dependence within the conducting system and ii) electrotonic modulation of repolarization by the basal activation sequence (sinus or paced).

In summary, our data suggest in agreement with clinical findings[41,42,44], that the left-sided His-Purkinje system is the preferred retrograde route of impulse conduction during both RV and LV premature stimulations. In particular, the reentry circuit within the conducting system elicited by RV premature stimulation involves both RBB and LBB, whereas the reentry circuit elicited by LV premature stimulation tends to occur preferably within the LBB alone.

4.5. IVR arrhythmias.

Another type of repetitive ventricular responses consists of those that are due to intraventricular reentry occurring near or at a short distance from the pacing site.

These repetitive responses, usually occurring at short coupling intervals with an R-on-T morphology, were induced in 40 of the 45 test sites through the RW-S protocol. In the present work, the term "R-on-T arrhythmias" is used to indicate non-sustained arrhythmias (no more than three reentries) characterized by a first reentry whose QRS complex occurs on the peak or shortly after the peak of the T wave of the stimulated beat (for example fig. 53).

In most cases, IVRs were obtained at higher stimulation strengths than BBRs (fig. 73). However, when IVRs occurred at the same stimulation strength of BBRs, they suddenly occurred when the coupling interval was decreased and were characterized by a sudden decrease of the AT1-AT2 interval by 20-30 ms**.** Moreover, IVRs continued to occur consistently at shorter coupling intervals near the ERP (fig. 74).

At many test sites, IVRs were obtained at lower stimulation strengths than VF and at the same coupling intervals (figures 73 and 74). In numerous cases, IVRs and VF arrhythmias alternatively occurred during premature stimulations characterized by the same strength and coupling interval (example: fig. 68). Frequently, IVRs at a test site were characterized by a first reentry whose activation pattern was very similar to the first reentry of the VFs obtained at higher stimulation strength. These findings suggest a high probability for the IVR to initiate VF arrhythmias.

In many cases, the premature beat that induced IVR was characterized by an activation pattern with UCB visible at the epicardium (example: fig. 56); However, IVRs triggered by premature beats were also obtained in the absence of a visible UCB at the epicardium (example: fig. 54).

IVRs showed two main activation patterns. At higher strengths they were often characterized by a local figure 8 reentry circuit (IVR-M). At lower strengths, they were characterized by a focal activation (IVR-P), with a BTP often localized at the proximal side of the UCB of the premature beat. In particular, when the premature beat originated at distance from the test site due to graded response[34], the BTP of IVR-Ps was usually localized near the distal source. In fact, the source region is the first to activate and consequently the first to repolarize (regions with lowest RTs). At many test sites, IVRs characterized by focal activation at the lower strengths, were characterized by figure 8 reentry at the higher strengths.

In summary, results of our study suggests that R-on-T arrhythmias occur by IVR circuits with the following characteristics.

a) When focal reentry activation initiates at distance from the pacing site, the reentry circuit occurs through the terminal Purkinje fibers of the paced ventricle (IVR-P).

According to this hypothesis, a premature stimulus at a coupling interval shorter than local ERP at the pacing site induces a local conduction block and an activation wave front originating with latency at a distal source from the pacing site. Moreover, retrograde block at PMJs in the region comprised between the distal source and test site inhibits impulse conduction toward the underlying terminal Purkinje fibers comprised between the peripheral conducting system and PMJs[48-56]. However, retrograde conduction can occur at distant PMJs in the region where the wave front originates from the distal source. Hence, the electrical impulse that enters the terminal Purkinje fibers can propagate toward resting Purkinje fibers not activated by the initially blocked PMJs. As soon as ventricular myocardium has regained excitability, antegrade conduction through the initially blocked PMJs can complete the IVR circuit. Hence, focal activation occurs with a BTP that gives rise to a wave front propagating in all directions and toward the blocked region at the pacing site. According to the recovery time of excitability at this site, the wave front can either cross over the block or surround the block with two wings, possibly initiating a second reentry circuit (for example figures 61 and 62).

According to this hypothesis, only terminal Purkinje fibers are involved in the reentry circuit, while the bundle branch of the stimulated ventricle is still refractory due to the early onset of R-on-T reentry arrhythmia. This interpretation is consistent with the fact that IVR-Ps are characterized by much shorter AT1-AT2 intervals than BBRs. Moreover, the location of reentry BTPs does not always coincide with sinus beat BTPs especially when the pacing site is located at distance from sinus beat BTPs. Thus, the BTP reentry pattern can reveal the existence of delayed functional PMJs in ventricular muscle activation that are not directly identified by the appearance of a BTP during sinus rhythm.

In the IVR circuit, the bundle branch of the conducting system of the stimulated ventricle is not involved and the BTP of the reentrant activation is not always located in correspondence with the BTPs of the sinus beat. However, coincidence of reentry and sinus beat BTPs occurred when the pacing site was located at the sinus beat BTP or very close to it. In fact, if the branch of the stimulated ventricle were involved in the reentry circuit, as it occurs with BBRs, functional PMJs that mediate the BTPs of the sinus beat should characterize the

reentry pattern. This hypothesis is also consistent with the fact that IVR-Ps are characterized by much shorter AT1-AT2 intervals than BBRs. Since the entire reentry circuit occurs within the stimulated ventricle, it would be shorter than the interventricular circuit of the BBRs and therefore could be completed more quickly. In addition, the short AT1-AT2 interval is consistent with the recovery time interval of the terminal Purkinje fibers.

In fact, as previously described in the thesis introduction, it has been demonstrated that action potential durations in the conducting system increase from the bundle branches distally. An area of maximum action potential duration occurs about 2 mm proximal to the termination of Purkinje cells in muscle, and then the durations progressively decrease through a sequence of Purkinje cells, transitional cells, and muscle cells[48]. At the PMJ action potential duration at the two sides of the junction coincides with that of ventricular myocardium. Hence, the terminal Purkinje fibers represent an intermediate conduction domain between peripheral conduction system and ventricular myocardium where intermediate recovery properties that can sustain local impulse conduction in a network electrically separated from the bundle branch.

According to this hypothesis, the BTP would be localized near the source of the stimulated beat or in the region between the test site and the source (the region where the graded response occurs in the stimulated beat) as those are the first regions of the myocardium to return excitable after the premature beat. The source region of the stimulated beat and the region in which the graded response occurs are the regions that first regions to recover their excitability for the following reasons:

- in the region where the graded response occurs, there is a prolongation of refractoriness of the previous sinus beat without development of a new action potential following the stimulus[34].
- the source region of the stimulated beat is the first region of myocardium to activate and consequently the first to recover.

Clinical electrophysiological studies of Farshidi et al[47], 1980, have also suggested similar mechanisms for IVR. "*Intraventricular reentry probably results from reentry within the ventricular myocardium and distal His-Purkinje system. This may occur locally in proximity to the site of stimulation, or at a distance and in relation to anatomic or ischemic lesions (especially in the left ventricle). Our data suggest that large segments of the proximal His-Purkinje system are not required. Unlike bundle branch reentry, intraventricular reentry cannot be prevented by appropriately time supraventricular impulses, which pre-excite the*

bundle of His. Furthermore, the dissociation between His bundle electrograms and intraventricular re-entrant responses suggests that the proximal His-Purkinje system does not form a portion of the reentrant pathway."

b) Focal reentry activation originating at the proximal side of the conduction block is likely mediated by local electrotonic current. According to this mechanism, the circuit is similar to a figure 8 reentry without apparent wave front conduction from the distal to the proximal side of the UCB that is still refractory. This mechanism can occur when the two wings of premature activation wave front surround the refractory region of the block and collide at the distal side. Hence, when repolarization initiates at the distal side and recovery is completed at the proximal side an electrotonic current flow across the block initiates focal activation wave front moving away from the proximal side of the block. The electrotonic mechanism is made possible when the blocked region extends a few millimetres, accounting also for the increase in space constant due to greater membrane resistance during repolarization. It cannot be excluded that the reentry circuit is completed in a graded conduction like manner across the blocked region and not by a simple electrotonic mechanism.

c) Figure 8 reentry circuit (IVR-M). The two wings of the premature activation wave front originating at distance from the pacing site surround the refractory region of the block and collide at the distal side of the functional conduction block. Successively, wave front reenters through the site of the initial block when it is no longer refractory, thus completing the first figure 8 reentry circuit. Wave front conduction velocity across the region of the amounts to approximately 0.1 m/s.

In conclusion, repetitive ventricular responses in our experiments are consistent with repetitive ventricular responses to programmed ventricular stimulation described in patients[46-47]. Moreover, epicardial mapping in animals adds complementary missing information to endocardial His bundle and right ventricular apex recordings in patients. Furthermore, important clinical implications are reported by Farshidi et al[47], 1980. "... *two different mechanisms of repetitive ventricular responses encountered during ventricular stimulation exist. One, bundle branch reentry, involves a macroreentrant circuit involving the bundle branches and is a benign phenomenon occurring in more than half the patients in whom ventricular stimulation is carried out. Intraventricular reentry, on the other hand, represents a pathological event closely related to clinical ventricular arrhythmias"*.

4.6. VFs.

VFs were induced in 36 of 45 test sites, through RW-S protocol. We remind that VF threshold, or VF lower limit of vulnerability, is defined by the pair of critical stimulation parameters, strength and coupling interval, that initiate ventricular tachyarrhythmia.

The RV was characterized by lower VF threshold than LV (fig. 72). Moreover, the RV anterior wall was characterized by lower VF threshold than the RV lateral free wall. In fact, VF occurred at all (10) endocardial test sites in the RV anterior wall while VF never occurred at the two endocardial test sites in the RV lateral free wall.

The reentry beat that initiated VF was characterized by either one of two activation patterns: focal with one or more BTPs (example: fig. 61) and figure 8 (example: fig. 64). At some test sites only VFs due to figure 8 reentries were obtained in the S-I plane; At other test sites VF with both focal and figure 8 reentries were obtained. VF focal reentry occurred at lower stimulus strength than VF figure 8 reentry. Moreover, AT1-AT2 interval for VF focal reentry was longer than VF figure 8 reentry. As in the case of IVR arrhythmias, the BTP of VF focal reentry was localized either at the source region or in the graded response region of the premature beat. In particular, VFs focal reentry was characterized by slightly shorter AT1-AT2 intervals than corresponding focal IVR. These findings suggest that critical focal IVRs with very short AT1-AT2 intervals can induce ventricular tachyarrhythmias. Moreover, the two mechanisms described for focal IVR arrhythmias can also induce VF focal reentry.

Overall, the AT1-AT2 intervals of the VF figure 8 reentry were 10-20 ms shorter than AT1-AT2 intervals of figure 8 IVRs.

At test sites in which both typologies of VFs (focal and figure 8 reentry) were obtained, the position of the BTP in VF focal reentry coincided with the position of figure 8 reentry (examples: fig. 61 for focal pattern and fig. 64 for figure 8 pattern).

At almost all test sites, when VF threshold was reached, then VF consistently occurred at higher strengths in a triangular vulnerable domain extending toward shorter coupling intervals.

However, one RV endocardial test site (experiment 15) was characterized by two different VF domains in the S-I plane, with VF threshold at a) 900 μA and b) 7 mA (fig. 67). Premature beat activation patterns at each point of S-I plane, were consistent with simultaneous activation of ventricular myocardium and peripheral Purkinje fibers.

a) VF threshold at 900 µA.

VF threshold was identified by one point in the S-I plane, with coordinates 900 µA and 48 ms. Repetitive stimulation at this strength and coupling interval induced only one VF episode while consistently induced IVR-Ps. Stimulations at coupling intervals shorter or longer than 48 ms consistently induced similar IVR-Ps.

Moreover, the vulnerable domain for IVR-Ps was centred about VF threshold and limited by points comprised between 800 µA and 1 mA strength in the S-I plane (fig. 67). Stimulation strengths above this vulnerable domain at 2 mA, 3 mA and 4 mA did not induce IVR-Ps while BBRs were consistently induced. It is important to underline that starting at 2 mA the activation pattern of the premature beat at short coupling intervals (close to ERP) changed compared to that at lower strengths; This change could be responsible for the absence of IVR-Ps and VFs within the 2-4 mA strength range.

These findings suggest that IVR-Ps, triggered at low stimulation strengths, could very rarely degenerate into VF.

b) VF threshold at 7 mA.

VF threshold occurred again at 7 mA and the VF vulnerable domain extended at higher stimulation strengths. VF vulnerable domain was fully comprised within the wider IVR-P vulnerable domain with lower limit at 5 mA threshold. IVR-Ps were characterized by a different activation pattern than in the corresponding lower vulnerable domain. Moreover, VFs that occurred at 7mA threshold and above were characterized by a different activation pattern than at 900 µA.

It is equally important to underline that both the VF obtained at 900 µA and the VF obtained at higher strengths were always characterized by focal activation although with BTPs at different locations. At this test site, VF originating with a figure 8 reentry was never obtained in either one of the two vulnerable domains. This finding suggests that the terminal Purkinje fibers are likely responsible for VF onset as in the case of IVR with focal activation pattern characterized by a BTP. Furthermore, whenever VF threshold is very low, terminal Purkinje fibers are the only likely responsible for the arrhythmia onset.

In summary, it should be emphasized that, at different test sites of numerous experiments, the VFs obtained at lower stimulation strengths were characterized by focal activation. Hence, lowering of VF threshold is likely due to an IVR circuit that comprises terminal Purkinje fibers. Moreover, for VF occuring above threshold, the VF onset can suddenly change to figure 8 reentry characterized by shorter AT1-AT2 interval. This finding suggests that the

reentry circuit suddenly shifts to a new circuit with shorter conduction time and path length entirely comprised within the myocardium.

In addition, these findings suggest that the onset of idiopathic ventricular fibrillation in normal ventricular myocardium is likely characterized by an IVR circuit through terminal Purkinje fibers that can occur at low VF threshold. Moreover, this is also consistent with clinical findings indicating that, in the majority of cases, VF is triggered by premature beats that originate from the Purkinje network.

Our findings also show that VF onset characterized by focal reentry circuit can be followed by multiple reentries with single or figure 8 rotation patterns. This would suggest that, in some instances, the initial reentry beats act like "premature stimulus equivalents" (i.e. S2, S3, S4) aiding the emergence of stable ventricular tachyarrhythmias.

4.7. Role of PMJs in the intraventricular reentry within terminal Purkinje fibers.

Whether short coupling premature ventricular stimulation during normal sinus rhythm might induce an intraventricular reentry (IVR) circuit that comprises ventricular myocardium, PMJs and terminal Purkinje fibers requires that the wavelength of the re-entrant impulse (conduction velocity x effective refractory period) must be shorter than the length of the pathway. Verification of this hypothesis requires that measured epicardial potentials be interpreted in terms of renowned cellular electrophysiological properties of the reentry pathway.

In particular, we refer to results of the following experiments where, by means of standard microelectrode techniques, action potential durations were measured a) along the course of canine conducting tissue from bundle branches to the termination of false tendons in ventricular muscle and b) at the terminal Purkinje fibers and ventricular muscle cells during antegrade and retrograde impulse conduction at PMJs.

a) It has been shown that a progressive increase in action potential duration occurs along the conducting system from the His bundle through the bundle branch to distal areas, or gates, of maximum action potential duration that occur about 2 mm proximal to the termination of Purkinje cells in muscle (peripheral conducting system). Then, action potential durations progressively decrease through a sequence of Purkinje cells, transitional cells, and ventricular free wall muscle cells (terminal Purkinje fibers). It has also been shown that low-resistance intercellular connections are present at the junction of terminal Purkinje fibers and ventricular muscle[56]. The functional geometry at these junctions seems to be such that ordinary ventricular muscle has an extensive electrotonic interaction with the terminal Purkinje fiber. The end result is that action potential durations of terminal Purkinje fibers are essentially the same as those of muscle fibers with which they make direct functional connections[57].

Moreover, conduction of premature impulses has been studied in preparations of a bundle branch and its multiple ramifications terminating in large blocks of free ventricular muscle wall[48]. When the bundle branch in such preparations is stimulated prematurely at a coupling interval less than the duration of the refractory periods at the distal gates, excitation of the proximal tissue by the premature impulse occurs, but the impulse remains confined proximal to the gates. When the muscle cells of the ventricular free wall are stimulated at a similar coupling interval, confinement of the premature impulse within the terminal Purkinje fibers occurs, as long as conduction velocities are not depressed, being unable to cross the gates and find a route back into the peripheral conducting system.

b) Mendez et al.[56] (1970) found in a canine right anterior papillary muscle preparation that the relatively long PMJ delays observed during antegrade impulse conduction were practically abolished during retrograde conduction confirming that the safety factor for propagation across the PMJs is higher in the muscle-to-Purkinje fiber direction. Using the same type of preparation Sasyniuk and Mendez[55] (1971) were able to obtain conduction block at the PMJs by premature stimulation of the attached false tendon. Under these conditions, the configuration of the action potentials of the terminal Purkinje fibers was extremely brief while the transmembrane potential from the neighbouring muscle showed only a subthreshold depolarization. Low intracellular resistance to current flow, high membrane resistance during the plateau and a particular functional geometry combine and cause the flow of electrotonic current that shape the extremely brief action potentials recorded from terminal Purkinje fibers during conduction block.

Moreover, solid proof that electrotonic interactions modulate action potential duration at the two sides of PMJs during antegrade conduction block has been obtained in sheep Purkinje fibers using the sucrose-gap technique[50].

These cellular electrophysiological findings can offer explanatory suggestions for the interpretation of epicardial activation patterns measured during premature stimulation in the rat.

1) During basal sinus rhythm, ventricular activation is characterized by the synchronized antegrade impulse conduction through functional PMJs. Epicardial emergence of the impulse occurs at a limited number of BTPs surrounded by accelerated impulse conduction that completes ventricular activation. A numerous number of functional PMJs, not identified by corresponding BTPs, participates in this entire activation pattern. However, among the numerous PMJs, those characterized by a long conduction delay may not be able to sustain impulse conduction being anticipated by local activation of ventricular myocardium. In addition, many PMJs that may be normally quiescent due to a source-load mismatch fail to conduct the impulse to ventricular myocardium. Evidence in murine and canine models has shown that propagation is successful only in determined subsets of the PMJs, and that dynamic coupling–uncoupling may influence physiological and pathological conduction[17-58-59-60].

Hence, conduction block that can occur at normally quiescent PMJs should be characterized by an initially brief action potential configuration of terminal Purkinje fibers that is soon after prolonged by the electrotonic interaction with local ventricular cells activated by impulse

conduction from neighbouring functional PMJs. We note that although action potential configuration of terminal Purkinje fibers and ventricular cells is the same at all PMJs, nevertheless active membrane properties of terminal Purkinje fibers are significantly different at functional and normally quiescent PMJs. At functional PMJs action potential duration of Purkinje fibers gradually decreases during antegrade conduction from the gate area toward the PMJ, while at normally quiescent PMJs the initially brief action potential duration is prolonged by electrotonic current from the ventricular cells.

The fact that two cells characterized by identical action potential can nevertheless be characterized by different electrophysiological properties has been demonstrated by simulation studies[61].

Hence, the existence of normally quiescent PMJs during sinus rhythm would therefore determine the presence of ~~a~~ non-uniform distribution of recovery properties at the level of the terminal Purkinje fibers.

2) During premature stimulation, at coupling intervals shorter than local ERP, prolongation of refractoriness occurs in the region surrounding the pacing site and cellular graded responses propagate toward a distant source where impulse conduction originates with latency. Consequently, retrograde conduction block occurs at PMJs at the pacing site where action potential prolongation is also induced within terminal Purkinje fibers. Moreover, non-uniform distribution of recovery times characterizes the network of terminal Purkinje fibers at the pacing site due to different restitution properties of action potential duration at functional and normally quiescent PMJs. However, latent ventricular activation at the distant source can initiate retrograde conduction through recovered PMJs. Hence, impulse conduction confined within terminal Purkinje fiber network can reach the fibers underlying the region of graded response at the pacing site characterized by non-uniform times. Finally, antegrade conduction through functional PMJs can occur in this region at the time of recovery of ventricular myocardium. Hence, completion of the intraventricular reentry circuit is accomplished with the emergence of BTPs that may coincide or not with those of sinus rhythm.

Direct verification of the proposed mechanism for intraventricular reentry should require the design of experimental studies that would enable appropriate electrophysiological measurements to be obtained along the circuit pathway.

4.8. Assessment of ventricular arrhythmia vulnerability.

Assessment of ventricular arrhythmia vulnerability by quantitative evaluation of critical stimulation parameters, i.e. stimulus strength S and coupling interval I, of all test sites represented in the S-I planes demonstrated that there are differences in RV and LV for the different types of arrhythmia.

We demonstrated that BBR threshold strength is higher in LV than RV. Similarly, higher threshold strength in LV, compared to RV, is also present for IVR and VF. It can be speculated that distinct structural and electrophysiological properties of RV and LV can account for differences in threshold strengths. Briefly, greater tissue volume of the thicker free wall, gradual increase in fiber rotation across the wall, peculiar architecture of specialized conducting system and higher ERP values measured with both S1-S2 or RW-S protocols can explain the higher values of threshold strength in LV compared to RV. Interestingly, threshold strength for BBR is lower compared to threshold strength for both IVR and VF induction. Moreover, threshold strength for IVR is lower than threshold strength for VF. This behaviour is counteracted by an increase of coupling interval I for BBR compared to both IVR and VF. We speculate that the lower threshold strength for BBR induction is associated to the longer coupling interval I. This interpretation is also valid for explaining the differences between IVR and VF, i.e. higher threshold strength is associated to shorter coupling interval I. Representation of vulnerable domains for the different types of arrhythmia in the S-I plane support this interpretation.

We observed increased threshold strength for unidirectional conduction block in the LV compared to RV. Also, this difference is probably due to thicker free wall and the higher ERP value in LV compared to RV.

AT1-AT2 interval for BBR is prolonged compared to AT1-AT2 interval for both IVR and VF. Moreover, AT1-AT2 interval for IVR is longer than for VF. The same behavior is also present in RV and LV.

Finally, longer ERP values consistently measured by means of S1-S2 protocol as compared to the RW-S protocol are likely due to the different electrotonic modulation of repolarization by the activation sequence[49].

5 Limitations.

Four main limitations were found in the present study:

1) Perhaps the most relevant limitation in the present work is the use of premature stimulation to simulate spontaneous extrasystoles. This is obviously an artificial condition that does not occur in the real case. On the other hand, alternative solutions were not possible; the use of drugs, for example, would have altered the normal heart substrate. At the same time, it is impossible to hypothesize to place the grid on the rat heart and wait for a spontaneous critical PVC to occur and to trigger IVF; in fact, it is an extremely rare event that with very low probability could develop spontaneously over the course of an experiment.

As for the characteristics of the stimulus, stimulation strength and coupling interval, all stimulations are artificial, even those with lower strengths and longer coupling intervals. However, to simulate a very premature PVC, high stimulation strengths are required in order to be able to approach the peak of the T wave of the previous sinus beat. Consequently, also from this point of view, the use of high stimulation strengths results to be mandatory.

In addition, it must be considered that the activation pattern of a stimulated beat with high strength and short coupling interval should quite faithfully simulate the pattern of a spontaneous PVC, resulting in an activation pattern with a small source, low conduction speed and possible presence of UCB.

It should also be taken into account that in the present study the premature stimulus was applied at the level of the ventricular myocardium, while in spontaneous IVFs in humans, PVCs (which trigger IVFs) more frequently originate at the level of the Purkinje system.

2) The second limit of the present study has been the possibility to map only a portion of the anterior face of the RV and LV and hence to miss the possibility to map the entire activation of the analysed beat, thus preventing the possibility, for example, of detecting any secondary sources at a distance from the stimulation point or reentry circuits located outside the matrix. In fact, in some cases, especially for test sites located near the edges of the grid, the reentry circuit occurred externally to the region mapped by the grid; in such cases it was not possible to determine the reentry circuit underlying the arrhythmia.

3) The lack of recordings of the activity of His of the two branches (RB and LB) has been another limit of the present study. This prevents the BBR reentry circuits from being determined with certainty. The reentry circuits at the base of the BBRs, in the present study, were in fact determined indirectly using the reentry activation pattern; however, experimental measures that can confirm with certainty what was indirectly determined are lacking. In particular, in the present work, it was not possible to determine with certainty the retrograde entry point into the conducting system in the circuits at the base of the BBRs.

4) The lack of recordings of the endocardial region during arrhythmias has been another limit of the present study; such recordings during IVRs and during VFs with focal pattern could in fact have clarified whether they were figure 8 reentries occurring at the endocardial level or whether they were IVRs.

6. Conclusion.

Premature stimulation applied during sinus rhythm in normal rat heart in vivo succeeded in triggering BBRs, IVRs, and VFs.

BBRs resulted to be the most inducible (lower stimulation strength threshold), most frequent and most benign arrhythmic events; according to the data reported in the present work, they are unable to degenerate into VF in the normal heart.

IVRs, on the other hand, resulted to be much more dangerous; the similarity in the activation pattern between these reentries and the VFs leads to the hypothesis that IVRs may degenerate into VF in critical conditions. In particular, according to the data reported in the present study, when an IVR is able to be completed in an extremely short time (short AT1-AT2 interval), it could degenerate into VF; when, on the other hand, it is completed in relatively longer times (a few milliseconds of difference are enough) it remains a non-sustained event.

Perhaps the most relevant novelty of the following work is that IVRs and VFs obtained at lower stimulation intensity for a test site were typically characterized by a focal activation pattern; as previously described, these focal reentries could be due to reentries through the terminal portions of the Purkinje system (IVR-Ps). If indeed these were IVR-Ps, the Purkinje system could be responsible for triggering IVF in humans. In fact, since in the present study, the VFs obtained at lower stimulation intensity with a test site were characterized by focal aspect, while the VFs due to figure 8 reentry circuits with the same test site were obtained at higher stimulation strengths, all of this would lead to the conclusion that the normal heart is more vulnerable to IVR-Ps rather than figure 8 reentries.

In addition, as already described in the discussion of the VFs, the first focal reentries are then followed by figure 8 reentries; from this point of view, the first IVR-Ps could act as further premature stimuli (S2 and S3) and thus favour the development of figure 8 reentries.

Therefore, what could happen in the healthy heart in humans is that a premature extrasystole (in the present work simulated by the stimulated beat) could trigger IVR-Ps, which in turn could favour the development of the figure 8 reentries and thus degenerate into VF.

7. Bibliography

1. H. A. Fozzard: “Cardiac muscle: Excitability and passive electrical properties",
Prog. Cardiovasc. Dis., vol. XIX, no. 5, 1977.
https://doi.org/10.1016/0033-0620(77)90015-9

2. Dobrzynski, H. et al.: Structure, function and clinical relevance of the cardiac conduction system, including the atrioventricular ring and outflow tract tissues.
Pharmacol. Ther. 139, 260–288 (2013).
https://10.1016/j.pharmthera.2013.04.010

3. J. R. Sommer, E. A. Johnson: Cardiac muscle. A comparative study of Purkinje fibers and ventricular fibers.
The Journal of cell biology. 36, 497–526 (1968).
https://10.1083/jcb.36.3.497

4. B. R. Eisenberg, I. S. Cohen: The ultrastructure of the cardiac Purkinje strand in the dog: a morphometric analysis.
Proceedings of the Royal Society B: Biological Sciences. 1983 Jan 22;217(1207):191-213.
https://10.1098/rspb.1983.0006

5. P. J. Podrid and P. R. Kowey: Cardiac Arrhythmia: Mechanisms, Diagnosis and Management. Lippincott Williams and Wilkins Publication, 2nd ed., 2001.

6. Oleg V. Aslanidi, Rakan N. Sleiman, Mark R. Boyett, Jules C. Hancox, Henggui Zhang: Ionic mechanisms for electrical heterogeneity between rabbit Purkinje fiber and ventricular cells.
Biophysical journal. 2010 Jun 2;98(11):2420-31.
https://doi.org/10.1016/j.bpj.2010.02.033

7. Bruno D. Stuyvers, Wen Dun, Scot Matkovich, Vincenzo Sorrentino, Penelope A. Boyden, and Henk E.D.J. ter Keurs: Ca^{2+} Sparks and Waves in Canine Purkinje Cells
A Triple Layered System of Ca^{2+} Activation
Circulation Research. 2005;97:35–43.
https://doi.org/10.1161/01.RES.0000173375.26489.fe

8. P. F. Cranefield: Action potentials, afterpotentials, and arrhythmias.
Circulation Research. 1977;41:415–423
https://doi.org/10.1161/01.RES.41.4.415

9. Zhen Song, Christopher Y. Ko, Michael Nivala, James N. Weiss 2, Zhilin Qu: Calcium-voltage coupling in the genesis of early and delayed afterdepolarizations in cardiac myocytes.
Biophys journal. 2015 Apr 21;108(8):1908-21.
https://10.1016/j.bpj.2015.03.011

10. Masanori Hirose, Bruno D. Stuyvers, Wen Dun, Henk E.D.J. ter Keurs, and Penelope A. Boyden: Function of Ca2+ Release Channels in Purkinje Cells That Survive in the Infarcted Canine Heart
A Mechanism for Triggered Purkinje Ectopy
Circulation: Arrhythmia and Electrophysiology. 2008;1:387–395.
https://doi.org/10.1161/CIRCEP.107.758110

11. Henk E. D. J. ter Keurs, and Penelope A. Boyden: Calcium and Arrhythmogenesis.
Physiological reviews. 2007 Apr;87(2):457-506.
https://doi.org/10.1152/physrev.00011.2006

12. Makarand Deo, Patrick M. Boyle, Albert M. Kim, Edward J. Vigmond: Arrhythmogenesis by single ectopic beats originating in the Purkinje system.
American Journal of Physiology-Heart and Circulatory Physiology. 2010 Oct;299(4):H1002-11.
https://10.1152/ajpheart.01237.2009

13. R. W. Joyner, E. D. Overholt: Effects of octanol on canine subendocardial Purkinje-to-ventricular transmission.
American journal of physiology. 1985 Dec;249(6 Pt 2):H1228-31.
https://10.1152/ajpheart.1985.249.6.H1228.

14. Patrick M. Boyle and Edward J. Vigmond: An Intuitive Safety Factor for Cardiac Propagation.
Biophysical Journal. 2010 Jun 16; 98(12): L57–L59.
https://10.1016/j.bpj.2010.03.018

15. R. F. Gilmour Jr., N. S. Moïse: Triggered activity as a mechanism for inherited ventricular arrhythmias in German shepherd Dogs.
Journal of the American College of Cardiology. 1996 May;27(6):1526-33.
https://10.1016/0735-1097(95)00618-4.

16. E. D. Overholt, R. W. Joyner, R. D. Veenstra, D. Rawling, and R. Wiedmann: Unidirectional block between Purkinje and ventricular layers of papillary muscles.
American Journal of Physiology-Heart and Circulatory Physiology. 247, H584–H595 (1984).
https://doi.org/10.1152/ajpheart.

17. Gregory E. Morley, Stephan B. Danik, Scott Bernstein, Yanjie Sun, Gregg Rosner, David E. Gutstein, Glenn I. Fishman: Reduced intercellular coupling leads to paradoxical propagation across the Purkinje-ventricular junction and aberrant myocardial activation. *Proceedings of the National Academy of Sciences of the United States of America, 102(11), 4126–4129.* 2005.
https://doi.org/10.1073/PNAS.0500881102

18. Michel Haissaguerre, Edward Vigmond, Bruno Stuyvers, Meleze Hocini, Olivier Bernus: Ventricular arrhythmias and the His-Purkinje system.
Nature Reviews Cardiology. 13(3):155-66. 2016.
https://doi.org/10.1038/nrcardio.2015.193

19. Sumeet S. Chugh: Sudden cardiac death in 2017: Spotlight on prediction and prevention. *International Journal of Cardiology*, *237*, 2–5. 2017. https://doi.org/10.1016/j.ijcard.2017.03.086

20. Bo Gregers Winkel, Reza Jabbari, Jacob Tfelt-Hansen: How to prevent SCD in the young? *International Journal of Cardiology*, *237*, 6–9. 2017. https://doi.org/10.1016/j.ijcard.2017.03.083

21. Pieter van der Bijl, Victoria Delgado, Jeroen J Bax: Sudden cardiac death: The role of imaging.
International Journal of Cardiology, *237*, 15–18. 2017. https://doi.org/10.1016/j.ijcard.2017.03.010

22. Michel Haïssaguerre, Morio Shoda, Pierre Jaïs, Akihiko Nogami, Dipen C. Shah, Josef Kautzner, Thomas Arentz, Dietrich Kalushe, Dominique Lamaison, Mike Griffith, Fernando Cruz, Angelo de Paola, Fiorenzo Gaïta, Mélèze Hocini, Stéphane Garrigue, Laurent Macle, Rukshen Weerasooriya, and Jacques Clémenty: Mapping and ablation of idiopathic ventricular fibrillation.
Circulation, *106*(8), 962–967. 2002.
https://doi.org/10.1161/01.CIR.0000027564.55739.B1

23. Oscar Campuzano, Georgia Sarquella-Brugada, Ramon Brugada and Josep Brugada: Genetics of channelopathies associated with sudden cardiac death.
Global Cardiology Science and Practice. 2015(3): 39.
https://10.5339/gcsp.2015.39

24. Michel Haïssaguerre, Josselin Duchateau, Remi Dubois, Mélèze Hocini, Ghassen Cheniti, Frederic Sacher, Thomas Lavergne, Vincent Probst, Elodie Surget, Ed Vigmond, Nicolas Welte, Remi Chauvel, Nicolas Derval, Thomas Pambrun, Pierre Jais, Wee Nademanee, and Olivier Bernus: Idiopathic Ventricular Fibrillation: Role of Purkinje System and Microstructural Myocardial Abnormalities.
JACC: Clinical Electrophysiology. 2020 Jun;6(6):591-608.
https://doi.org/10.1016/j.jacep.2020.03.010

25. Ghassen Cheniti, Konstantinos Vlachos, Marianna Meo, Stephane Puyo, Nathaniel Thompson, Arnaud Denis, Josselin Duchateau, Masateru Takigawa, Claire Martin, Antonio Frontera, Takeshi Kitamura, Anna Lam, Felix Bourier, Nicolas Klotz, Nicolas Derval, Frederic Sacher, Pierre Jais, Remi Dubois, Meleze Hocini and Michel Haissaguerre: Mapping and Ablation of Idiopathic Ventricular Fibrillation.
Frontiers in Cardiovascular Medicine, *5*, 123. 2018.
https://doi.org/10.3389/fcvm.2018.00123

26. Charles Antzelevitch, Alexander Burashnikov: Overview of Basic Mechanisms of Cardiac Arrhythmia.
Cardiac Electrophysiology Clinics. 2011 Mar 1;3(1):23-45.
https://doi.org/10.1016/j.ccep.2010.10.012

27. S. Viskin , M. D. Lesh, M. Eldar, R. Fish, I. Setbon, S. Laniado, B. Belhassen: Mode of onset of malignant ventricular arrhythmias in idiopathic ventricular fibrillation.
Journal of Cardiovascular Electrophysiology, 8(10), 1115–1120. 1997. https://doi.org/10.1111/j.1540-8167.1997.tb00997.x

28. A. Leenhardt, E. Glaser, M. Burguera, M. Nürnberg, P. Maison-Blanche, P. Coumel: Short-coupled variant of torsade de pointes: A new electrocardiographic entity in the spectrum of idiopathic ventricular tachyarrhythmias.
Circulation, 89(1), 206–215. 1994
https://doi.org/10.1161/01.CIR.89.1.206

29. Martyn P. Nash, Ayman Mourad, Richard H. Clayton, Peter M. Sutton, Chris P. Bradley, Martin Hayward, David J. Paterson, and Peter Taggart: Evidence for multiple mechanisms in human ventricular fibrillation.
Circulation, *114*(6), 536–542. 2006. https://doi.org/10.1161/CIRCULATIONAHA.105.602870

30. Nicholas Jackson, Stéphane Massé, Nima Zamiri, Mohammed Ali Azam, Patrick F. H. Lai, Marjan Kusha, John Asta, Kenneth Quadros, Benjamin King, Peter Backx, Raymond E. Ideker, Kumaraswamy Nanthakumar: Mechanisms of long-duration ventricular fibrillation in human hearts and experimental validation in canine Purkinje fibers.
JACC: Clinical Electrophysiology, 1(3), 187–197. 2015. https://doi.org/10.1016/j.jacep.2015.04.003

31. Henk E D J Ter Keurs 1, Penelope A Boyden: Calcium and arrhythmogenesis.
Physiological Reviews. 87(2):457-506. 2007.
https://doi.org/10.1152/physrev.00011.2006

32. M. A. Allessie, F. I. Bonke, F. J. Schopman: Circus movement in rabbit atrial muscle as a mechanism of tachycardia. III. The "leading circle" concept: a new model of circus movement in cardiac tissue without the involvement of an anatomical obstacle.
Circulation Research, 41(1), 9–18. 1977.
https://doi.org/10.1161/01.RES.41.1.9

33. N. El-Sherif, R. A. Smith, K. Evans: Canine ventricular arrhythmias in the late myocardial infarction period. VIII. Epicardial mapping of reentrant circuits.
Circulation Research, 49(1), 255–265. 1981.
https://doi.org/10.1161/01.RES.49.1.255

34. Masamichi Gotoh, Takumi Uchida, William J. Mandel, Michael C. Fishbein, Peng-Sheng Chen, and Hrayr S. Karagueuzian: Cellular graded responses and ventricular vulnerability to reentry by a premature stimulus in isolated canine ventricle.
Circulation, 95(8), 2141–2154. 1997.
https://doi.org/10.1161/01.CIR.95.8.2141

35. P. S. Chen, P. D. Wolf, E. G. Dixon, N. D. Danieley, D. W. Frazier, W. M. Smith, and R. E. Ideker: Mechanism of ventricular vulnerability to single premature stimuli in open-chest dogs.
Circulation Research. 62:1191–1209. 1988.
https://doi.org/10.1161/01.RES.62.6.1191

36. D. W. Frazier, P. D. Wolf, J. M. Wharton, A. S. Tang, W. M. Smith, R. E. Ideker: Stimulus-induced critical point. Mechanism for electrical initiation of reentry in normal canine myocardium.
The Journal of clinical investigation. 83(3):1039-52. 1989
https://doi.org/10.1172/JCI113945

37. P. S. Chen, Y. M. Cha, B. B. Peters, and L. S. Chen: Effects of myocardial fiber orientation on the electrical induction of ventricular fibrillation.
American Journal of Physiology - Heart and Circulatory Physiology, 264(6 33-6). 1993.
https://doi.org/10.1152/ajpheart.1993.264.6.h1760

38. C. Antzelevitch, J. Jalife, and G. K. Moe: Characteristics of reflection as a mechanism of reentrant arrhythmias and its relationship to parasystole.
Circulation, 61(1), 182–191. 1980
https://doi.org/10.1161/01.CIR.61.1.182

39. G. J. Rozanski, J. Jalifé, and G. K. Moe: Reflected reentry in nonhomogeneous ventricular muscle as a mechanism of cardiac arrhythmias.
Circulation, 69(1), 163–173. 1984.
https://doi.org/10.1161/01.CIR.69.1.163

40. S. C. Krishnan, C. Antzelevitch: Flecainide-induced arrhythmia in canine ventricular epicardium. Phase 2 reentry?
Circulation. 87(2):562-72. 1993.
https://doi.org/10.1161/01.cir.87.2.562

41. Masood Akhtar, Anthony N. Damato, William P. Batsford, Jeremy N. Ruskin, J. Bimbola Ogunkelu, and Guillermo Vargas: Demonstration of re entry within the His Purkinje system in man.
Circulation, 50(6), 1150–1162. 1974.
https://doi.org/10.1161/01.CIR.50.6.1150

42. Masood Akhtar: Editorial: The Clinical Significance of the Repetitive Ventricular Response.
Circulation. 63:773–775. 1981.
https://doi.org/10.1161/01.CIR.63.4.773

43. M. Akhtar, A. N. Damato, A. R. Caracta, W. P. Batsford, S. H. Lau: The Gap Phenomena During Retrograde Conduction in Man.
Circulation. 49(5):811-7. 1974.
https://doi.org/10.1161/01.cir.49.5.811.

44. Ali Akbar Mehdirad, Stephen Keim, Kevin Rist, Todor Mazgalev, Patrick Tchou: Asymmetry of retrograde conduction and reentry within the His-Purkinje system: A comparative analysis of left and right ventricular stimulation.
Journal of the American College of Cardiology, 24(1), 177–184. 1994.
https://doi.org/10.1016/0735-1097(94)90560-6

45. J. C. Bailey, D. A. Lathrop, D. L. Pippenger: Differences between proximal left and right bundle branch block action potential durations and refractoriness in the dog heart.
Circulation Research. 40:464–468. 1977.
https://doi.org/10.1161/01.RES.40.5.464

46. Mark E. Josephson: Clinical Cardiac Electrophysiology: Techniques and Interpretations.

47. A. Farshidi, E. L. Michelson, A. M. Greenspan, S. R. Spielman, L. N. Horowitz, M. E. Josephson: Repetitive responses to ventricular extrastimuli: incidence, mechanism, and significance.
America Heart Journal. 100(1):59-68. 1980.
https://doi.org/10.1016/0002-8703(80)90279-3

48. Robert J. Myerburg: The gating mechanism in the distal atrioventricular conducting system.
Circulation, 43(6), 955–960. 1971.
https://doi.org/10.1161/01.CIR.43.6.955

49. Macchi E., Musso E., Rossi S. (2018) Role of Electrotonic Current in Excitable Cells. In: Boffi D., Pavarino L., Rozza G., Scacchi S., Vergara C. *(eds) Mathematical and Numerical Modeling of the Cardiovascular System and Applications. SEMA SIMAI Springer Series, vol 16. Springer, Cham.*
https://doi.org/10.1007/978-3-319-96649-6_5

50. C. Méndez: The Role of Electrotonus in Cardiac Electrophysiology.
In: Rosenbaum M.B., Elizari M.V. (eds) Frontiers of Cardiac Electrophysiology. Developments in Cardiovascular Medicine, vol 19. Springer, Dordrecht. 1983.
https://doi.org/10.1007/978-94-009-6781-6_2

51. Richard D. Walton, Olivier Bernus: Electrotonic effects on action potential duration in perfused rat hearts.
2009 Annual International Conference of the IEEE Engineering in Medicine and Biology Society. 2009:4190-3. 2009.
https://doi.org/10.1109/IEMBS.2009.5334052

52. S. Rohr, B. M. Salzberg: Characterization of impulse propagation at the microscopic level across geometrically defined expansions of excitable tissue: multiple site optical recording of transmembrane voltage (MSORTV) in patterned growth heart cell cultures.
The Journal of general physiology. 104(2):287-309. 1994.
https://doi.org/10.1085/jgp.104.2.287.

53. S. Rohr, J. P. Kucera: Involvement of the calcium inward current in cardiac impulse propagation: induction of UCB by nifedipine and reversal by Bay K 8644.
Biophysical Journal, 72(2 Pt 1), 754–766. 1997.
https://doi.org/10.1016/S0006-3495(97)78710-1

54. Jack JJB, Noble D, Tsien RW: Electrical current flow in excitable cells.
Jack JJB, Noble D, Tsien RW, eds. Oxford Press, Oxford, 1975.

55. B. I. Sasyniuk, C. Mendez: A mechanism for reentry in canine ventricualar tissue.
Circulation research. Jan;28(1):3-15. 1971.
https://doi.org/10.1161/01.res.28.1.3

56. C. Mendez, W. J. Mueller, and X. Urguiaga: Propagation of Impulses across the Purkinje Fiber-Muscle Junctions in the Dog Heart.
Circulation Research. 26:135–150. 1970.
https://doi.org/10.1161/01.RES.26.2.135

57. D. J. Huelsing , K. W. Spitzer, J. M. Cordeiro, A. E. Pollard: Conduction between isolated rabbit Purkinje and ventricular myocytes coupled by a variable resistance.
The American journal of physiology. Apr;274(4):H1163-73. 1998.
https://doi.org/10.1152/ajpheart.1998.274.4.H1163

58. R. W. Joyner, J. Picone, R. Veenstra, D. Rawling: Propagation through electrically coupled cells. Effects of regional changes in membrane properties.
Circulation research. Oct;53(4):526-34. 1983.
https://doi.org/10.1161/01.res.53.4.526

59. R. D. Veenstra, R. W. Joyner, D. A. Rawling: Purkinje and ventricular activation sequences of canine papillary muscle. Effects of quinidine and calcium on the Purkinje-ventricular conduction delay.
Circulation research. May;54(5):500-15. 1984.
https://doi.org/10.1161/01.res.54.5.500

60. F.S. Ng E. Behradfar M.T. Debney A. Nygren A. Hartley A.R. Lyon I.R. Efimov E. Vigmond N.S. Peters: Gap junction uncoupling during ischaemia activates normally quiescent purkinje-myocardial junctions resulting in accelerated and more complex activation patterns.
EP Europace, Volume 17, Issue suppl_5, October 2015, Pages v16–v17.
https://doi.org/10.1093/europace/euv328

61. Massimiliano Zaniboni, Irene Riva, Francesca Cacciani, Maria Groppi: How different two almost identical action potentials can be: a model study on cardiac repolarization.
Mathematical Biosciences 228(1):56-70. 2010.
https://doi.org/10.1016/j.mbs.2010.08.007